Flood Estimations

A View on Time Dependency in Flood-Calculation

Oliver Wieder

Department of Water - Atmosphere - Environment
University of Natural Resources and Life Sciences

This dissertation is submitted for the degree of
Master of Science

Institute of Water Management,
Hydrology and Hydraulic
Engineering

August 2016

Statutory Declaration

I declare that I have authored this thesis independently, that I have not used other than the declared sources/resources, and that I have explicitly marked all material which has been quoted either literally or by content from the used sources.

Vienna, _____ _____

Date Signature

Eidesstattliche Erklärung

Ich erkläre an Eides statt, dass ich die vorliegende Arbeit selbstständig verfasst, andere als die angegebenen Quellen/Hilfsmittel nicht benutzt, und die den benutzten Quellen wörtlich und inhaltlich entnommenen Stellen als solche kenntlich gemacht habe.

Wien, am _____ _____

Datum Unterschrift

Acknowledgements

I would first like to thank my two thesis advisers Priv.-Doz. Dr. Matthias Bernhard and Univ.Prof. Dipl.Geoökol. Dr.rer.nat. Karsten Schulz of the Institute for Water Management, Hydrology and Hydraulic Engineering at the University of Natural Resources and Life Sciences who's office doors were always open whenever I ran into a trouble spot or had a question about my research or writing. Without their passionate participation and input, the validation survey could not have been successfully conducted.

Moreover, I must express my very profound gratitude to my parents, my brother and to my girlfriend for providing me with unfailing support and continuous encouragement throughout my years of study and through the process of researching and writing this thesis. This accomplishment would not have been possible without them. Thank you very much.

Abstract

River Discharge is assumed to follow a stationary process. Engineers do calculate design discharge for structures depending on that crucial assumption, but rarely take a closer look on the length of time window and its effects on the variability of the flood return value. Our goal was to find out, based on the guidelines used in Austria and Germany, how much the length and point of time matters in flood estimation and that the current minimum sample size of 30 years may be too short for a precise HQ value. Moreover, even under strict stationarity, how many years are mandatory in order to reduce the uncertainty and variability of the return level to an acceptable level.

Die zerstörenden Auswirkungen von Hochwasser sind unbestreitbar und wiederholen sich - Ein hundert jähriges Hochwasser jagt das Nächste. Ingenieure berechnen Hochwasserwelle mit Statistiken Hilfsmittel und der Annahme, dass sich das hydrologische System stationär verhält. Doch sind diese Annahmen haltbar? Wie groß ist der Einfluss der Zeitreihenlänge auf den Hochwasserscheitel? In Österreich und Deutschland gelten Zeitreihen ab einer länge von 30 Jahre als geeignet für die statistische Berechnung - doch ist diese Länge gerechtfertigt? Das Ziel dieser Arbeit ist es, die Länge der Zeitreihe kritisch zu hinterfragen und die dadurch entstehenden Unsicherheiten aufzuzeigen.

Keywords: Flood estimation, Extreme value statistics, Annul maxima, Stationarity

Contents

List of Figures

List of Tables

Nomenclature

AD	Anderson Darling Test
AM	Annual Maximum
AMS	Annual Maximum Series
BMLFUW	Federal Ministry of Agriculture, Forestry, Environment and Water Management
CoV	Coefficient of Variation
GRDB	Global Runoff Database
GRDC	Global Runoff Data Center
HQ_X	Flood return level with a return interval of X years
IQR	Inter Quartile Range
LMRD	L-Moment-Ration Diagram
$List_{yx}$	List of gauging sites with X years of length
MAD	Mean Absolute Deviation
PDS	Partial Duration Series
TS	Time Series

Chapter 1

Introduction

1.1 Introduction and Research Question

Along with storms, floods account for the most devastating natural hazards in Europe in terms of human losses and economic damage (Munich Re, 2013). But not only their direct and tangible impacts are disastrous, but also their indirect and intangible effects are tremendous as adverse influences go far beyond the flooded areas, such as production losses caused by damaged transport or energy infrastructure as well as adverse effects on human health, the environment and cultural heritage (FOEN, 2016, Parliament and Comission, 2007, EEA, 2012).

River floods are mainly caused by intense precipitation events and or snow melt within a catchment. Important criteria for precipitation are intensity, duration, amount as well as spacial distribution and elevation. Moreover temperature as well as infiltration rate of the soil within the catchment, debris flow and condition of dams and levees, which, if not maintained properly, can lead to structural failures and a possible increase of the damage, as well as natural or artificial retention space, riparian vegetation and land-use. So it is important to understand that there is not one criteria that makes a flood but it is the complex interaction of different climatical, geological, anthropogenic and biological factors which led to the most devastating floods people experienced in Europe.

In general there is a long lasting, broad understanding that flood risk is increasing throughout Europe and that its reasons are many-fold and complex and that it is of crucial importance to look at the main drivers in order to be able to make assumptions about the possible impacts and make predictions. (Merz et al., 2010, Hallegatte et al., 2013, Alfieri, Feyen, Dottori et al., 2015, IPCC, 2014, Liu et al., 2013, Wentz et al., 2007, Cai, Borlace and Lengaigne, 2014, Feyen, Jos. I. Barredo and Dankers, 2009, Palmer and Räisänen, 2002, Milly et al., 2002, Munich Re, 2013). One of those drivers

is Climate Change. As the IPCC, 2014 Report points out, the evidence for a change in the earth's climate is striking and the anthropogenic influence is "extremely likely" to be the main cause for it. Moreover, by changing the climatic component, more uncertainty is involved in the first part of the risk equation (Fuchs, 2014) - namely the probability of the occurrence of a scenario or event with certain characteristics like magnitude and frequency. As the temperature rises and the Greenland Antarctic ice sheets as well as Glaciers around the world are loosing mass, sea levels are rising as well as the energy level within the system is rising leading to a higher water vapor concentration within the atmosphere, which might - according to the IPCC, 2014 Report - lead to the effect that extreme precipitation events become more intense and frequent in many regions, including most of the mid-latitude land masses and the wet tropical regions. Moreover, it is estimated that due to climate change, the variability of occurrence of floods is higher in general (Jeneiová et al., 2015). Due to changing precipitation patterns or abnormal snow and or ice melt, parts of the hydrological systems are being altered (Wentz et al., 2007, IPCC, 2014), which might lead to climate-related extremes such as floods but also droughts, cyclones, heat waves and wildfires, threatening ecosystems all around the world and in many respects posing significant danger to humans (IPCC, 2014). Within the scientific community, climate change is accepted as a mostly anthropogenic driven change of the earth's climate, however, its impacts are still basis of broad discussion and highly uncertain (Liu et al., 2013).

Nevertheless, even though climate change is happening and there is an increase in flood risk, climate change might play a less significant role than suggested on short time scales, while on the long run, it does (Jha, Bloch and Lamond, 2012). And that natural variability and other non-climatic risks are in fact expected to pose a higher impact on flood risk than long term climate trends (Alfieri, Feyen, Dottori et al., 2015, Schwerdtfeger, 1993, O'Connell et al., 2007, Genovese, 2006). J. I. Barredo, 2007 puts it like this :"... changes in climate cannot be understood as the main reason for increasing flood damage in Europe ...". Which puts the short-term focus on other drivers. Especially those of changes in socio-economic systems, land surface and land-use (Pinskwar et al., 2012) e.g. population growth in combination with a fast urbanization and its current implications Jha, Bloch and Lamond, 2012) which lead to a higher vulnerability and susceptibility of society towards ever more extreme events (IPCC, 2014, EEA, 2012). Alfieri, Feyen and Baldassarre, 2016 estimates that there will be an increase on the impact on the population affected as well as in economic-damage by an average of 220% till 2050 due to climate change alone. Moreover, that when current socio-economic pathways are included in the assessment, the annually affected population ranges between 500,000 and 640,000 and the annual flood damage

will increase to 20 to 40 billion euros. Hallegatte et al., 2013 even goes as far as to estimate the approximate global flood losses with projected socio-economic change and climate change to approximately US$1 trillion for major coastal cities by 2050 per year. Those risks, however, are unevenly distributed and are generally greater for disadvantaged people and communities in countries at all levels of development with an overall increase of human casualties and financial losses (IPCC, 2014,Alfieri, Feyen, Dottori et al., 2015). Also people who believe in a false sense of absolute security, the so called "levee-effect" (Merz et al., 2010, Alfieri, Feyen and Baldassarre, 2016), are at higher risk to move to flood prone areas. This uneven rise of flood risk and how to share this burden evenly is greatly debated (Penning-Rowsell and Priest, 2014). It is therefore easy to see that not only technical but also non-technical flood mitigation measurements need to be broadly discussed and taken into account when dealing with flood risk. Which was tried by introducing two major directives on an European wide basis, namely the European Comission, 2000 and the Parliament and Comission, 2007. Those two guidelines interact and complement each other (European Commission, 2014) and are a major step towards an integrated flood risk management by introducing flood risk maps and flood risk management plans for all river districts within the MS of the European Union. Nevertheless, these two directives create "only" a framework in which member states have a lot of ample scope in order to integrate their own standards and measurements regarding floods, leaving dozens of inconsistent national regulations and guidelines.

In Austria for example, the Federal Ministry of Agriculture, Forestry, Environment and Water Management (BMLFUW) is responsible for the technical/structural flood protection (RIWA-T, 2015) and is therefore issuing a guideline (BMLFUW, 2011) for the calculation of the flood characteristics. It is mandatory to estimate the risk for settlements and important economic structures as well as infrastructure. This risk needs to be calculated for a flood with a return period of 30 (HQ_{30}), 100 (HQ_{100}) and 300 years (HQ_{300}). For a reservoir a return period of 5000 years is necessary to calculate (RIWA-T, 2015). However, floods, as all extreme events, do have a high variability in space and time and with respect to socio-economic changes and climate change, face an even greater space of uncertainties. Moreover, there are periods with a higher appearance and periods with lower appearance of floods and therefore the statistical and hydrological estimations can vary a lot in not only the quality but also in the representativety. The BMLFUW, 2011 refers to those uncertainties as well as it suggests that one needs to take the quality of the measured data, the experience of the expert, statistical uncertainties, limited sample space as well as other hydrological relevant Information into account. Most relevant are the quantification of the peak discharge and the design flood discharge and their confidence interval. In Austria, the

design flood discharge needs to be calculated for the three scenarios mentioned above, namely HQ_{30}, HQ_{100} and HQ_{300} by estimating the return level of such a return period - which is from a hydraulic-hydrological point of view quite arbitrary. Nevertheless, the foundation for setting a certain return period are the potential damage to either life or material values, the cost of implementation as well as the impact on the environment e.g. for a settlement a HQ_{100} is defined. So in order to design, plan, construct, run, maintain and or reconstruct a project related to e.g. flood protection, an analysis of the flood events and the resulting flood characteristics need to be considered and therefore calculated, which is done via extreme value statistics. According to the BMLFUW, 2011 several uncertainties in the process of data collection, specifically data accuracy and plausibility, need to be checked for and eventually corrected. This is also true for the assumptions of Independency, Homogeneity, Consistency and Representativety regarding the sample as well as for outliers. The BMLFUW, 2011 explains these procedures quite well and points out that time series longer than 30 years are usable for these calculations (Table 1.2).

Table 1.1 Shows the statistical usability for different time series sample lengths according to the BMLFUW, 2011

Sample Time [Years]	Statistical Applicability
<10	No
10 - 20	Weak
20 - 30	Limited
>30	Yes

The question if it is appropriate to assume stationarity, which is normally not the case (Westra et al., 2015, Jain and Lall, 2001, Villarini et al., 2009) but is necessary for any extreme value statistic (BMLFUW, 2011) is not being challenged in this thesis, as people assume it and calculate return levels based on it. Nevertheless, even if the assumption of stationarity was assumed to be true, are 30 years of sample length enough in order to get a precise design flood return levels or is it more like throwing a dice as Bloschl and Montanari, 2010 suggested? And if not, how many years are necessary in order to get a stable return level?

As mentioned above, any kind of water related structure or simulation that is being calculated using either the national guidelines of Germany (DWA, 2012) or Austria (BMLFUW, 2011) suggests that under stationary conditions the assumption of 30 years of sample length is enough to calculate a reliable return value.
Therefore, the main research questions where:

1. Are 30 years enough to calculate a "precise" return level?

2. How many years are necessary in order to get a "precise" return level? And,
3. how do 30, 40 and 50 years of time series length impact the return level with regard to the variability of the estimate?

Those questions have been tried to answer by following the BMLFUW, 2011 in order to calculate a flood return level. The procedure described in this guideline and used in this thesis is described in the following sections.

1.2 Flood Return-Level Calculation

There exist several ways of flood return level calculations (DWA, 2012, BMLFUW, 2011, Parliament and Comission, 2007). Nevertheless, this thesis follows strictly the BMLFUW, 2011 in order to be in the position of an average user of this guideline. It concurs most of the time with another prominent guideline, namely the DWA, 2012. This section gives an overview of the procedure of how the BMLFUW, 2011 suggests the user to calculate flood return levels, about the assumptions to be made and the uncertainties of the calculation and how it was calculated.

1.2.1 Errors and Assumptions Regarding the Data-Set

In the beginning, a short introduction of the main errors of hydrological data in general and the assumptions necessary for extreme value statistics are given. The BMLFUW, 2011 provides an overview of the most prominent errors within the hydrological data and suggests procedures of how to detect them and correct them under certain conditions. The assumptions necessary for the statistical analysis of the flood return level calculation are according to the BMLFUW, 2011 the following: The data needs to be

- Unbiased: The sample data-set needs to be unbiased
- Independent: The sample data-set needs to be independent
- Homogeneous: The gauging station should not be influenced by either natural or anthropogenic disturbances during the sampling
- Representative: The data should show the (populations) discharge pattern

Some of these assumptions can be tested according to the BMLFUW, 2011:

- For Independence: *Wald-Wolfowitz*

- For Trend: *Mann-Kendall,Spermanns Rho, Sneyers*
- For Homogeneity: *Wilcoxon*

In this thesis it was assumed that the data-set provided by the GRDC was unbiased. Nevertheless, the data was checked for plausibility, the corrected values were used and every gauging site with missing values was excluded. Furthermore, the "Annual Maxima Series" -Methode was used in order to get the extreme values for the flood return level estimation (See section 1.2.3 for more details), which is according to the BMLFUW, 2011 another way to make sure, that the data set is independent. As mentioned above, the corrected values were chosen so if there have been any anthropogenic disturbances and they were detected and corrected by the provider of the data, it was used.

The main focus, however, did lay on the time series length and the assumptions made by the BMLFUW, 2011 regarding it: "A sample length of 30 years is enough, to estimate flood return levels".

Table 1.2 Shows the statistical usability for different time series sample lengths according to the BMLFUW, 2011

Sample Time [Years]	Statistical Applicability
<10	No
10 - 20	Weak
20 - 30	Limited
>30	Yes

Any further errors have been neglected, as the attention lay on the precision of the repeated return level outcomes with different time window lengths and not so much on the accuracy of the estimation.

1.2.2 Return Period

Before flood return levels can be calculated, the **return period** (T_n) needs to be defined. One can distinguish between either frequency of exceedance (Equation 1.1, P_e), non-exceedance (Equation 1.2, P_n) or occurrence probability (Equation 1.3, P). In this thesis it was defined as the number of years (e.g. 100 years), in which a certain event occurs on average once or is exceeded. This means that within a discrete time interval of 100 years, the return period for a hundred-year-flood is each year the same (P=0.01) - this event does not return every 100 years, but on average it occurs or exceeds once within 100 years. The BMLFUW, 2011 defines them as:

$$P_e = P(X \geq x_1) = \frac{1}{T_n} \tag{1.1}$$

$$P_n = P(X < x_2) = 1 - \frac{1}{T_n} \tag{1.2}$$

$$P(x_1 < X < x_2) = P_{u,x_2} - P_{u,x_1} \tag{1.3}$$

There is a simple relationship between the P_e and the P_n:

$$P_n + P_e = 1 \tag{1.4}$$

According to the BMLFUW, 2011, the probability or "Statistical Security" (S) that a flood (HQ) is greater or equal a flood with a certain return period (HQ_n) does not occur within m years is:

$$S = (1 - \frac{1}{1 - T_n})^m \tag{1.5}$$

and

$$T_n = \frac{1}{1 - S^{1/m}} \tag{1.6}$$

1.2.3 Extraction of the Extreme Values

The next step of a flood return level estimation is to extract the extreme values of a time series. Both, the German DWA, 2012 and the Austrian BMLFUW, 2011 for flood estimation offer two different types of doing this. On the one side, there is the *annual maximum series* (AMS) approach, and on the other side, there is the *partial duration series* (PDS) method. Both have advantages and disadvantages and it is up to the user to decide which one of them should be used. For the AMS method, one has to extract the annual maximum of a time series whereas for the PDS method, one has to extract all the values which exceed a certain threshold value (ξ_0).

According to the BMLFUW, 2011, there are several ways to calculation the ξ_0 e.g by assuming a Poisson-Distributed occurrence or by extracting the five biggest events of the time series first and afterwards add the next smaller event till a goodness of fit test suggests that the fitted distribution cannot adequately fit the chosen subset of the data anymore. This last event can then be seen as the ξ_0.
Furthermore, the guideline suggests, that the ξ_0 should be chosen in a manner, that for each year there are around two extremes to be extracted - under the assumption of independence (See Subsection 1.2.1). In practice, there will be two to three exceeding events per year that are over the ξ_0. Therefore the PDS is assumed to be more powerful than the AMS method, because with the AMS some information is lost and not all the extreme events within one year are being taken into account or events that might not be extreme are.
Nevertheless, results for very extreme return levels do not differ much (Table 1.3) but one can assume that in general with lower return period, the difference gets higher and vice versa.

Table 1.3 Comparison of the return period for a PDS and an AMS according to the BMLFUW, 2011.

T_n in years	
PDS	AMS
0.50	1.16
1.00	1.58
1.40	2.00
2.00	2.54
5.00	5.52
10.00	10.50
20.00	20.50
50.00	50.50
100.00	100.50

For the conversion of the probabilities P into return periods the following functions were used (BMLFUW, 2011):

for the AMS:

$$T_{AMS} = \frac{1}{1 - P_{U,AMS}} \tag{1.7}$$

$$P_{U,AMS} = 1 - \frac{1}{T_{AMS}} \tag{1.8}$$

or for the PDS:

$$T_{PDS} = T_{AMS}\frac{n}{j} \tag{1.9}$$

$$P_{U,PDS} = 1.1\frac{1}{T_{PDS}} = 1 - \frac{1}{T_{AMS}}\frac{j}{n} \tag{1.10}$$

j: Number of years
n: Number of samples

For $T_n < 10$ Years, the return levels differ significantly between the PDS and the AMS method, and are better described by the PDS, however, for larger T_n they are assumed to be nearly even. In this thesis, only the AMS method has been taken into account and the T_n was always a T_n =100, which means that the occurrence of such an event is assumed to have a probability of $p = 0.01$.

1.2.4 Choosing the Extreme Value Distributions Function

The next step is to chose an extreme value distribution that fits the AMS or PDS of the time series best. These distributions are described by extreme value functions. There are several types of theoretical extreme value distribution functions for fitting extreme events (BMLFUW, 2011). In general, functions with a higher number of parameters are more flexible and adjustable than functions with fewer parameters, however over-fitting due to too many parameters is not desirable, as it might lead to a bigger influence of outliers.

According to the BMLFUW, 2011, the two most prominent families of extreme value distributions are the Generalized Extreme Value distributions (GEV) and the Generalized Pareto distributions (GPD). The GEV is more related to the AMS method, whereas the GPD is more related to the PDS method. The GEV distribution family consists of three distributions; the Frechet distribution (EV2), which has a lower limit, the Weibull distribution, which has an upper one and the Gumbel distribution, which is unlimited in both directions. Only the EV1 and EV3 distribution have been used in this thesis, as well as the very commonly used, and also recommended by

the DWA, 2012 and the BMLFUW, 2011, Pearson-Type-3 (PE3) and Log-Normal-3 (LN3) distributions. All except the Gumbel distribution, use three parameters namely ζ, α and k, which stand respectively for the location, the scale and the shape of the distribution. The Gumbel distribution sets $k = 0$. The ordinary Weibull distribution sets $\zeta = 0$ and is rather used in reliability applications (Works, Technology and Statistics, 2002) - in the extreme value theory, ζ is > 0.
As the standard set by the BMLFUW, 2011 was used, the parameters were named as listed above. This is important to know, as different sources use different mathematical nomenclature for the parameters. They are described according to Jenkinson, 1955 as following:

$$F(x) = \left\{ \begin{array}{llll} \exp(-(1-k\frac{x-\zeta}{\alpha})^{\frac{1}{k}}) & \zeta + \frac{\alpha}{k} \geq x & k < 0 & (EV2) \\ \exp(-\exp(-\frac{x-\zeta}{\alpha})) & x \in \Re & k = 0 & (EV1) \\ \exp(-(1-k\frac{x-\zeta}{\alpha})^{\frac{1}{k}}) & x \geq \zeta + \frac{\alpha}{k} & k > 0 & (EV3) \end{array} \right\} \tag{1.11}$$

According to the BMLFUW, 2011, the PE3 distribution contains the normal distribution, the shifted three-parameter Γ distribution with a finite lower bound and positive skewness and the reverse three-parameter Γ distribution with a finite upper bound and negative skewness. The distribution's parameters are the first three ordinary moment ratios μ as a location parameter, σ a scale parameter and γ a shape parameter and is usually parametrized by α, β and ζ. If a random variable x has a PE3 distribution, then its probability density function (PDF) is described according to the BMLFUW, 2011 as:

$$f(x) = \frac{1}{a\gamma(b)}(\frac{x-c}{1}) \tag{1.12}$$

The LN3 distribution is similar to the two-parameter Log-Normal distribution (BMLFUW, 2011), except that x is shifted by an amount ζ which represents a lower bound. The distribution function, with a lower bound ζ, the mean on log scale μ and the standard deviation on log scale σ is defined according to Aristizabal, 2012 as

$$F(x) = \Phi(y), \tag{1.13}$$

x > 0, where

$$y = \{log(x - \zeta) - \mu\} \backslash \sigma \tag{1.14}$$

and Φ(y) is the distribution function of the standard normal distribution.

1.2.5 Estimation of the Parameters

After an extreme value function has been chosen, one needs to estimate its parameters. Several possibilities for the parameter estimation exist (BMLFUW, 2011), each having advantages and disadvantages, like the Method by KREPS, the Gumbel-Method, the Method of Moments, the Probability Weighted Moments (PWM), the L-Moments and the Maximum-Likelihood Estimation Method (MLE). The usefulness of different estimators can be judged by looking at their properties such as consistency, efficiency, asymptotic normality, robustness and being unbiased. In this thesis the L-Moment Method (LMOM) were used because the MLE Method shows significantly bad results with low sample size (BMLFUW, 2011, Subsection 1.2.5). In the following two subsection a short overview of the most commonly used estimation methods following the BMLFUW, 2011 guideline is given.

L-Moments Estimation Method (LMOM)

Introduced by Hosking (Hosking, 1990), the LMOM has several advantages over other product moments, such as probability weighted moments or the simple method of moments. They tend to be more robust against extreme values and exist whenever the mean of the distribution exists. Furthermore, the estimators for the location, scale and shape are nearly unbiased. The r^{th} LMOM is defined by Hosking (Hosking, 1990) as:

$$\lambda_r = \frac{1}{r} \sum_{k=0}^{r-1} (-1)^k \binom{r-1}{k} E(X_{r-k:r}) \tag{1.15}$$

The theoretical LMOM for real valued random variables x with a quantile function x(F) are derived from the expectations of order statistics (Hosking, 1990). The order statistics of sample size r are formed by ascending order $X_{1:n} \leqslant X_{2:n} \leqslant \ldots \leqslant X_{n:n}$. From

equation 1.6, the first four LMOM can be derived as:

$$\lambda_1 = E(X_{1:1}) \tag{1.16}$$

$$\lambda_2 = \frac{1}{2}E(X_{2:2} - X_{1:2}) \tag{1.17}$$

$$\lambda_3 = \frac{1}{3}E(X_{3:3} - 2X_{2:3} + X_{1:3}) \tag{1.18}$$

$$\lambda_4 = \frac{1}{4}E(X_{4:4} - 3X_{3:4} + 3X_{2:4} - X_{1:4}) \tag{1.19}$$

The first four LMOM, λ_1, λ_2, λ_3 and λ_4, can be seen as the location, the scale, the skewness and the kurtosis and are being used, depending on how many parameters are needed, in order to calculate the desired function.

Maximum Likelihood Estimation Method

The Method of Maximum Likelihood tries to find the function parameters that maximize the likelihood function. Theoretically speaking, it has many advantages like minimum variance, however, with values below 500, the error for such estimations using the Generalized extreme value distribution (GEV) are bigger than with the LMOM or PWM. Therefore, only the L-Moment parameter estimation method was used in this thesis. For reasons of completnes, however, a short overview over the MLE is given as well. The first step for a parameter estimation with the MLE is to specify the joint density function (JDF) for all observations - for an independent and identically distributed sample the JDF is defined according to the BMLFUW, 2011 as:

$$f(x_1, x_2, ..., x_n|\theta) = f(x_1|\theta) * f(x_1|\theta) * ... f(x_1|\theta). \tag{1.20}$$

θ: Function Parameter
$x_{1:n}$: Observed Values

Then the observed values $x_1, x_2, \cdots, x_n$ need to be fixed, allow θ to be the function's variable and let it vary freely. This function can be called likelihood and is defined according to the BMLFUW, 2011 as:

$$\mathscr{L}(\theta;x_1,x_2,...,x_n) = f(x_1,x_2,...,x_n|\theta) = \prod_{i=1}^{n}) \tag{1.21}$$

In practice it is often more convenient to work with the logarithm of the likelihood function, called the **log-likelihood**:

$$ln\mathscr{L}(\theta;x_1,x_2,...,x_n) = \sum_{i=1}^{n} lnf(x_i|\theta) \tag{1.22}$$

or the average log-likelihood:

$$\hat{l} = \frac{1}{n} ln\mathscr{L}. \tag{1.23}$$

An MLE parameter has to be found numerically using an optimization method. For some problems, there may be multiple estimates, for others, no MLE exists.

1.3 Goodness-Of-Fit Tests

After the theoretical distribution has been fitted to the data sample extracted via the AMS method and the parameters have been estimated, one should use some kind of goodness of fit (GoF) test in order to evaluate, how well the function describes the observed sample. Both, the DWA, 2012 and the BMLFUW, 2011 suggest different test like the **Kolmogorov-Smirnow-Test** (KS), the χ^2**-Test**, the **nw**^{2}**-Test**, the **probability plot correlation coefficient test** or the **L-Momentratiodiagram - Test** (LMRD). In this thesis no GoF-Tests was used, nevertheless, as for reasons of completeness some of them suggested by BMLFUW, 2011 are still mentioned.

1.3.1 Plotting Position Method

Another way is the Plotting Position, also called empirical Probability. It is a simple way to visualize the relation between the CDF of the estimates versus the time using a log-log scale. There are several different formulas, of which the following is generally accepted (BMLFUW, 2011:

$$P_e(X \geq x_i) = \frac{1-\alpha}{n+1-2\alpha} \qquad with\ (x_1 \geq x_2 \geq,...,x_n) \tag{1.24}$$

P_e: Exceedance Probability
α: Parameter (0,...,1)
n: Total Number

1.3.2 L-Moment-Ratio Diagram Method

The L-Moment-Ratio diagram (L-MRD) uses the L-Moments coefficient of variation (τ_2, a scale parameter), the L-Skewness ratio (τ_3, a shape parameter) and the L-Kurtosis ratio (τ_4, a shape parameter) as a measure of GoF by comparing them with the theoretical distributions parameters. τ_3 is a dimensionless measure of asymmetry, whereas the L-CV is dimensionless measure for variability. The best fitting function lays closest to either the weighted-average regional τ_3 or τ_4 and can be visualized via the LMRD. They ratios are being calculated according to BMLFUW, 2011 by:

$$\tau_2 = L_2/L_1 \tag{1.25}$$
$$\tau_3 = L_3/L_2 \tag{1.26}$$
$$\tau_4 = L_4/L_2 \tag{1.27}$$

where:

$$L_1 = \beta_0 \tag{1.28}$$
$$L_2 = 2\beta_1 - \beta_0 \tag{1.29}$$
$$L_3 = 6\beta_2 - 6\beta_1 + \beta_0 \tag{1.30}$$
$$L_4 = 20\beta_3 - 30\beta_2 + 12\beta_1 - \beta_0 \tag{1.31}$$

and where the data ($x_{1:n}$) are first ranked in ascending order from 1 to n and:

$$\beta_0 = n^{-1}\sum_{j=1}^{n} x_j \tag{1.32}$$
$$\beta_1 = n^{-1}\sum_{j=2}^{n} x_j[(j-1)]/(n-1) \tag{1.33}$$
$$\beta_2 = n^{-1}\sum_{j=3}^{n} x_j[(j-1)(j-2)]/[(n-1)(n-2)] \tag{1.34}$$
$$\beta_3 = n^{-1}\sum_{j=4}^{n} x_j[(j-1)(j-2)(j-3)]/[(n-1)(n-2)(n-3)] \tag{1.35}$$

1.3.3 Kolmogorov-Smirnow Test (KS) and Anderson-Darling Test (AD)

The KS-Test gives a measure of how well a certain function fits the sample data. It uses the *theoretical cumulative distribution function* (CDF) of a certain function with random values and plots it against the *empirical cumulative distribution function* (ECDF) of the sample data and calculates the maximum distance between those two curves - This distance is called the test statistic. Moreover, a critical value is being calculated, which should not be exceeded by the test statistic. If that is the case, the According to Chakravarti, Laha and Roy, 1967, there are several limitations to the test:

- It only applies to continuous distributions.
- it tends to be more sensitive near the center of the distribution than at the tails.
- If location, scale and shape parameters are estimated from the data, the critical region of the KS Test is no longer valid.

The AD-Test tries to answer the same question, however, it gives more weight to the tails of the distribution (Chakravarti, Laha and Roy, 1967).

1.4 Confidence Interval Method

The guidelines (BMLFUW, 2011) suggest several options in order to calculate confidence intervals (CI). Two different processes are being used in the thesis, one is a non-parametric technique (bootstrap - Method) and the other is a parametric one, where a **theoretical distribution function** is being fitted to the sample data. The main disadvantage of the bootstrap-method is that it cannot be reproduced exactly anymore. The CI calculated in this thesis were done via the bootstrap method with a significance level of 0.05 and 5000 repetitions (BMLFUW, 2011).

Chapter 2

Methods

2.1 Calculation Environment and Data Source

The programming language *R* was the main tool for the calculations (Chambers, n.d.). It is freely available under the "General Public License" (GNU) and mainly used for statistical analysis. Due to its package extensions, *R* can be used for multiple purposes and offers a wide range of applications. During the calculations for this thesis, numerous R-Packages have been used and can be viewed in the Appendix (Chapter A).

The data set used in this thesis was provided by the "Global Runoff Data Center" (GRDC) in June 2015 for all European countries. The Center itself is seated in Koblenz and hosted by the German Federal Institute of Hydrology (BfG). It is under the supervision of the World Meteorological Organisation (WMO) and does not only provide the largest database of the world's river discharge and meta-data, but also participate in research concerning climate variability and global change (GRDC, 2014). Figure 2.2 shows the global distribution of the GRDC gauging stations and Figure 2.1 gives a short statistical overview. Its main objective is to support water and climate related programs and projects of the United Nations (UN), its agencies as well as scientific research on water and climatic related topics in general. It does not collect the data itself but gets provided by national, trans-national and partner institutions all over the world. Everyone can contribute to it, starting from national hydrological survey institutions to private energy suppliers. Nevertheless, the national Hydrological and Hydro-Meteorological Services of the WMO are the main contributors to the "Global Runoff Database" (GRDB) (GRDC, 2014).

From the raw data provided by the GRDC, two lists have been extracted. The first one consists of all the gauging sites with a daily available discharge of more than for 60 years starting with the 01.01.1948 - all in all 227 gauging stations. This list will

be called $List_{y60}$ from now on. The second list consists of all the gauging sites with a daily available discharge of more than 100 years starting with the 01.01.1908 - overall 45 gauging stations and it is called $List_{y100}$. For the gauging site details (GRDC. Nr, Station-Names, River-Name, Country and coordinates) go to Table A.1 and A.2 in the Appendix. As explained in Section 1.2 no gauging site with missing values has been used but the corrected discharge. The spatial distribution of the two lists can be seen in (Figure 3.1) and (Figure 3.2) in section 3.1.

	WMO Region	data from 9 countries	number of stations [-]	station-years [y]	individual values [-]	average time series length [years]	shortest record [years]	longest record [years]	earliest data [year]	latest data [year]	latest import [year]
all	World	monthly data (total)	2.412	90.906	1.090.572	37,7	1	130	1877	2013	2014
		original monthly data	2.191	71.374	856.488	32,6	1	123	1877	2001	
		original daily data	1.046	40.549	14.800.385	38,8	1	128	1883	2013	
1	Africa	monthly data (total)									
		original monthly data									
		original daily data									
2	Asia	monthly data (total)	1.186	42.214	506.568	35,6	1	109	1891	2011	2013
		original monthly data	1.184	41.925	503.100	35,4	1	109	1891	2000	
		original daily data	98	2.870	1.047.550	29,3	1	82	1918	2011	
3	South and Central America	monthly data (total)									
		original monthly data									
		original daily data									
4	North America	monthly data (total)	859	33.465	401.460	38,9	1	115	1892	2013	2013
		original monthly data	663	16.525	198.300	24,9	1	95	1902	2001	
		original daily data	858	33.285	12.149.025	38,8	1	115	1892	2013	
5	Australia and Oceania	monthly data (total)									
		original monthly data									
		original daily data									
6	Europe	monthly data (total)	357	15.237	182.844	41,5	5	130	1877	2013	2014
		original monthly data	344	12.924	155.088	37,6	4	123	1877	2001	
		original daily data	90	4.394	1.603.810	48,8	2	128	1883	2013	

Figure 2.1 Shows the GRDC gauging station distribution worldwide as of June 2015 (GRDC, 2014).

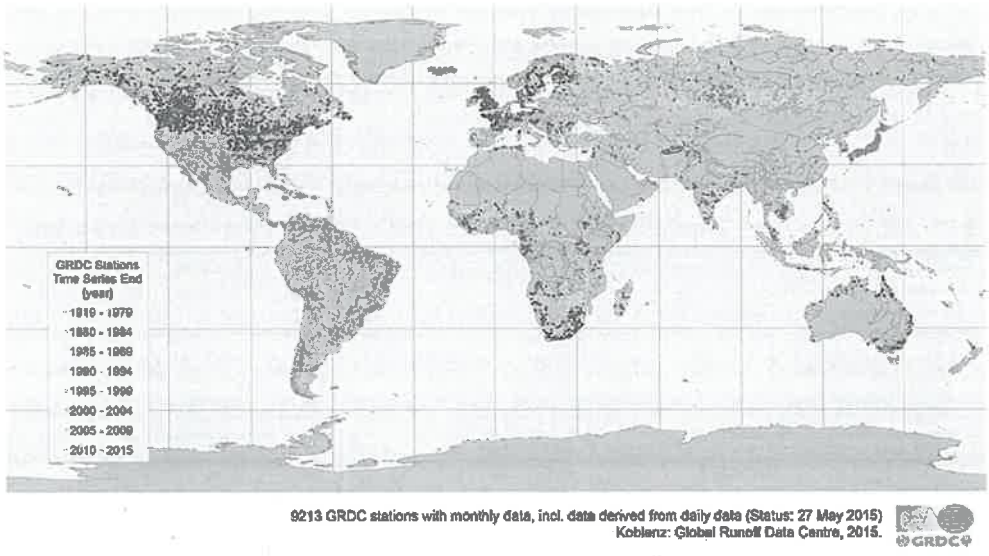

Figure 2.2 Shows the GRDC gauging station locations worldwide as of May 2016 with respect to the ending of the time series - starting in red with 1919-1979. Then each 5 year interval is marked with a different color till 2010-2015 in dark blue (GRDC, 2014).

2.2 Window Shift over the 60 Year-Long Time-Series

The $List_{y60}$ is a list consisting of the 227 gauging sites shown in detail in Table A.1 in the Appendix and with a spacial distribution shown in Figure 3.1 in section 3.1. Each Station has a daily discharge length of 60 years, starting with the 01.01.1948. For every gauging site in the $List_{y60}$, a time window of 30 years, which begun with the 01.01.1948 (Figure 2.3) has been sampled. For each time-window, the annual maxima were extracted via the AMS-Method (See section 1.2.3 for details) and a Weibull, Gumbel, Log-Normal-III and Pearson-III distribution (Shown in detail in section 1.2.4, Figure 2.4 shows the graphical procedure) was fitted separately to the annual maxima using the L-Moment parameter estimation method (See section 1.2.5 for more details regarding the L-Moment Method). From the cumulative distribution function (CDF) of each fitted function, the return level T_n=100 (HQ_{100}) as well as the confidence intervals were calculated as explained in subsection 1.2 and subsection 1.4 and afterwards standardized according to Kryszig, 1979 as:

$$z_i = \frac{X_i - \mu_p}{\sigma_p} \tag{2.1}$$

z_i: Standardized annual maxima i
X_i: Extracted annual maxima i
μ_p: The mean for the extracted annual maxima
σ_p: The standard deviation for the extracted annual maxima

The value calculated is called z-score, however, it can be used synonymously for standard deviation. In this thesis standard deviations (sd) are being used for the scale of the standardized values and not z-values. This procedure was repeated 30 times (Figure 2.4) every 365.25 days for all 227 gauging sites until the time series reached the window between 01.01.1979 to 01.01.2008. Overall 30 return values were calculated for each of the four fitted distributions and put into a matrix. For each column of this matrix, which stands for one of the four distributions, the mean of the 30 return levels was taken (As it was standardized, the mean was $\mu = 0$, and the standard deviation was sd = 1) as a reference of under- and overestimation within the 60 years of the time series. Blue was taken as a signal for underestimation and red as overestimation. This was done in order to get a quick overview of the flood return level spread.

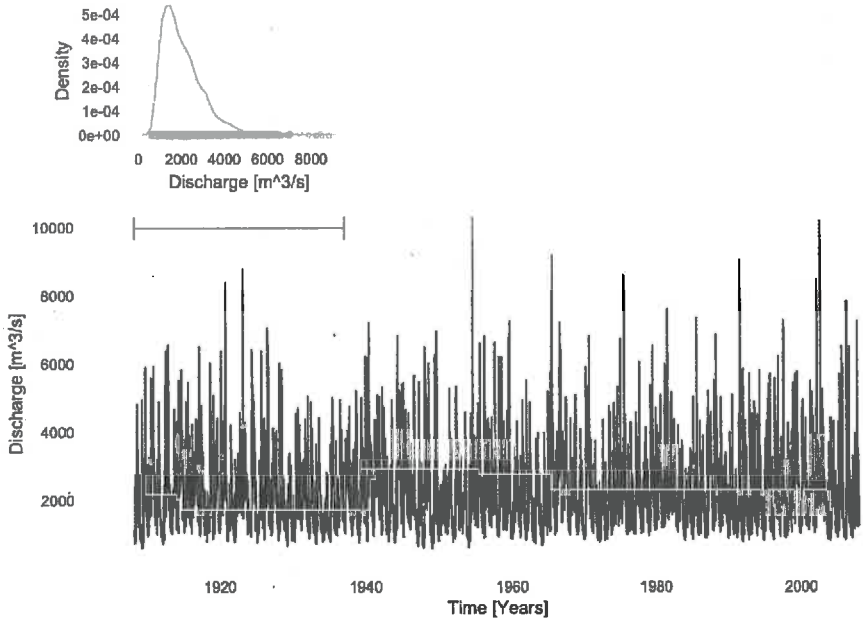

Figure 2.3 Shows at the bottom of the graph the time series of the daily discharge of the Danube at the Bratislava Gauging Station (GRDC Nr. 6142200). There is a black bar above it, which shows a 30 year time window for the annual maxima extraction and at the top of the graph, the density for this time window's annual maxima is shown.

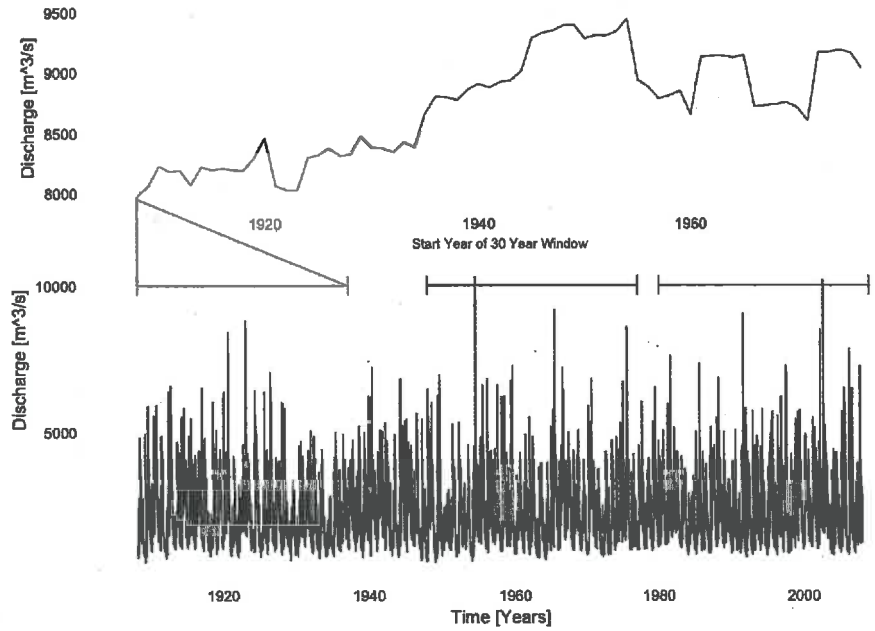

Figure 2.4 Shows the graphical procedure of how the HQ_{100} return level were extracted and put into a time series. At the bottom of the graph the time series of the daily discharge of the Danube at the Bratislava Gauging Station (GRDC Nr. 6142200) is plotted. This graph shows the method of how several HQ_{100} have been calculated separately for different time windows. With each shift of one year, there is a recalculation of a HQ_{100}, which are all shown in the top line-graph. So each window stands for a point(=HQ_{100}) in the upper line.

2.2.1 Comparison of all the return levels for all gauging sites

Afterwards a correlation matrix containing all 227 gauging sites using the standardized HQ_{100} return levels calculated with the Weibull function was computed. Every gauging sites 30 standardized return values for the 60 year of time series length was compared with every other gauging stations 30 standardized return levels and correlations where computed. Out of this matrix six correlating regions were derived with the method of complete-linkage clustering (also called farthest neighborhood clustering) and mapped. The clustering Method is described by Defays, 1977 as:

$$D(X,Y) = \max_{x \in X, y \in Y} d(x,y) \tag{2.2}$$

X,Y: Two sets of elements (cluster)
d(x,y): Distance Between Elements $x \in X and y \in Y$

This clustering method puts each river is in its own cluster. Then, at any further step, it joins the cluster with the shortest distance to its own cluster. The finite number of clusters was 6, which is in this case an arbitrary number. These 6 clusters were then named region one to region six, and a linear regression as well as a LOESS (Local Regression) have been fitted. This was done in order to show that simply by the point of time when the return period was calculated with a 30 year time window, one can derive a tendency of an increase or decrease at certain gauging stations and merged into regions.

2.2.2 Calculation of the overall variability of the window shift

In order to calculate the variation of each calculated time series of HQ_{100} values, the coefficient of variation (CoV), the inter quartile range (IQR) as well as the median absolute deviation (MAD) were calculated and plotted. Each one of these variation values was calculated out of all the HQ_{100} values for both, the list containing all the 227 gauging sites with 60 years of time series length and its 30 year-long shift as well as the 30, 40 and 50 year-long window shift for all the 45 gauging sites with 100 year time series length. As for the CoV, the un-standardized values have been taken as calculation basis. Whereas for the IQR and the MAD the standardized values have been used, so their values always stand for the standard deviation (sd). This was done for each river independently and each CoV, IQR and MAD value was then plotted via a box-plot for each function separately. The CoV, also called the relative standard deviation, is a useful tool in order to compare the variability of different scales with each other. In Everitt, 1998, it is defined as the ratio of standard deviation to the mean

and expressed as percentage of difference from whatever value is used (in this case cubic meters of discharge per seconds) and calculated as:

$$C_v = \frac{\sigma}{\mu} * 100 \tag{2.3}$$

σ: Standard Deviation
μ: Mean

The IQR range is a robust measure of scale and defined according to Upton and Cook, 1996 as:

$$IQR = Q_3 - Q_1 \tag{2.4}$$

Q_1: First Quartile of the Data
Q_3: Third Quartile of the Data

It always stands for 50% of the data points between the first and third quartile and if normal distributed the IQR has a range of 1.345 standard deviations. The calculations have been done using the standardized data sets so in order to compare the gauging sites using the IQR and the MAD. The MAD, another robust measure of variability, is defined by Venables and Ripley, 1999 as:

$$MAD = median(|X_i - median(X_i)|) \tag{2.5}$$

X_i: Data Point i

2.3 Window Shift over the 100 Year-Long Time-Series

The same procedure as for $List_{y60}$ (See Subsection 2.2 for the detailed method) was applied for $List_{y100}$, except that there were three different time windows. The $List_{y100}$ is a list consisting of the 45 gauging sites in Table A.2 in the Appendix with a daily discharge length of 100 years, starting with the 01.01.1908 and an spatial distribution shown in Figure 3.2 in section 3.1. The first window contained 30 years (365.25*30 days) and was shifted over the 100 years lasting time series starting with the 01.01.1908 (Figure 2.5) with overall 70 return values. The second window had 40 years (365.25*40 days) and 60 return values were calculated. The third window had 50 years (365.50*50

days) and 50 values were returned. For each time window heat maps were plotted and the confidence intervals with a significance level of 0.05 were calculated with the bootstrap method. As a representation for the measure of variability, the CoV, IQR and MAD have been calculated as well (See Subsection 2.2.2) and plotted.

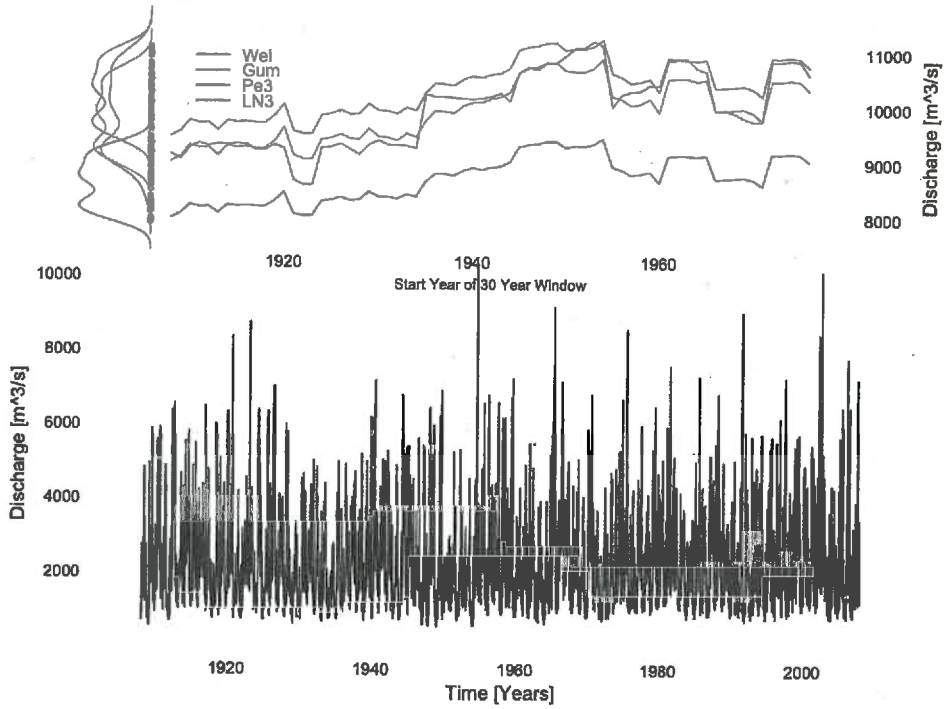

Figure 2.5 Shows as in Figure 2.4 the daily discharge of the Danube at the Bratislava Gauging Station (GRDC Nr. 6142200) on the bottom of the graph as well as the HQ_{100} estimated return level line of the Weibull function (black line) on the top. Moreover, it shows the Gumbel (red line), Log-Normal III (blue line) and Pearson III (green line) estimated return levels with their densities on the left side.

2.4 Generation of a Stationary Annual Maxima Series

In order to get a better understanding of how many years are necessary to calculate a stable return level, a "gauging station" was created, which follows the assumptions needed for extreme value statistics (See subsection 1.2.1) - Especially the assumption of strict stationarity. The gauging site with the GRDC Nr. 6142200 (Danube River - Bratislava) and the time series length of 100 years between the 01.01.1908 and 01.01.2008 was taken in order to fit a Weibull distribution function with the procedure described in section 1.2 with the following parameter values: the location parameter was 0, the scale parameter was 6230.387832 and the shape parameter was 4.553004.

Then the fitted Weibull distribution was taken in order to generate 2000 random values. This was done by setting the set.seed function of the "base" package in *R* to 1 - in order to be reproduceable - and use the inverse of the Weibull distribution function described in subsection 1.2.4. So an annual maxima series with a length of 2000 values and strict stationary conditions following a known Weibull distribution was generated. On these random and stationary generated annual maxima, all four distribution functions (Weibull, Gumbel, Pearson III and Log-Normal III distribution function seen in subsection 1.2.4) have been fitted following the same procedure as described in section 1.2 and tested with the One-sample Komogorov-Smirnov Test. The annual maxima basis for each HQ_{100} value was provided by a cumulative shifting window starting with a 30 year-long long window (=30 annual maxima), and then for each further value, the next generated annual maxima was added to the 30 year-long window until the calculation basis reached 2000 annual maxima, which leads to 1970 HQ_{100} values in total. Therefore, the first HQ_{100} value was calculated using 30 annual maxima, whereas the last HQ_{100} value has an annual maxima basis of 2000. For each additional annual maxima, the confidence intervals (CI) were calculated using the bootstrap method with 5000 repetitions and a significance level of 0.05. In order to get a number for the variability of the CI-spread in relation to the mean, the lower CI was subtracted from the upper CI, divided it by the mean and multiplied it by 100. Afterwards, as a measure of variability for the mean, the Coefficient of Variation (CoV), the Inter Quartile Range (IQR) and the Median Absolute Deviation (MAD) have been calculated starting with the HQ_{100} window between the first and the 10^{th} HQ_{100} value, then for each further 10^{th} HQ_{100} values. So the second CoV, IQR and MAD value was the range between the 11^{th} and 20^{th} HQ_{100} value. The third variation value was for the range between the 21^{th} and 30^{th} HQ_{100} value and so on. These values have been calculated till it reached the end of the 1970 HQ_{100} values - all in all 197 variation values for the CoV, IQR and MAD each. The IQR and MAD have been calculated with the standardized values.

Chapter 3

Results

3.1 Spatial Distribution of the Gauging Sites

This section shows the spatial distribution of the gauging sites used for the $List_{y60}$ and $List_{y100}$ described in Section 2 and the Appendix A.

Figure 3.1 Spatial distribution of the 227 gauging sites with 60 year-long time series (List of the gauging sites can bee seen in the Appendix A.1).

Figure 3.2 Spatial distribution of the 45 gauging sites with 100 year-long time series (List of the gauging sites can bee seen in the Appendix (A.2).

3.2 Window Shift Results for the 60 Year-Long Gauging Sites

In this Section the overall spread of the list with 60 years of gauging site length is presented. The details of this list can be viewed in Table A.1 in the Appendix A. This section is separated in two parts. The first shows the individual spread of all the 227 gauging sites. This is done via heat-map plots. Each field in these heat-maps is a HQ_{100} value. The second part shows the overall spread of all the 227 gauging sites with regard to different spread methods, which are described in detail in the Methods in Chapter 2.

3.2.1 Graphical Results for the 30 Year-Long Window Shift

As described in Section 2.2, the shift of the 30 year window return levels have been put in a matrix, standardized and colored according to the deviation from the mean of the HQ_{100} series for each function separately, ranging from blue to red - the darker the color, the more it diverges from the mean of the series with a mean $\mu = 0$ and a standard deviation $sd = 1$. The color scale for all the heat-maps is displayed in Figure 3.3 on the right side next to the biggest heat-plot. The scale on the left side shows the value of the standard deviations (sd) from the mean of this gauging sites flood return level. The scale is set for this and all the other heat-plots ranging from -4 to 4 sd. Each heat-map shows a gauging site of the $List_{y60}$ (For the detailed overview see Table A.1 in the Appendix), with its GRDC Nr. on top of it (e.g. 6119030), whereas on the bottom, one can the see the functions used for the calculation. Each column represents one of the four functions described in Section 1.2.4. They are always in the same order, respectively Wei, Gum, PeII and LNIII, which stand for the Weibull, Gumbel, Pearson III and Log-Normal III distribution function. The rows of each heat-plot start with the year 1979, which means that this value stands for the 30 year time window starting on the 01.01.1948 till the 01.01.1978. The next row is the time window ranging from the 01.01.1949 to the 01.01.1979 and is named 1980, and so on. The first big heat-plot is an example for all the other heat-maps and how they look like in detail, but for a better overview, the small ones have been stripped off their row and column names. Nevertheless, all the other heat-maps have the same structure as the first one. In Figure 3.3, 3.4, 3.5, 3.6, 3.7 and 3.8 one can see the result for the gauging sites of the $List_{y60}$. The Wei, Gum and LNIII functions most of the time show very similar patterns, whereas the PEIII function does not. Overall one can see that throughout the window shift, the HQ_{100} values change a lot. Often not only once from blue to red but several times within the window shift (e.g. gauging site with the GRDC Nr. 6233700, 6233800 or 6335200 in Figure 3.4). Moreover, changes of more than three sd within a few years are also not unusual (e.g. gauging site with the GRDC Nr. 6731140, 6731260 or 6401601 in Figure 3.6).

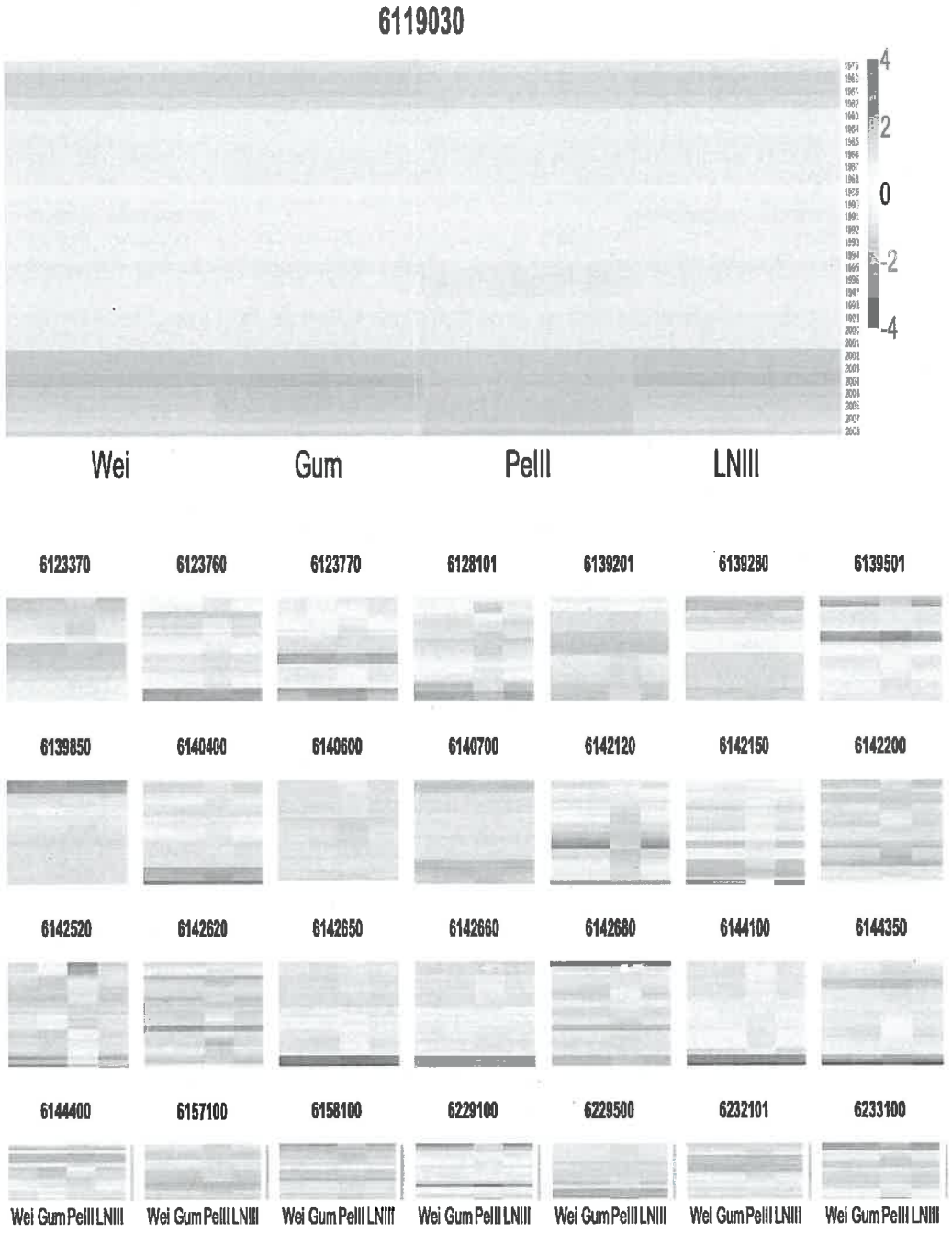

Figure 3.3 Shows the standardized return flood levels for all the 227 gauging sites of the $List_{y60}$. Each field represents a HQ_{100} return level for a 30 year time window starting with the window from the 01.01.1948 to 01.01.1978 for each gauging site. The GRDC Nr. is displayed as the header. The mean of each column has been taken and each deviation from it colored in either red (increasing - see the legend on the top right) or blue (decreasing). The legend ranges for all heat-maps from -4 to 4 standard deviations (sd). Wei, Gum, PeII and LNIII and stand for the Weibull, Gumbel, Pearson III and Log-Normal III distribution function. The smaller heat-maps have the same row and column names as the bigger upper one, however, due to reasons of representation, the row and column names have been deleted as well as the legend.

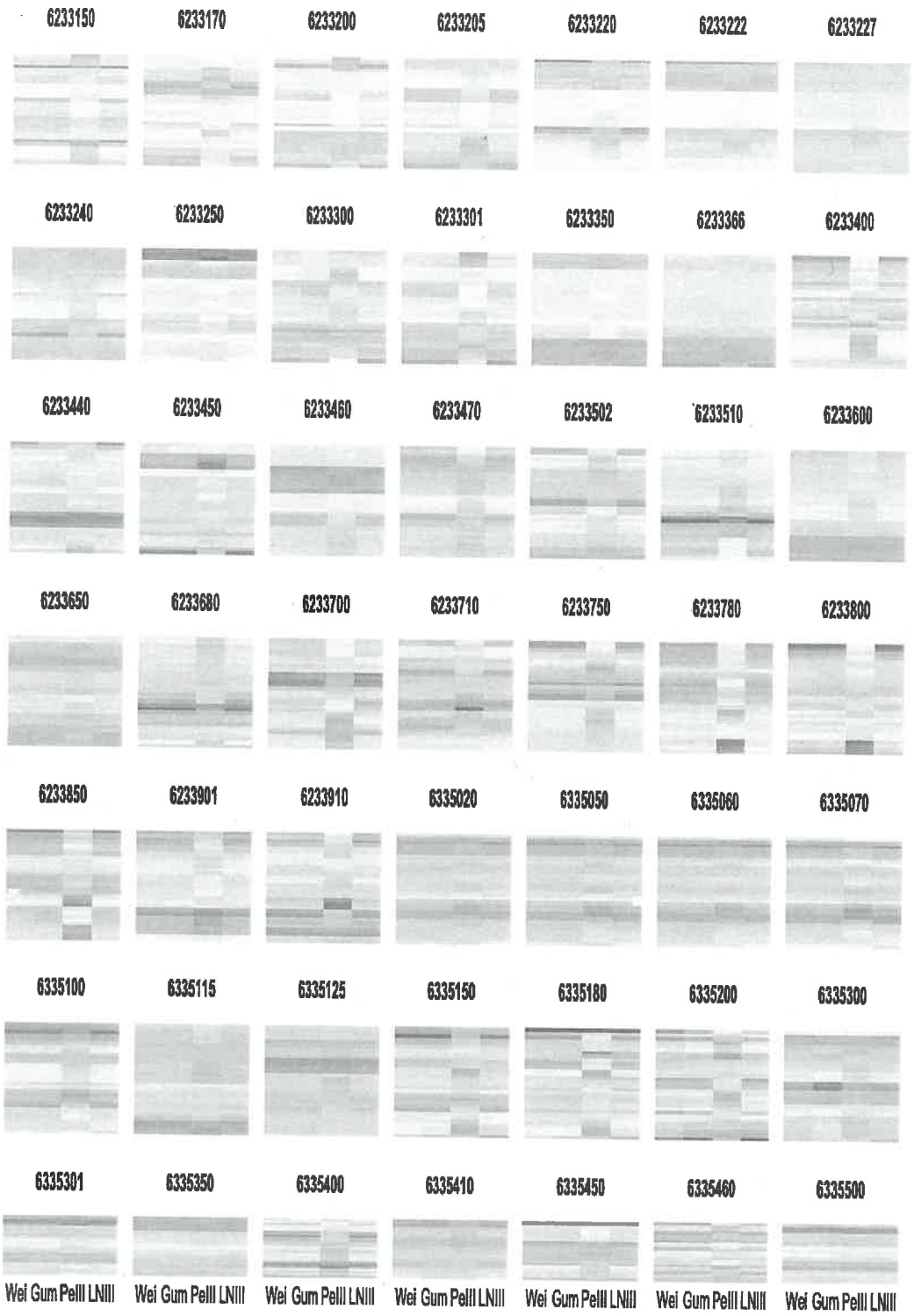

Figure 3.4 See Figure 3.3 and Section 2.2 for further details.

Figure 3.5 See Figure 3.3 and Section 2.2 for further details.

Figure 3.6 See Figure 3.3 and Section 2.2 for further details.

Figure 3.7 See Figure 3.3 and Section 2.2 for further details.

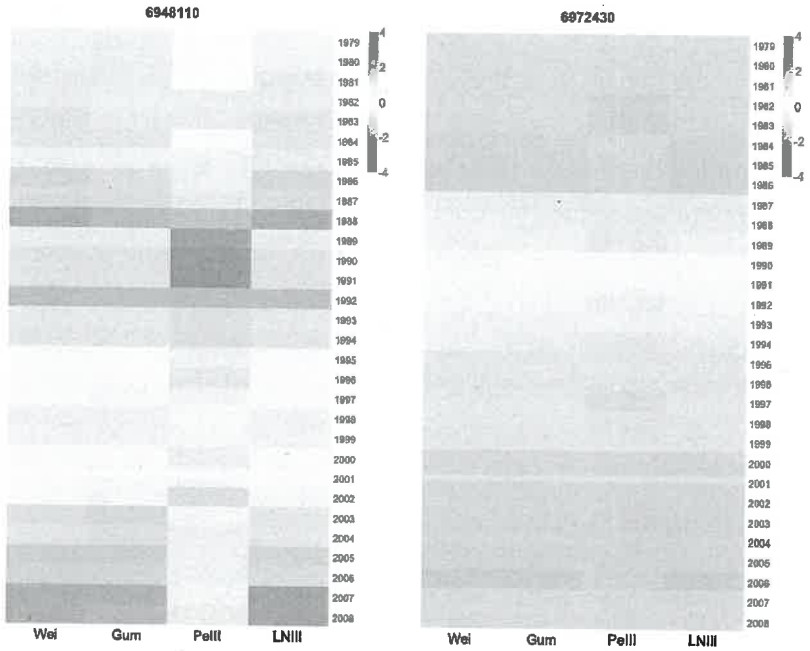

Figure 3.8 See Figure 3.3 and Section 2.2 for further details.

3.2.2 Overall Variability of the Window Shift

In this Subsection the overall deviation of the standardized HQ_{100} values with regards to the function used for all 227 gauging sites combined is shown. In Figure 3.10 one can see the overall spread of the flood return levels (HQ_{100}) in standard deviations (sd). As the standardized values have been used, it is not surprising that the mean as well as the median are located at around 0. The mean for all four functions is at 0 sd (around 10^{-16}), whereas the median for the Weibull distribution is -0.03 sd, for the Gumbel distribution it is -0.02 sd, for the Pearson III distribution it is -0.05 sd and for the Log-Normal III it is -0.03 sd. The first and third quartile for all four functions are very similar as well, between around -0.73 and 0.74 sd. So on average, 75% of the HQ_{100} values for all the 227 gauging sites combined lie within 1.47 sd, independent of the function being used.

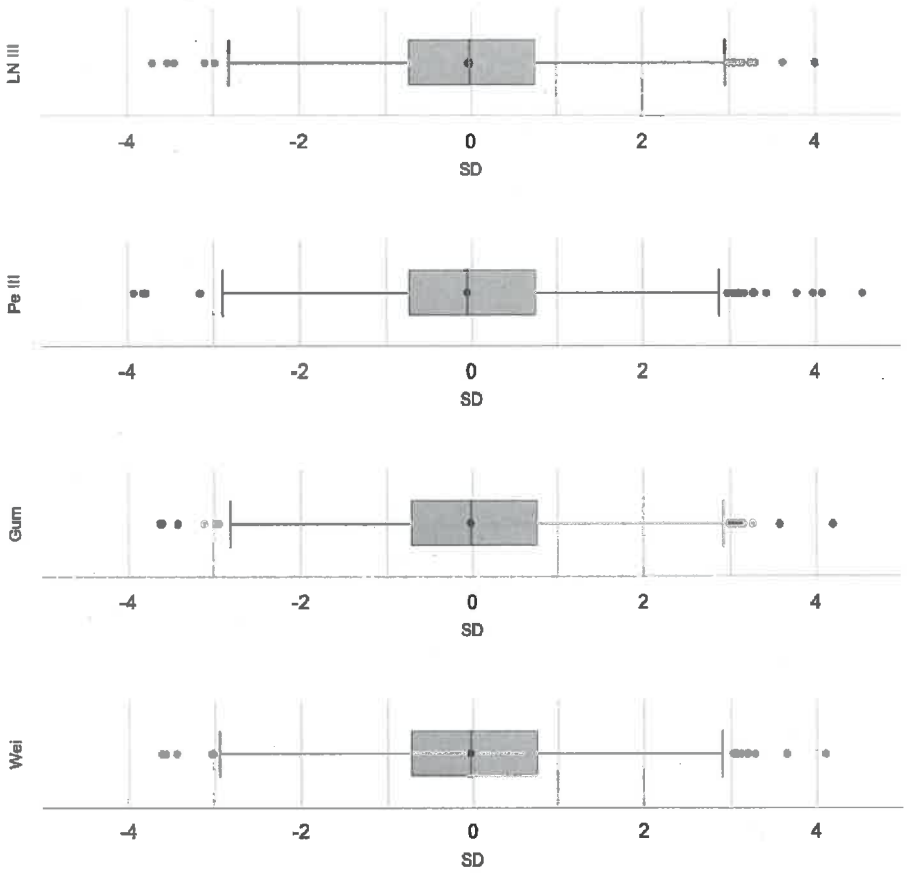

Figure 3.9 This box-whisker plot shows the spread of the standardized HQ_{100} values for all the 227 gauging sites. On the x-axis one can see the standard deviations and on the y-axis the function used for the HQ_{100} calculation.

3.2.3 Coefficient of Variation (CoV) Calculation Results

Figure 3.11 shows the CoV (For the exact calculation see at Subsection 2.2.2) for all the gauging stations for the four functions separately. It gives an overview of how the values can differ for each stations' HQ_{100} values and each function. Some sites have very extreme CoV values, whereas others show almost no spread. The median ranges from 5.23% for the Gumbel distribution, to 6.70% for the Pearson III function (The Weibull distribution has a median of 5.31% and the Log-Normal distribution of 6.01%). The Inter Quartile Range (IQR) of the CoV for the Weibull and Gumbel is between 3.8% and 8%, the Pearson III has a IQR between 4.8% and 10.9% CoV and the Log-Normal III distribution one between 4% and 9.8%. Figure 3.10 shows the range of the CoV for all the 227 stations combined for each of the four functions separately. One can see that the Pearson III distribution has the highest variability of the CoV values, whereas the Gumbel and Weibull function give similar results.

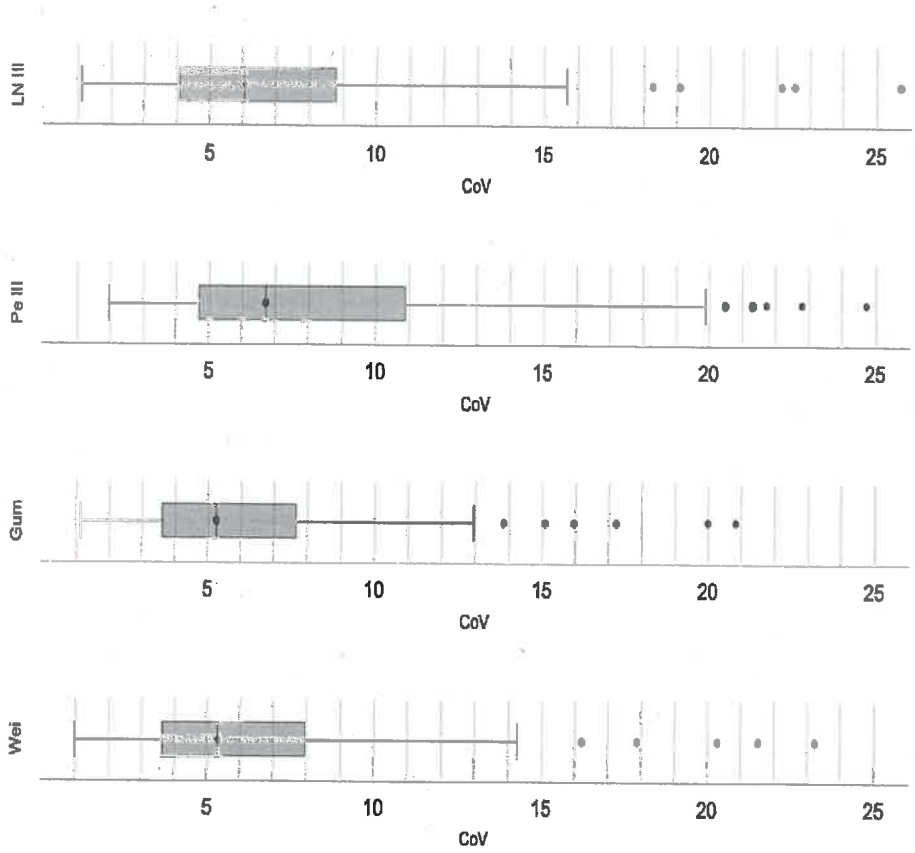

Figure 3.10 This box-whisker plot shows the overall Coefficient of Variation (CoV) for the Weibull (Wei), Gumbel (Gum), Pearson III (PeIII) and Log-Normal III (LNIII) distribution function for all 227 rivers combined. The point within the first and third quartile is the median. The CoV values on the x-axis are percentages.

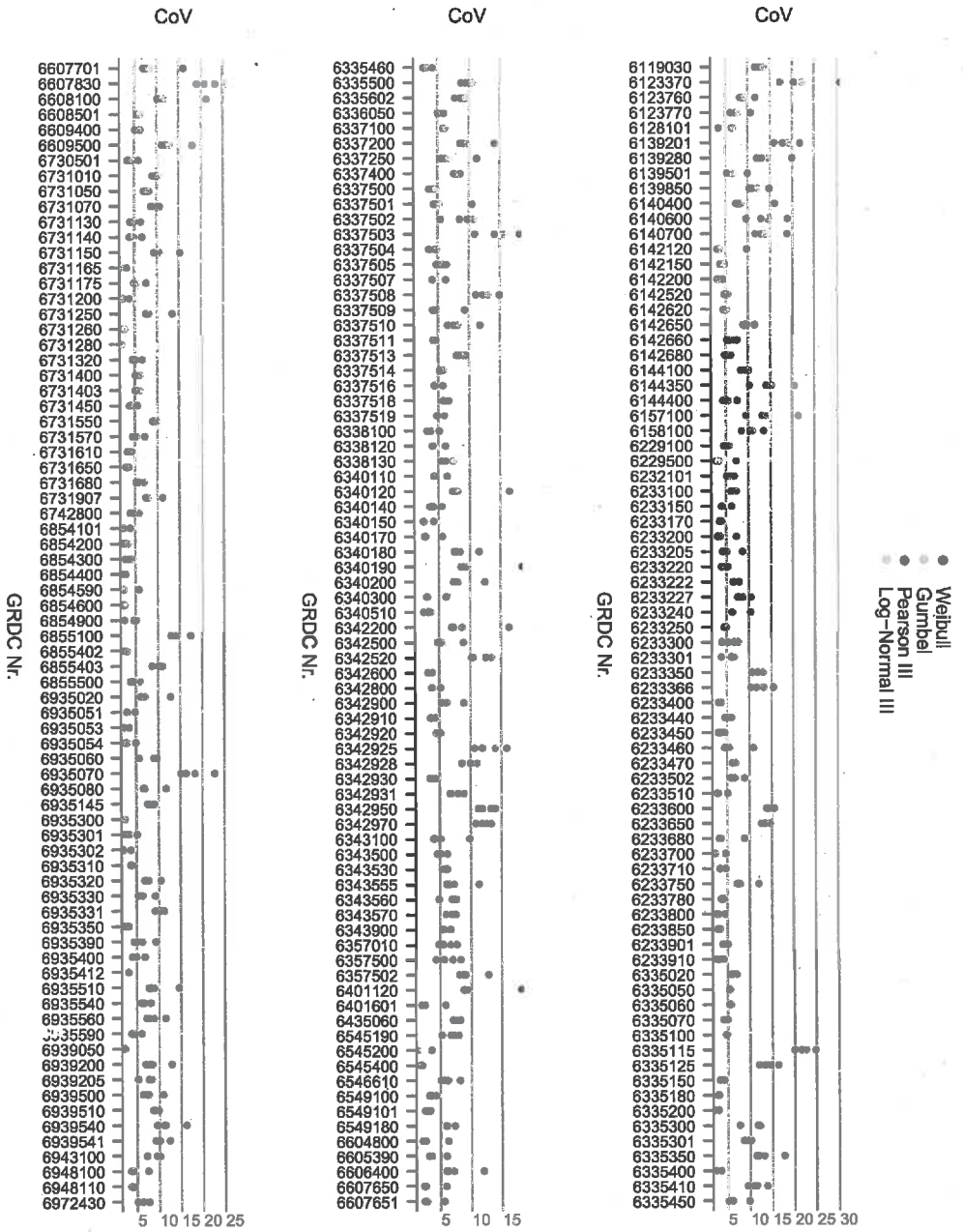

Figure 3.11 Shows the CoV values (Percentage on the y-axis) for each gauging station (GRDC Nr. on the x-axis) for all four functions separately.

3.2.4 Inter Quartile Range (IQR)

As described in Subsection 3.2.3, this has also been done for the IQR, but for the standardized discharge, so the values stand for standard deviations (sd). The IQR median for the Weibull distribution is 1.44 sd, for the Gumbel distribution it is 1.42 sd, for the Pearson III it is 1.44 sd and for the Log-Normal distribution it is 1.42 sd (See Figure 3.12). In Figure 3.13, one can see the IQR for each gauging site separately. Some sites have very extreme IQR values, whereas others show almost no spread. Overall, one can see that the first and third quartile range of the Pearson III distribution function has the highest spread, whereas the Log-Normal III function has the lowest. Moreover, the upper limit for all functions are very similar, so there is almost no gauging site with an IQR with more than 2 sd.

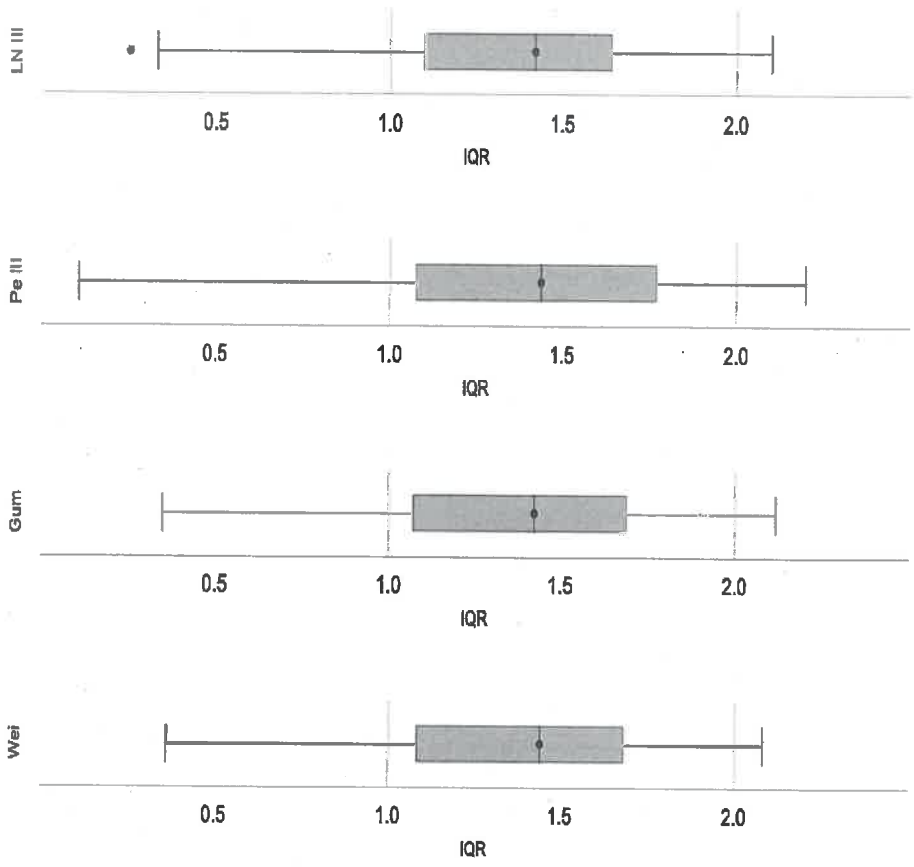

Figure 3.12 This box-whisker plot shows the overall Inter Quartile Range (IQR) values for the for the Weibull (Wei), Gumbel (Gum), Pearson III (PeIII) and Log-Normal III (LNIII) distribution function for all 227 rivers combined. The point within the first and third quartile is the median. The IQR values are standard deviations.

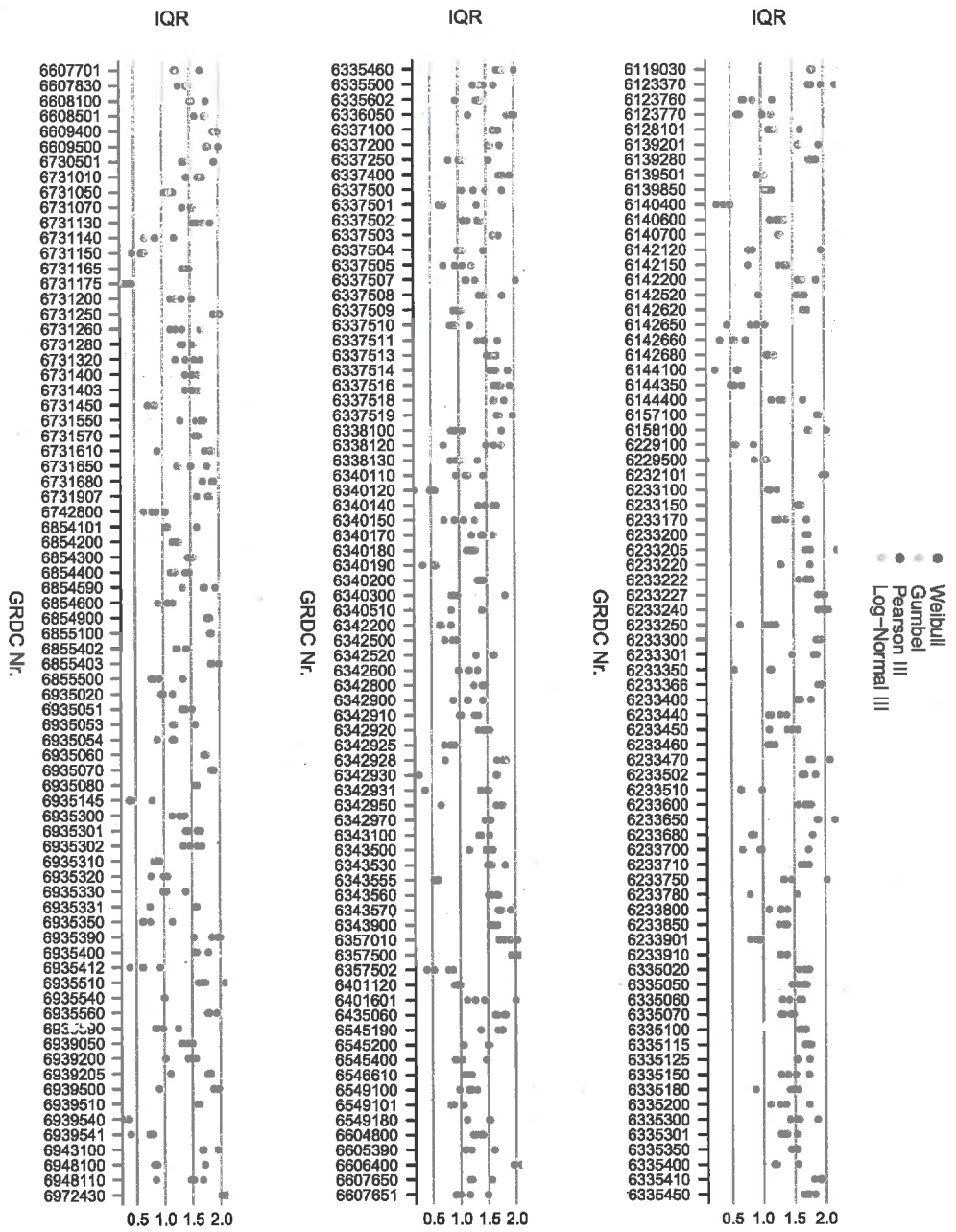

Figure 3.13 Shows the IQR values (standard deviation on the y-axis) for each gauging station (GRDC Nr. on the x-axis) separately for all four functions.

3.2.5 Median Absolute Deviation (MAD)

The same as described in Subsection 3.2.4 has been done for the MAD, so the values stand for standard deviations (sd). The MAD median for the Weibull distribution is 0.95·sd, for the Gumbel distribution it is 0.95, for the Pearson III it is 0.91 and for the Log-Normal distribution it is 0.96. This means that the median deviation of the median flood return level for all four functions is more than 0.91 sd (3.14). In Figure 3.15, one can see the MAD for each gauging site separately. Some sites have very extreme MAD values, whereas others show almost no spread. Overall, the Pearson III distribution function shows again the highest spread between the first and third quartile, however, all the functions give similar results. The Gumbel and Weibull distributions' MAD are almost identical, whereas the Log-Normal III function shows the smallest spread between the first and third quartile.

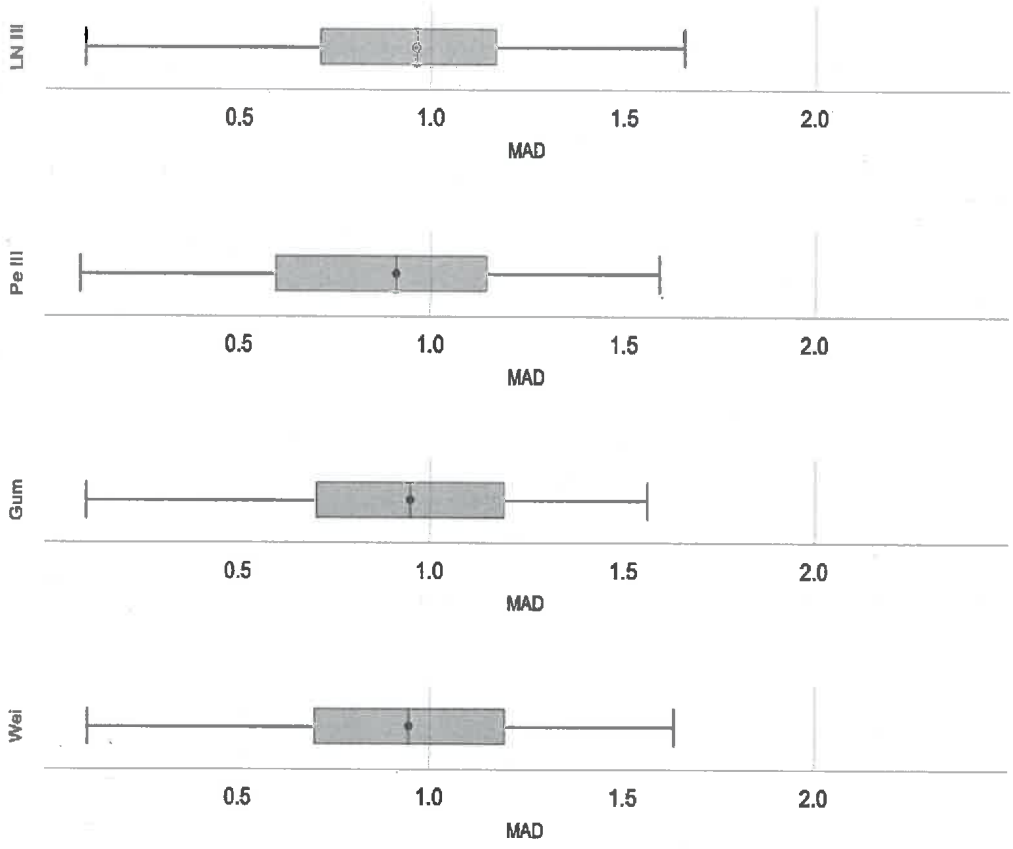

Figure 3.14 This box-whisker plot shows the Median Absolute Deviation (MAD) values for the Weibull (Wei), Gumbel (Gum), Pearson III (PeIII) and Log-Normal III (LNIII) distribution function for all 227 rivers combined. The point within the first and third quartile is the median. The MAD values are standard deviations.

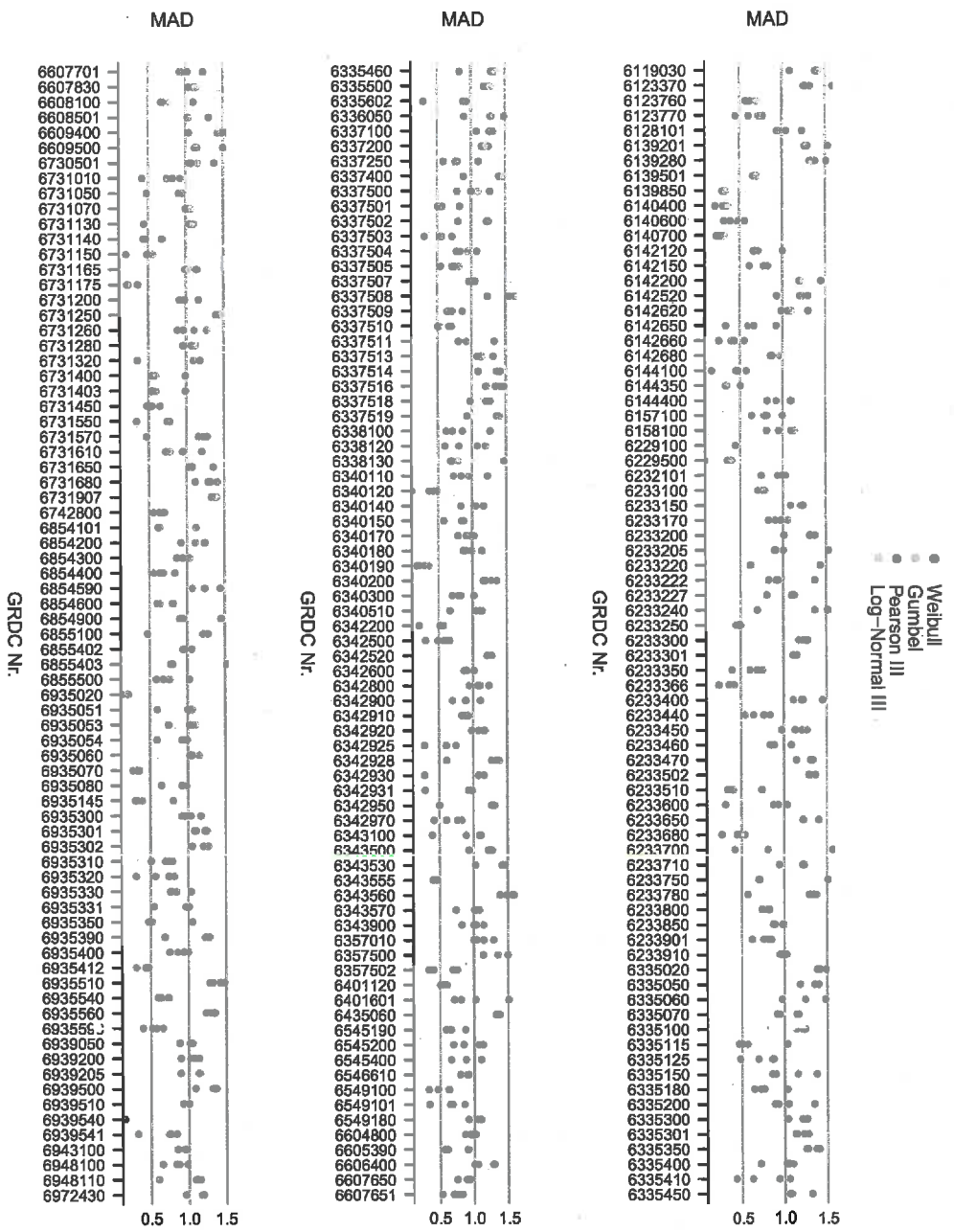

Figure 3.15 Shows the MAD values (standard deviation on the y-axis) for each gauging station (GRDC Nr. on the x-axis) separately for all four functions.

3.2.6 Correlation Calculation for the Gauging Sites

As shown in Subsection 3.2, some heat-maps show similar patterns regarding their increase or decrease throughout the time window shifts. These similar patterns were tried to be extracted via a correlation matrix (For the exact procedure see Section 2.2.1). Each gauging sites' HQ_{100} list of flood return levels calculated with the Weibull distribution function was compared with each other - Positive correlations were colored in blue whereas negative ones were colored in red. As one can see in the overall correlation matrix in Figure 3.16, each of the regions is surrounded by a black rectangle. However, as the first overall plot was too big in order to let the GRDC Nr. for all gauging sites be displayed properly (See Figure 3.16), each of the six regions was plotted separately in order to identify them properly in Figure 3.17, Figure 3.18, Figure 3.19, Figure 3.20, Figure 3.21 and Figure 3.22. In Figure 3.23 the standardized values of each gauging site within one of the 6 regions have been plotted separately in order to identify certain tendencies regarding their HQ_{100} values and find geographic similarities. The x-axis stands for the year when the calculation shift starts. So the first value on the x-axis is named 1948, which stands for the HQ_{100} value for the time window between the 01.01.1948 and 01.01.1978. The next year is 1949, which stands for the HQ_{100} value for the time window between 01.01.1949 and the 01.01.1979 and so on. Afterwards a linear regression and its R^2 value in black and a LOESS function in orange have been calculated and plotted. The blue cloud shows the HQ_{100} values density - the darker the cloud, the more HQ_{100} values are there. The LOESS function represents the "behaviour" of the Regions better than the regression line. Region one tends to higher HQ_{100} values, Region 2 to lower HQ_{100} values, the HQ_{100} values in Region 3 tend to increase slightly and then decrease, the HQ_{100} values in Region 4 decrease in the beginning and the increase whereas Region 5 decreases for more HQ_{100} values and then increases again and the HQ_{100} values for Region 6 stays quite stable and then increases. Region one has the highest gauging sites number, however, region two has the highest R^2 value with 0.629. It is important to note, that all Regions have gauging sites, which do not follow the overall tendency and sometimes even have a negative correlation. Figure 3.24 shows the spatial distribution of these six Regions. They are colored according to the Region Names underlying color in the density plots. As mentioned above, Region two has the highest R^2 value, however, as one can see in Figure 3.24, the gauging sites are spread throughout Europe.

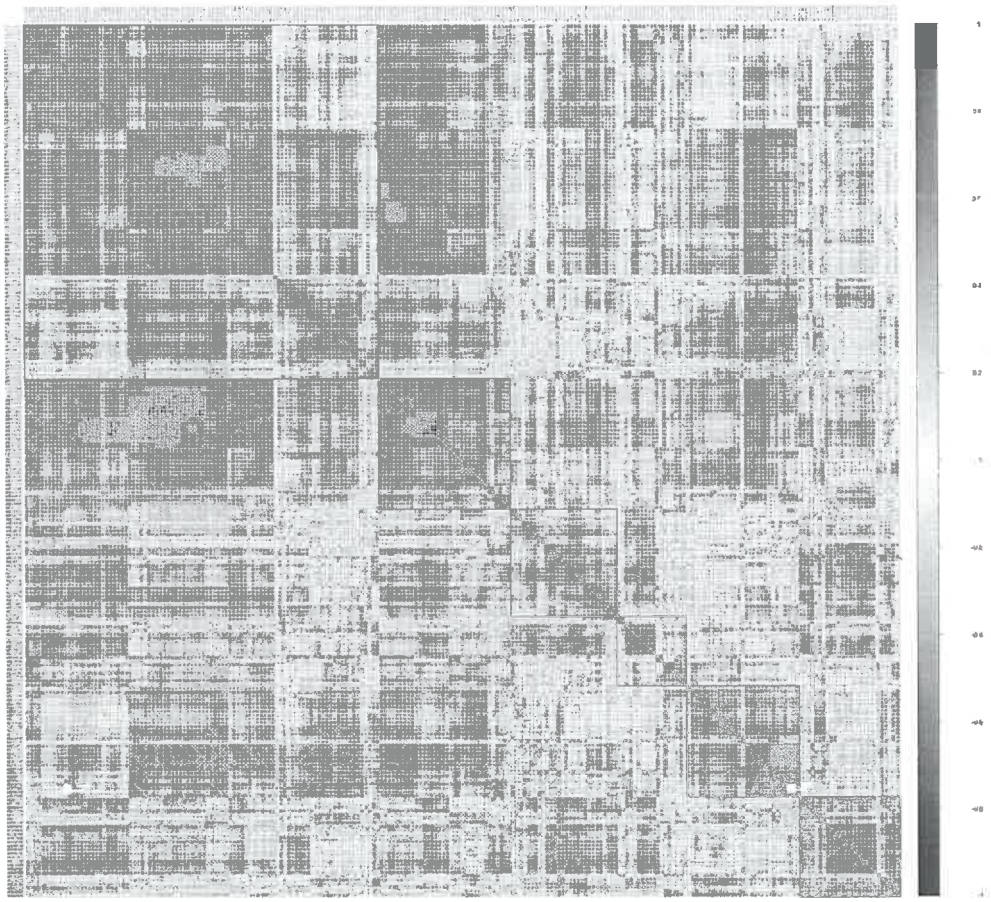

Figure 3.16 Shows all the 227 gauging sites of the $List_{y60}$. Each sites' HQ_{100} values are compared with every other station and grouped together (See Subsection 2.2.1 for the calculation details). The colored dots show if one river has a high or low positive (blue) or negative (red) correlation with this rivers' HQ_{100} values - the correlation scale is located on the right side. The six regions are surrounded with black rectangles and plotted separately in the following plots in order to have a better view on the GRDC Nrs. on the y-axis and upper x-axis in red.

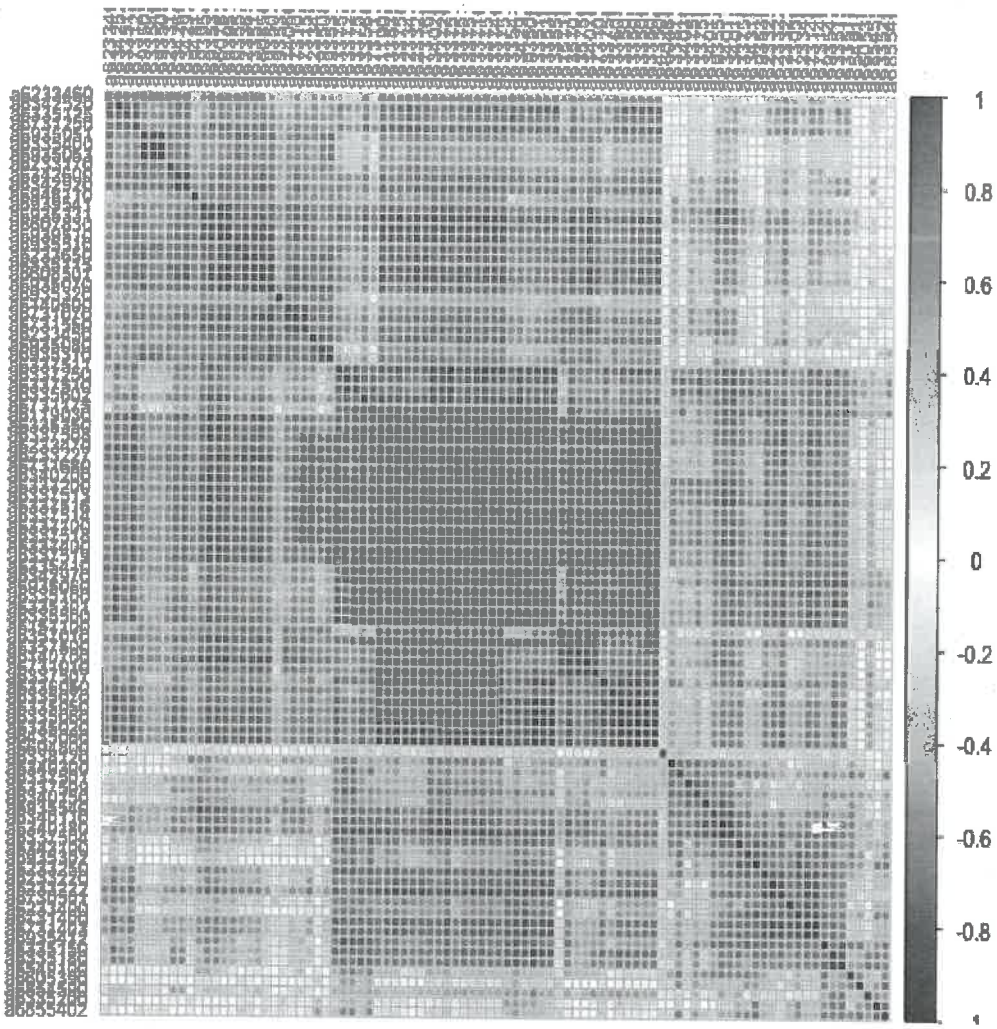

Figure 3.17 Shows the correlations of **region one** as described in Figure 3.16 and Subsection 2.2.1. The GRDC Nrs. are plotted on the x-, and y-axis. The colored dots show if one river has a high or low potive (blue) or negative (red) correlation with this rivers HQ_{100} values - the correlation scale is located on the right site.

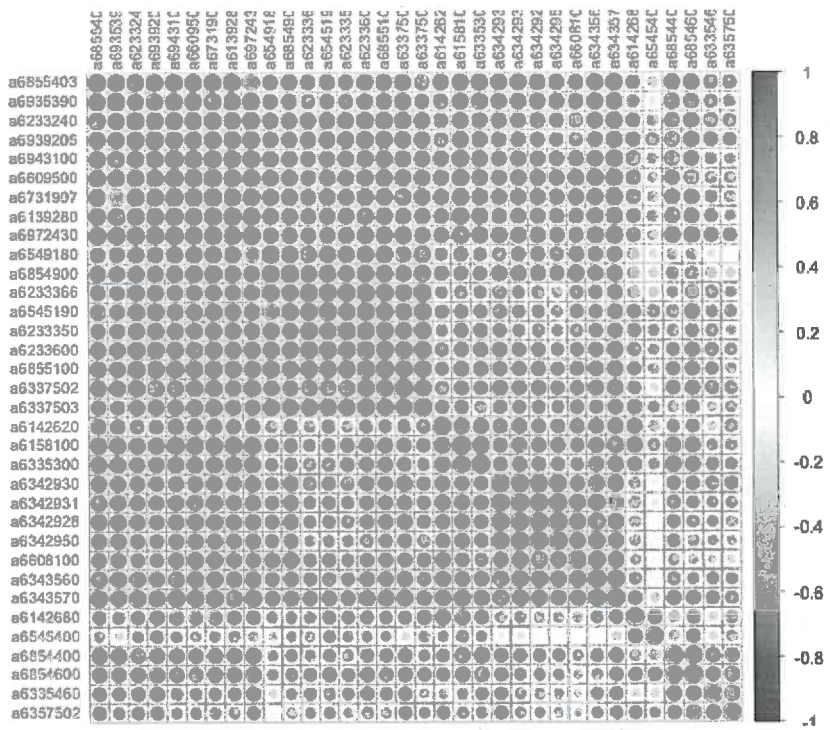

Figure 3.18 Shows the correlations of **region two** as described in Figure 3.17 and Subsection 2.2.1.

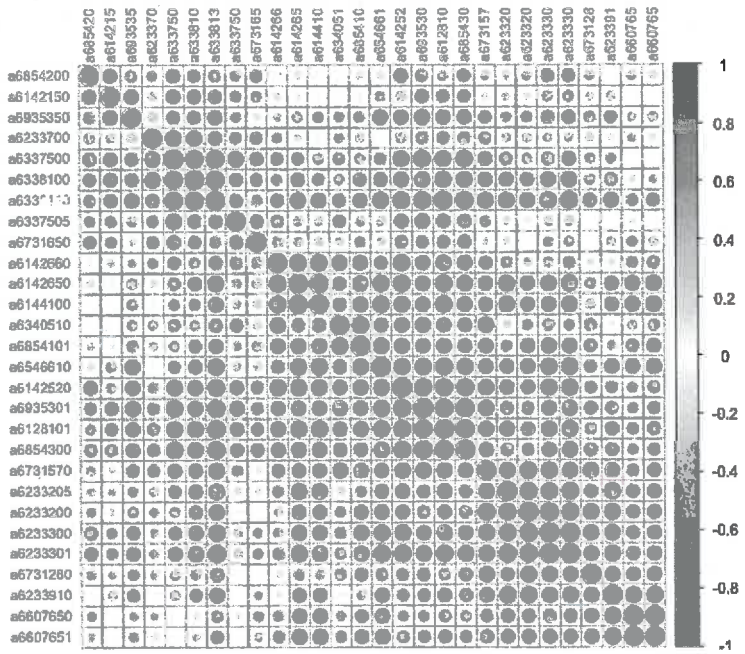

Figure 3.19 Shows the correlations of **region three** as described in Figure 3.17 and Subsection 2.2.1.

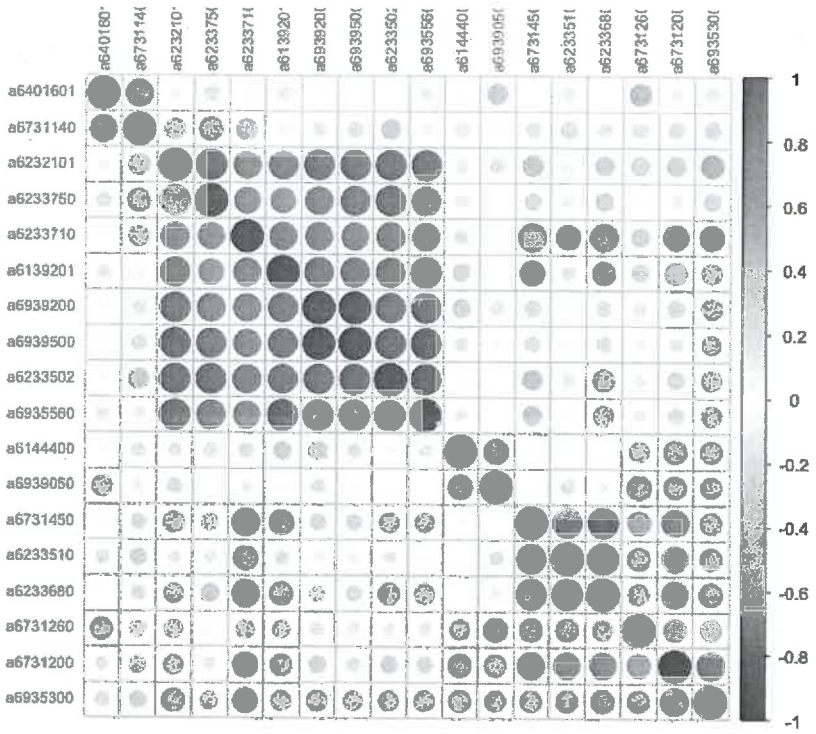

Figure 3.20 Shows the correlations of **region four** as described in Figure 3.17 and Subsection 2.2.1.

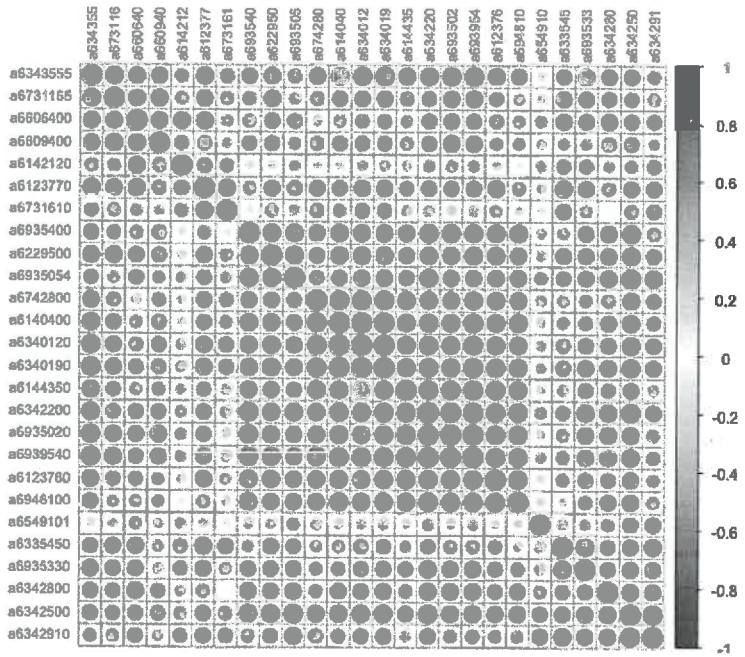

Figure 3.21 Shows the correlations of **region five** as described in Figure 3.17 and Subsection 2.2.1.

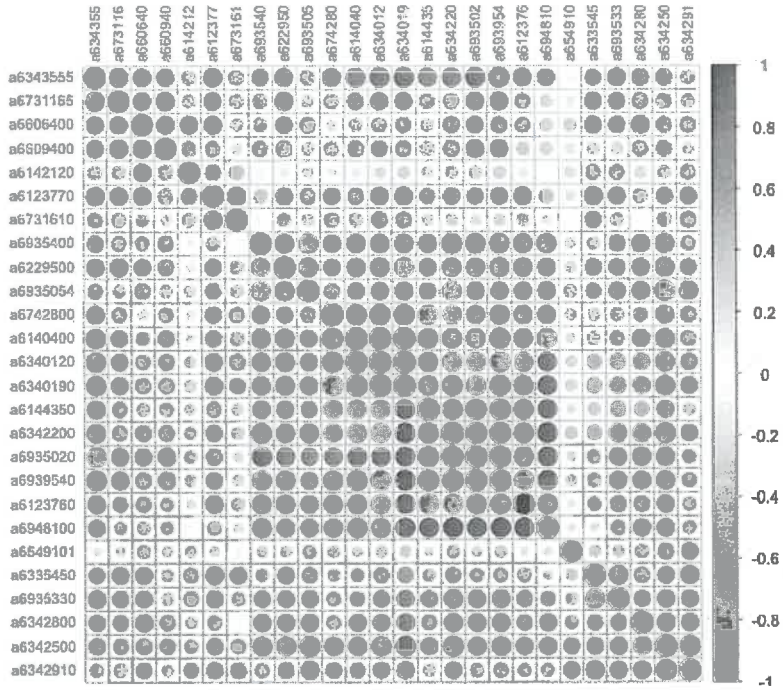

Figure 3.22 Shows the correlations of **region six** as described in Figure 3.17 and Subsection 2.2.1.

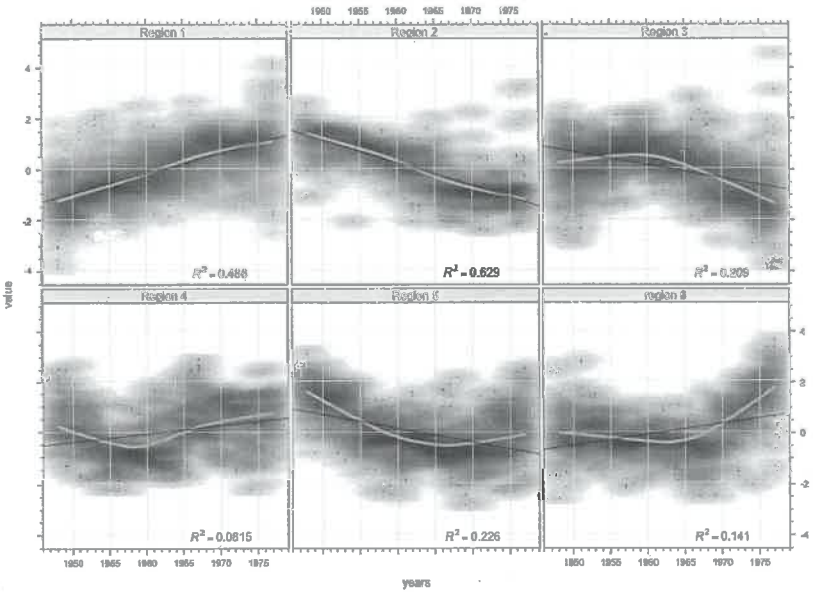

Figure 3.23 Shows the tendency of the HQ_{100} values over time for all six regions. The R^2 values for the black linear regression line are shown as well as the LOESS line in orange. The y-axis shows the standardized HQ_{100} values whereas the y-axis shows the first year of the 30 year-long window for the HQ_{100} calculation, starting with 1948 (See Subsection 3.2.6 for more details). The blue cloud shows the densities of the values - the darker, the more HQ_{100} values and the more weight on the LOESS function.

Figure 3.24 Shows the spatial distribution of all six regions according to the color scale underlying the region names in the tendency of the HQ_{100} values over time on the lower left side. For the explanation of the tendency plot see Figure 3.23 above and the text in Subsection 3.2.6.

3.3 Window Shift Results for the 100 Year-Long Gauging Sites

The same procedure as for the 60 year-long gauging sites calculations in section 2.2 has been done for the 100 year-long gauging sites. The difference, however, was the length of the time series from which the annual maxima have been extracted and the length of the time window for the flood return level. In this section the gauging sites were 100 years long and three different time windows of 30, 40 and 50 years were applied. The spatial distribution can be seen in Section 3.1.

3.3.1 Graphical Results for the 30 Year-Long Window Shift

As described in Section 2.2, the shift of the 30 year window return levels have been put in a matrix, standardized and colored according to the standard deviation (sd) ranging from blue to red - the darker the color, the more it diverges from the mean ($\mu = 0$). The color scale for all the heat-maps is displayed in Figure 3.25 on the upper right side, next to the big heat-plot. The range was set to between -3 and 3 in order to be comparable with the other two time windows (40 and 50 year-long ones). The same has been done for the 40 year window shift as well as the 50 year window shift. In Figure 3.25 and 3.26 one can see the results for the individual spread for the 30 year-long window shift for the gauging sites in the $\text{List}_{\mathbf{y100}}$, which can be seen in Table

Overall one can see that throughout the window shift for the 100 year-long gauging sites, the HQ_{100} values change a lot and more often from blue to red than the HQ_{100} values in the 60 year-long gauging sites list. 70 HQ_{100} values have been calculated.

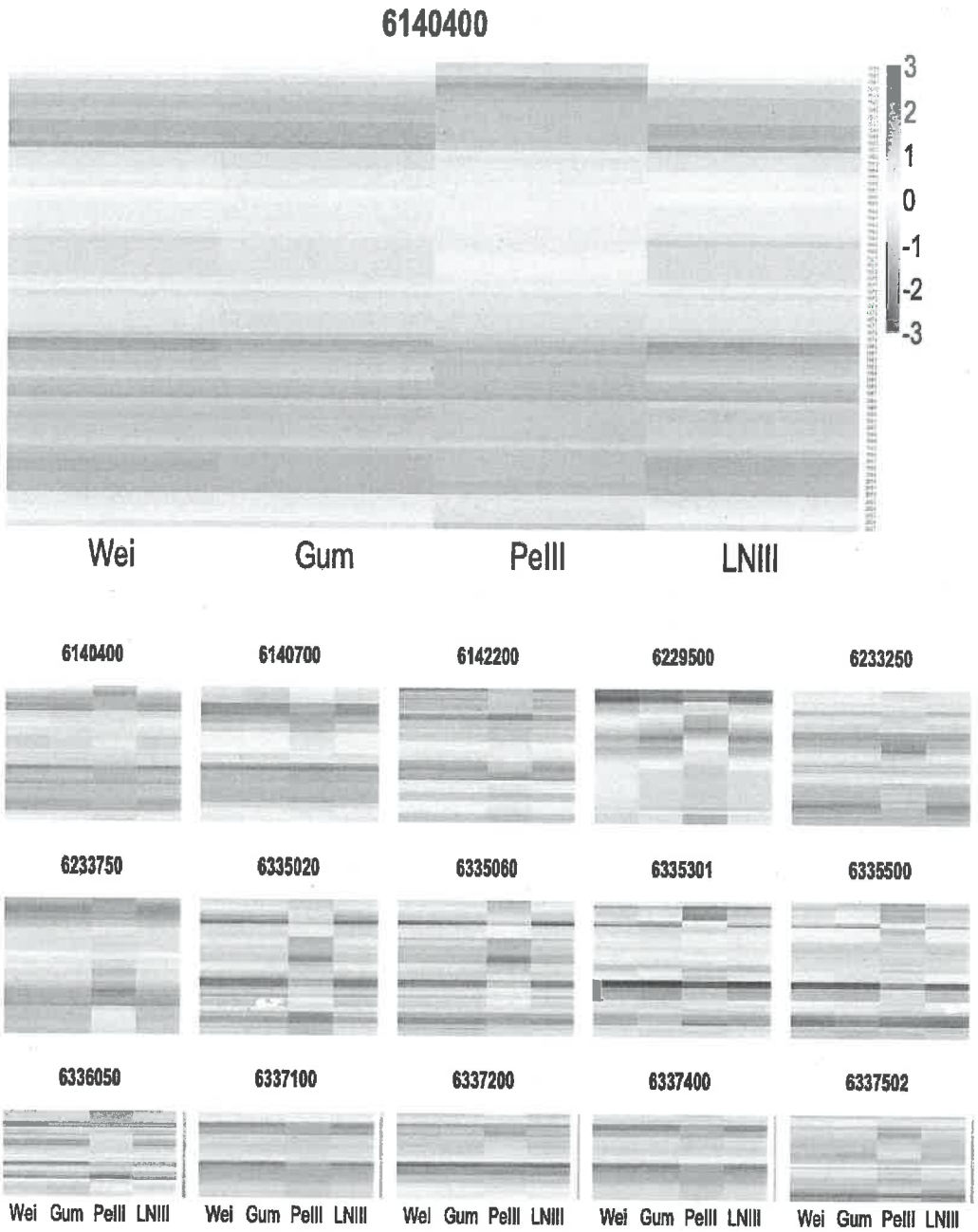

Figure 3.25 Shows the standardized return values for all the 45 gauging sites of the $List_{y100}$. Each field represents a HQ_{100} return level value for a 30 year-long time window starting with the window from the 01.01.1908 to 01.01.1938 for each gauging site. The representing GRDC Nr. is listed as the header. The mean of each column has been taken and each deviation from it colored in either red (positive values - as shown in the legend on the top right) or blue (minus values) - see Subsection 2.2 for more details.

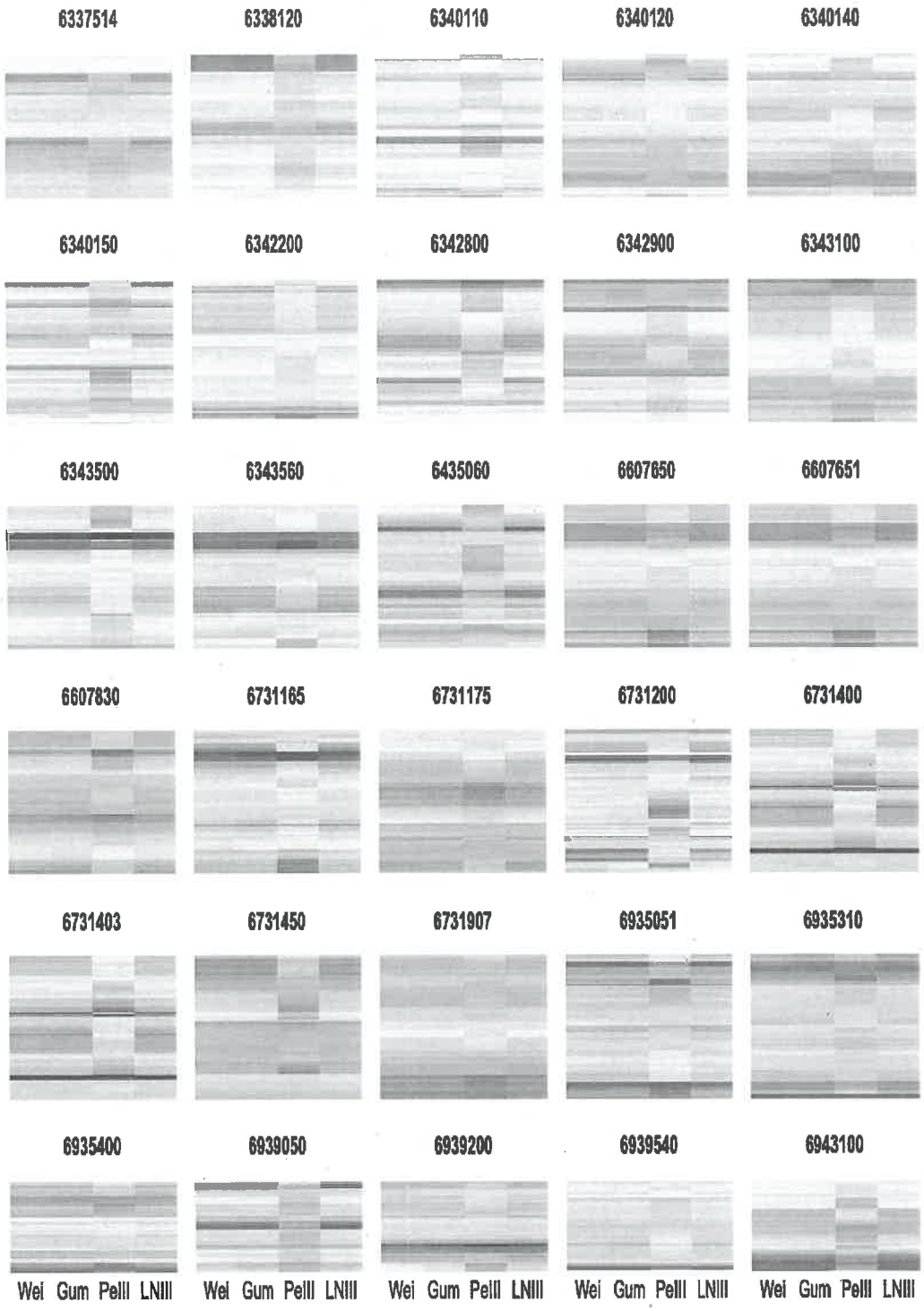

Figure 3.26 See Figure 3.25 for further details.

3.3.2 Graphical Results for the 40 Year-Long Window Shift

The individual gauging sites' HQ_{100} values spread for the 40 year-long window shift can be seen in Figure 3.27 and Figure 3.28. For the detailed description of the heat-maps see subsection 3.3.1. The scale is between -3 and 3 standard deviations as the heat-maps for the 30 year-long time window, which can be seen in the previous subsection 3.3.1. The HQ_{100} values differ for the individual gauging sites from minus values to plus values very often and this change can happen within only a few years. Nevertheless, as they use a longer time window for the HQ_{100} calculation, they tend to have a smoother change between the blue and red "phase" than the 30 year-long window shift in the previous subsection 3.3.1. 60 HQ_{100} values have been calculated.

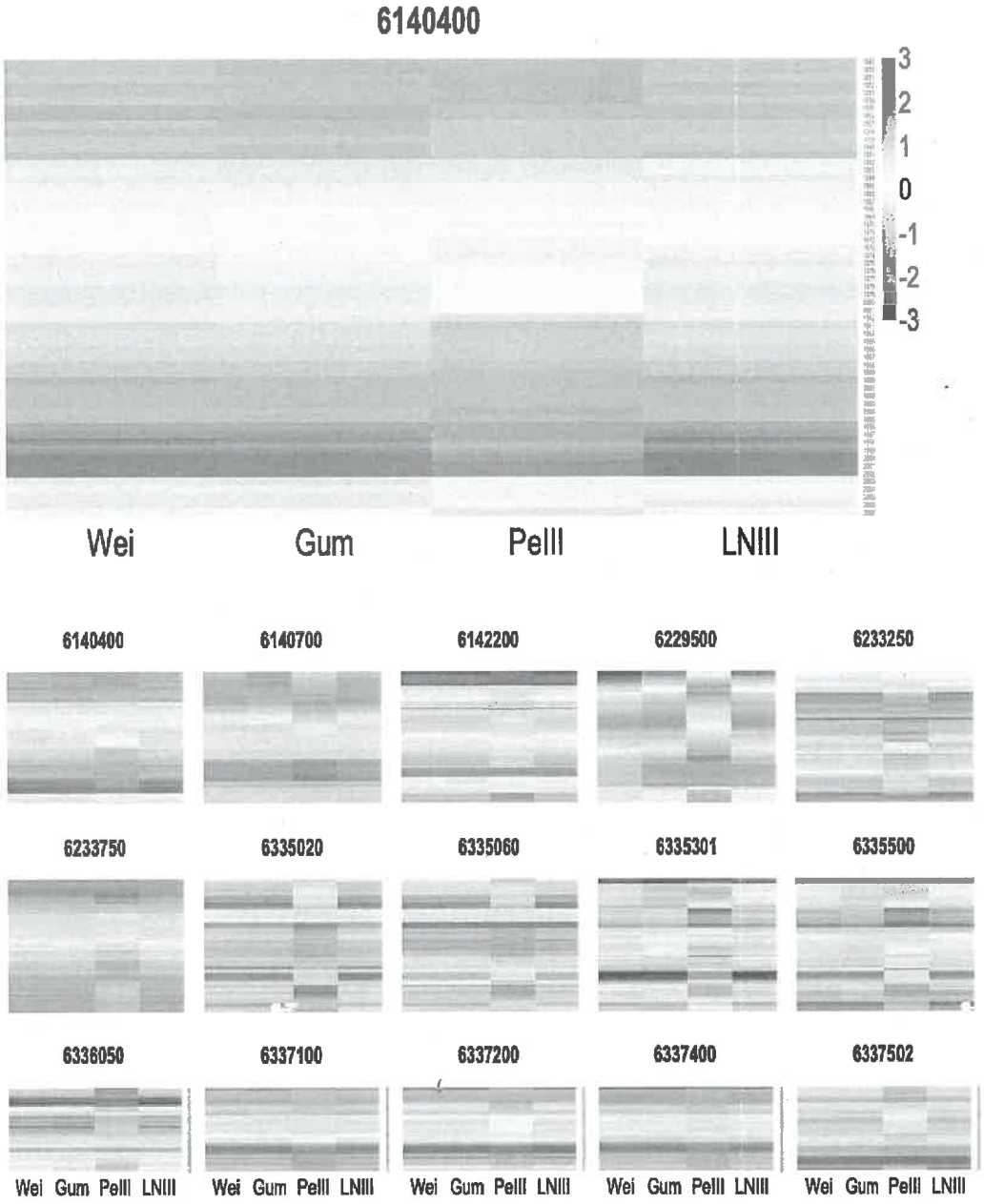

Figure 3.27 Shows the standardized return values for all the 45 gauging sites of the $List_{y100}$. Each field represents a HQ_{100} return level for a 40 year time window starting with the window from the 01.01.1908 to 01.01.1948 for each gauging site. The representing GRDC Nr. is listed as the header. The mean of each column has been taken and each deviation from it colored in either red (positive values - as shown in the legend on the top right) or blue (minus values) - see Subsection 2.2 for more details.

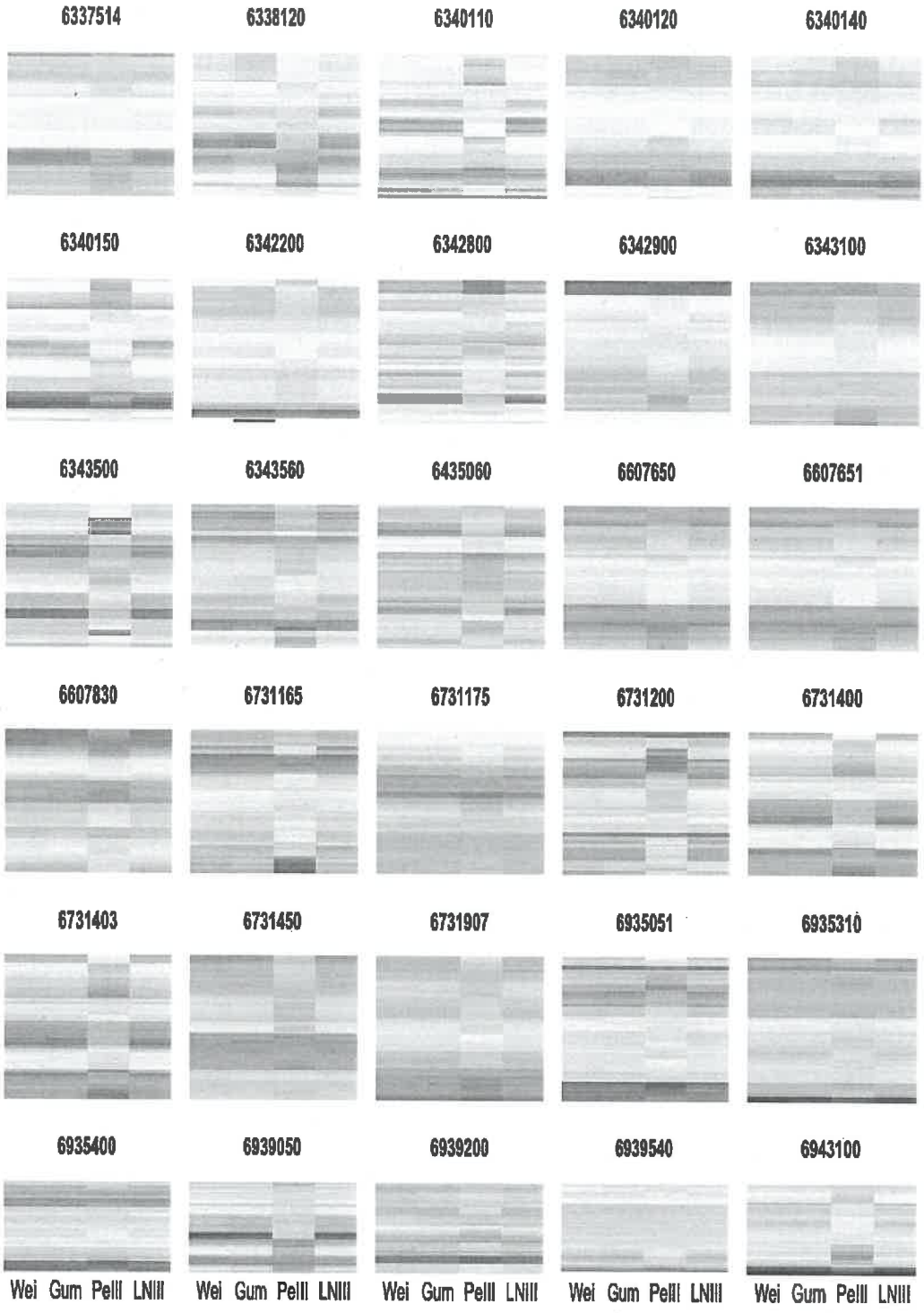

Figure 3.28 See Figure 3.27 for further details.

3.3.3 Graphical Results for the 50 Year-Long Window Shift

3.29 and 3.30 The individual gauging sites' HQ_{100} values spread for the 50 year-long window shift can be seen in Figure 3.29 and Figure 3.30. For the detailed description of the heat-maps see subsection 3.3.1. They have the same scale between -3 and 3 standard deviations as the heat-maps for the 30 and 40 year-long time window, which can be seen in subsection 3.3.1. The HQ_{100} values differ for the individual gauging sites a lot and can change within a few years from minus to plus values. Nevertheless, as they use a longer time window for the HQ_{100} calculation, they tend to have an even smoother change between the blue and red "phase" than the 40 and 30 year-long window shift in the previous subsections 3.3.1 and 3.3.2. 50 HQ_{100} values have been calculated.

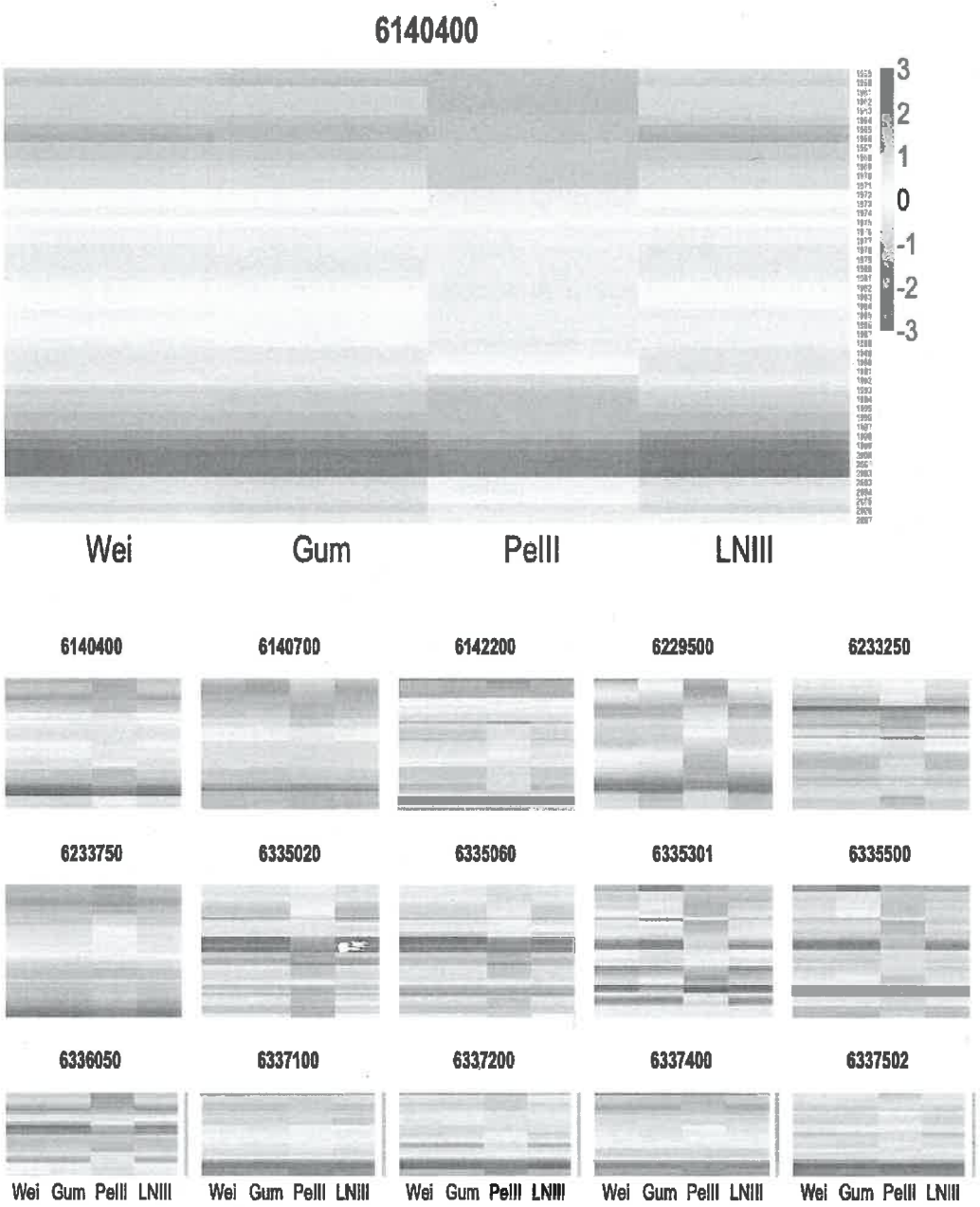

Figure 3.29 Shows the standardized return values for all the 45 gauging sites of the $List_{y100}$. Each field represents a HQ_{100} return level for a 50 year time window starting with the window from the 01.01.1908 to 01.01.1958 for each gauging site. The representing GRDC Nr. is listed as the header. The mean of each column has been taken and each deviation from it colored in either red (positive values - as shown in the legend on the top right) or blue (minus values) - see Subsection 2.2 for more details.

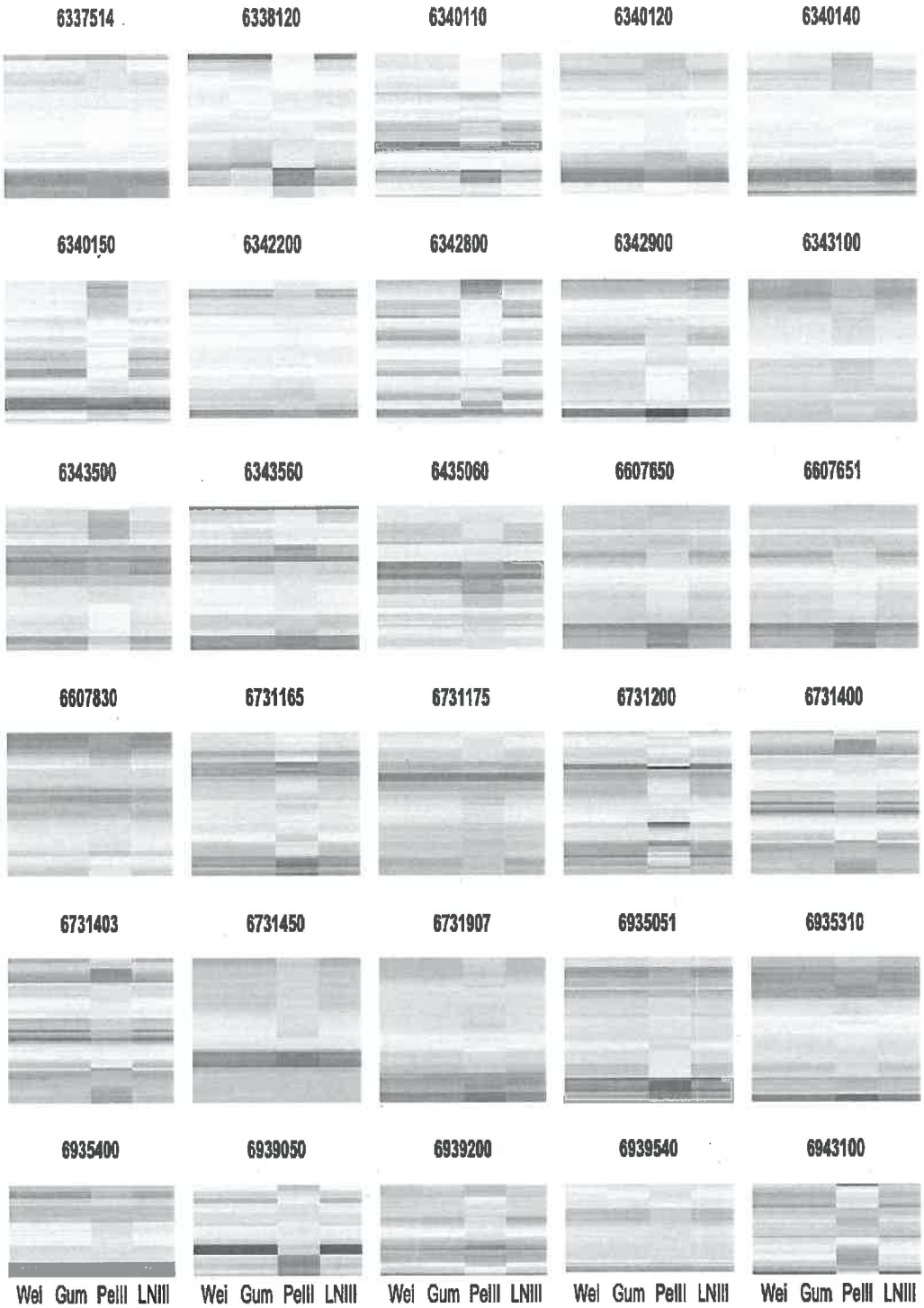

Figure 3.30 See Figure 3.29 for further details.

3.3.4 Comparison of the Overall Spread of the 30, 40 and 50 Year-Long Window Shift

In this section, the standardized 30, 40 and 50 year-long windows are compared with regards to the function used. As the standardized flood return levels were used, the mean for all three different window lengths for all functions are the same at around 0. Moreover, the median does not differ from 0 too much either as visible in Figure 3.31, Figure 3.32, Figure 3.33 and Figure 3.34. Nevertheless, there is a clear tendency, that with a longer time window length, independent of which function has been used, the overall spread does decrease. The first quartile for all the functions for the 30 year-long window shift is between -0.93 and -0.98 standard deviations (sd) and for the third quartile between 0.93 and 0.95 sd (See Table 3.4). This means that on average, the return levels spreads almost 2 sd between the first and the third quartile for the 30 year-long window shift. As for the 40 year-long window shift, this spread decreases to between -0.72 and -0.80 sd for the first quartile and 0.71 and 0.74 sd for the third quartile. The 50 year-long window shifts spread lays for the first quartile between -0.47 and 0.49 sd and between 0.51 and 0.53 sd for the third quartile. So the spread decreases from almost 2 sd for the 30 year window shift to 1 sd for the 50 year-long window shift. When looking at the difference of the spread between the four different, one can see that the functions do not influence the spread too much. They are all at around the same level (See Table 3.4), nevertheless, the Pearson III distribution function (df) shows the biggest spread for the 30 year-long window with 1.936 sd, whereas the Log-Normal III df has the smallest spread with 1.878 sd. As for the 40 year-long window shift, the Pearson III df shows the biggest spread with 1.770 sd and the Weibull df shows the smallest spread with 1.44 sd. The biggest spread for the 50 year-long window shift shows the Gumbel df with 1.027 sd and the Log-Normal III df has the smallest spread of 0.988 sd.

Distribution	Window length	first Quartile	Median	third Quartile
	[Years]	[SD]	[SD]	[SD]
Weibull	30	-0.933	-0.032	0.949
	40	-0.721	0.067	0.719
	50	-0.492	0.022	0.529
Gumbel	30	-0.950	-0.031	0.939
	40	-0.722	0.069	0.743
	50	-0.488	0.023	0.539
Pearson III	30	-0.984	0.02	0.952
	40	-0.802	0.108	0.748
	50	-0.474	0.049	0.514
Log-Normal III	30	-0.939	-0.055	0.939
	40	-0.73	0.059	0.718
	50	-0.482	0.025	0.523

Table 3.1 Shows the results for the overall spread in standard deviations for all four functions with respect to the length of the time window applied to the 100 year-long gauging sites time series.

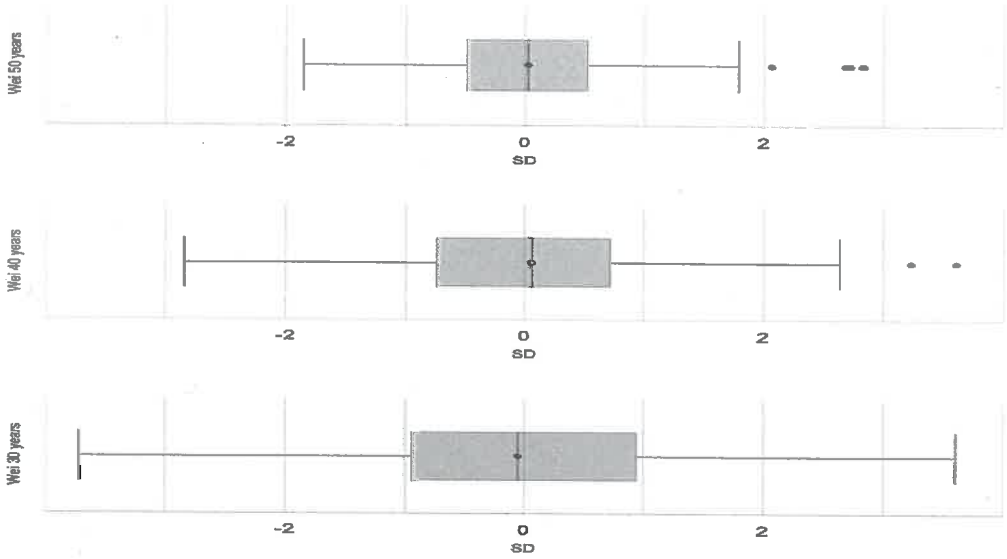

Figure 3.31 Shows the overall HQ_{100} value spread for the Weibull function, with respect to the window length used. On the x-axis the standard deviation (sd) is plotted.

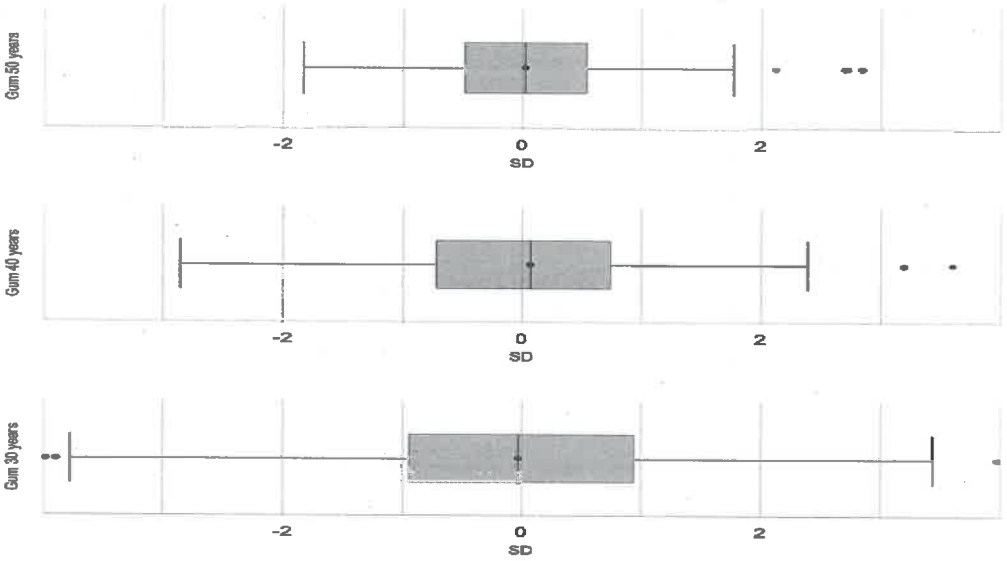

Figure 3.32 Shows the overall HQ_{100} value spread for the Gumbel function, with respect to the window length used. On the x-axis the standard deviation (sd) is plotted.

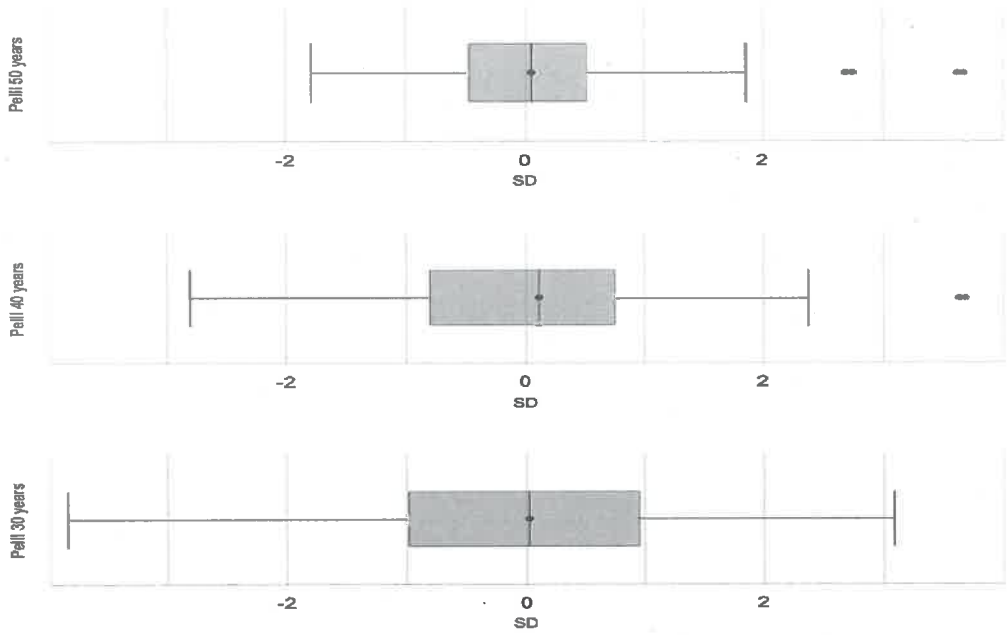

Figure 3.33 Shows the overall HQ_{100} value spread for the Pearson III function, with respect to the window length used. On the x-axis the standard deviation (sd) is plotted.

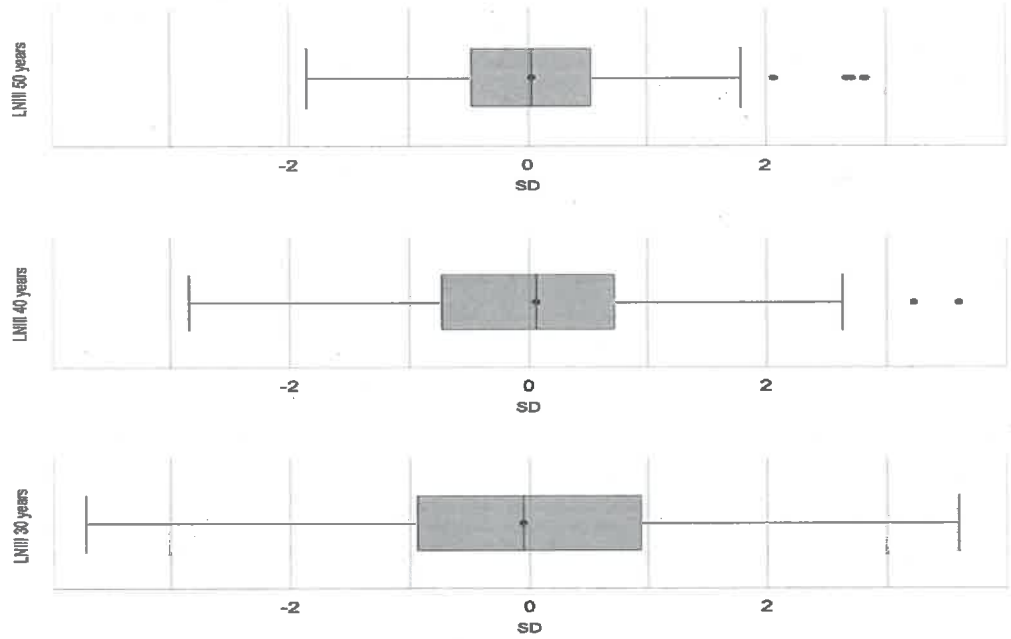

Figure 3.34 Shows the overall HQ_{100} value spread for the Log-Normal III function, with respect to the window length used. On the x-axis the standard deviation (sd) is plotted.

3.3.5 Coefficient of Variation (CoV) Comparison of the 30, 40 and 50 Year-Long Window Shift

Figure 3.35 shows the CoV values as percentage for all the gauging stations separately. Each value shows a CoV value calculated out of all the HQ_{100} values for the 30, 40 or 50 year-long window shift over a 100 year-long time series of a gauging station within the $List_{y100}$ (For more details regarding the calculation see subsection 2.2.2). Afterwards, all the CoV values for all four functions separately are shown as box-whisker plots, depending on the time window shift (30, 40 or 50 year-long window shifts can be seen in Figure 3.36, Figure 3.37, Figure 3.38 and Figure 3.39). In Table 3.4 one can see the results for the comparison of the CoV between the 3 different time window lengths. For the 30 year-long window shift, the highest spread can be seen when using the Pearson III distribution function (df) of 14.42% CoV for the third quartile. This value decreases for this df to 8.97% when using the 50 year-long window shift. There is a clear tendency towards a smaller CoV with increase time window length.

Distribution	Window length	first Quart-ile	Median	third Quart-ile
	[Years]	[%]	[%]	[%]
Weibull	30	5.40	7.47	11.07
	40	4.20	5.94	9.10
	50	2.79	4.34	6.18
Gumbel	30	5.54	7.87	10.24
	40	4.24	6.20	8.70
	50	2.84	4.43	6.09
Pearson III	30	6.87	10.27	14.42
	40	5.97	7.79	11.54
	50	3.90	6.44	8.97
Log-Normal III	30	6.14	8.22	11.52
	40	4.73	6.25	9.40
	50	3.19	4.83	7.00

Table 3.2 Shows the results for the CoV in percentage for all four functions with respect to the length of the time window applied to the 100 year-long gauging sites' time series.

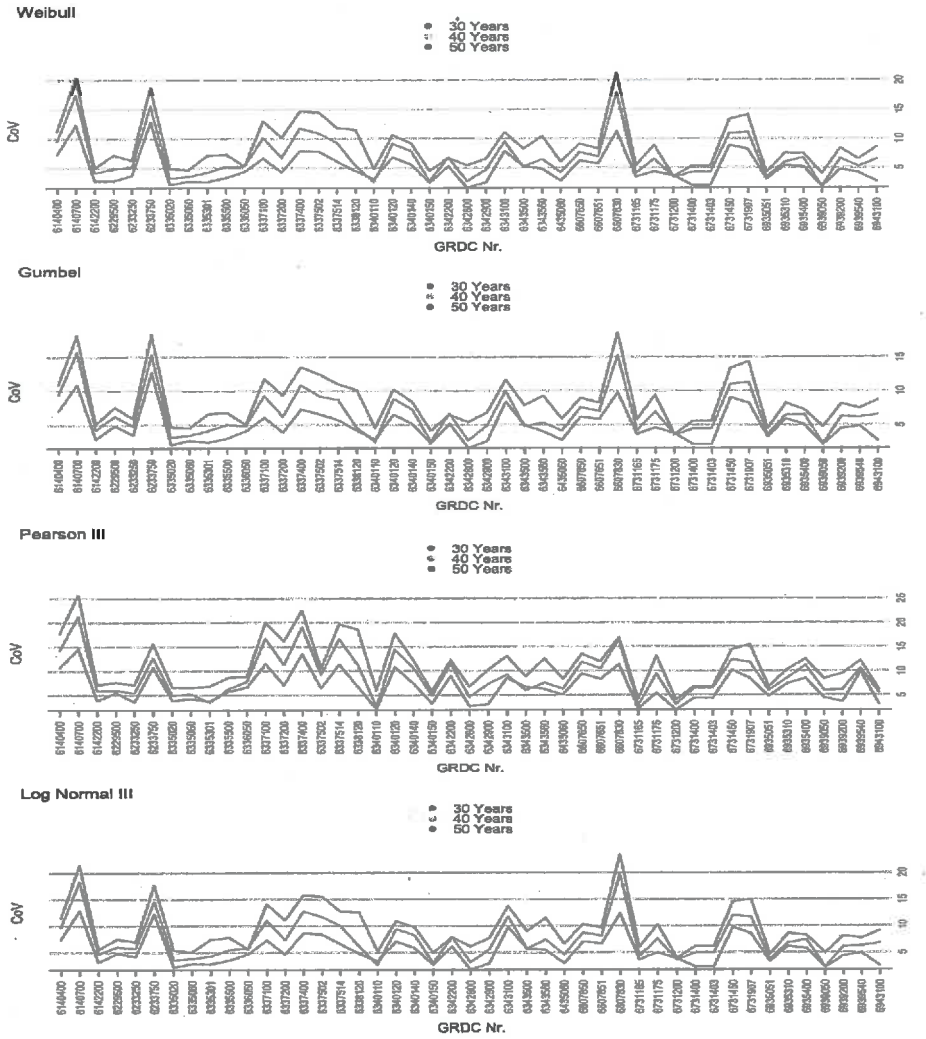

Figure 3.35 Shows the difference of the CoV values for the 30, 40 and 50 year-long time window shift. The name of the function used is displayed as header. The y-axis stands for the CoV values in percentage. The x-axis shows the GRDC Nr. for the gauging sites.

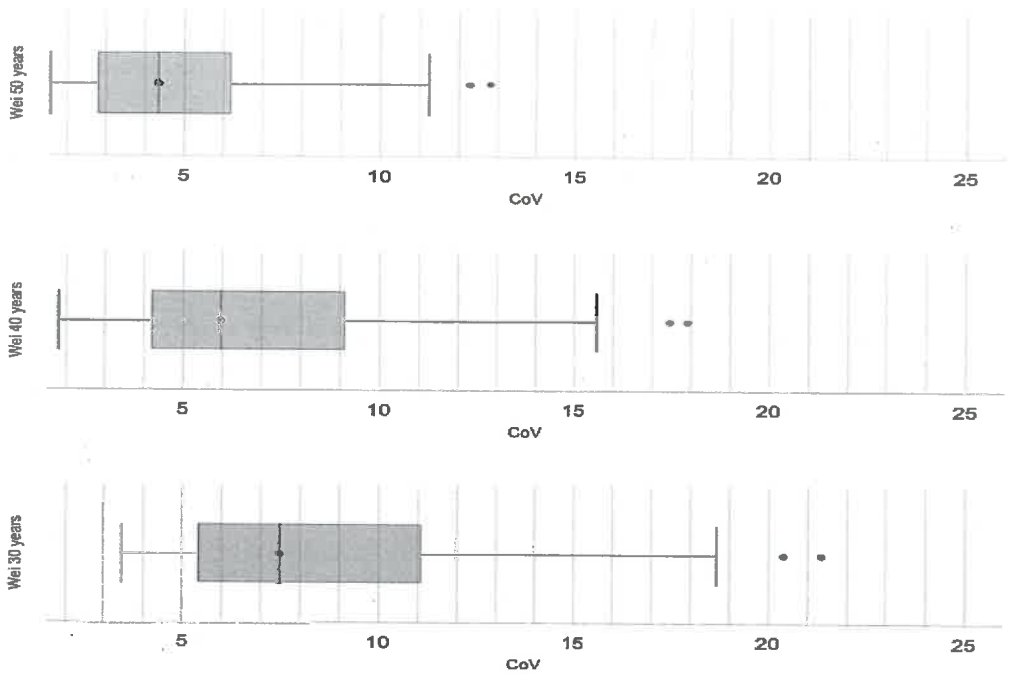

Figure 3.36 Shows the CoV percentages on the x-axis and the function used on the y-axis (Wei stands for Weibull). The dot between the 2 and 3 quartile is the median. The upper box-whisker plot shows the 50 year, the middle stands for the 40 year and the lower for the 30 year-long shift.

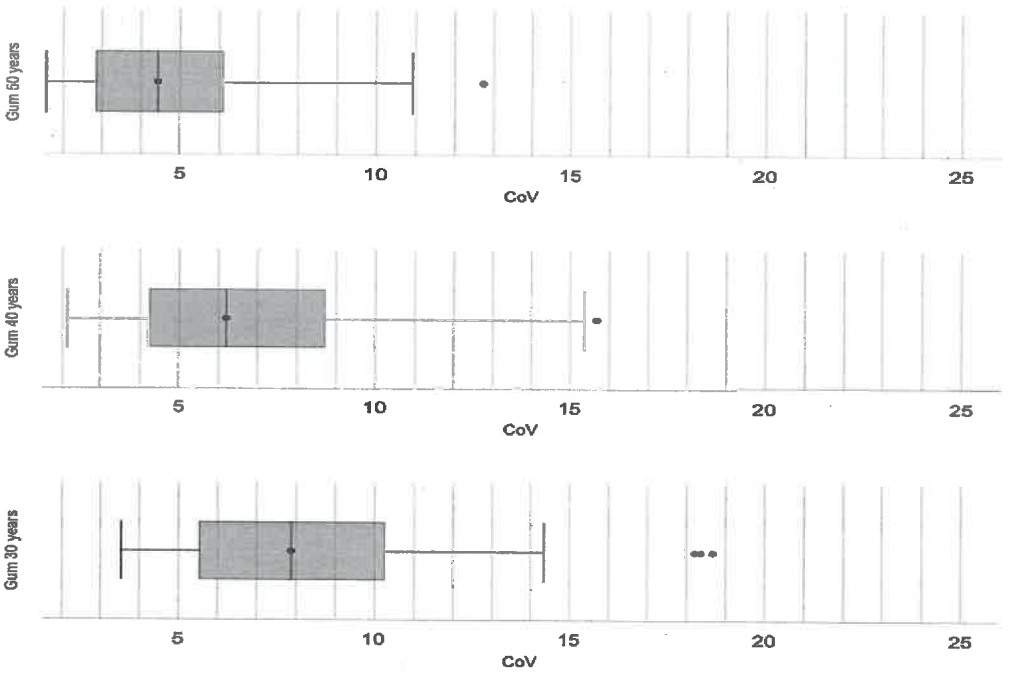

Figure 3.37 Shows the CoV percentages on the x-axis and the function used on the y-axis (Gum stands for Gumbel). The dot between the 2 and 3 quartile is the median. The upper box-whisker plot shows the 50 year-long, the middle stands for the 40 year-long and the lower for the 30 year-long shift.

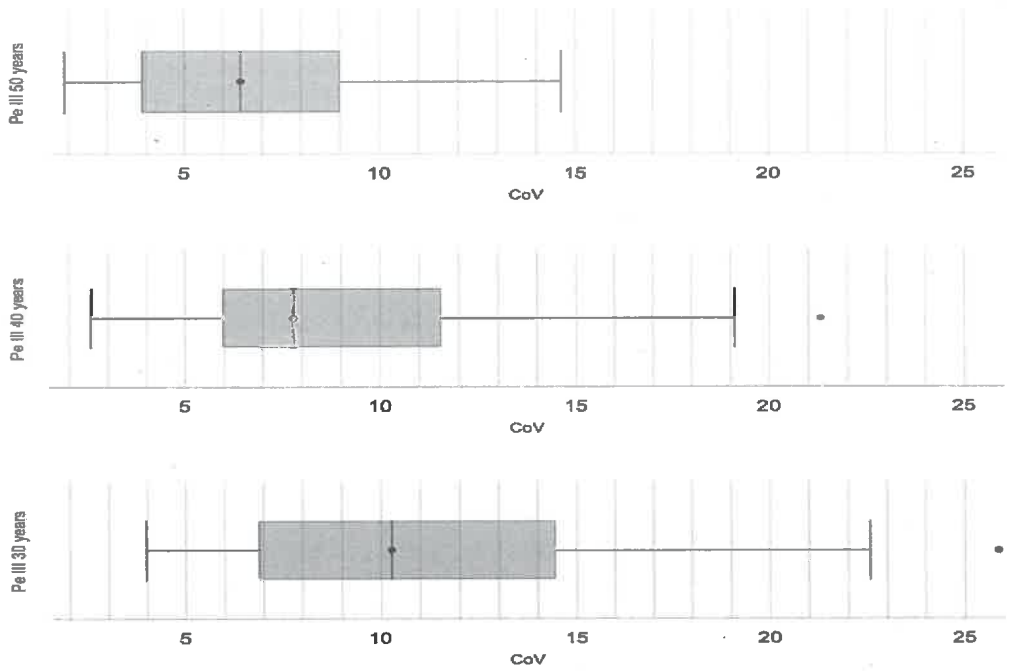

Figure 3.38 Shows the CoV percentages on the x-axis and the function used on the y-axis (PeIII stands for Pearson III). The dot between the 2 and 3 quartile is the median. The upper box-whisker plot shows the 50 year-long, the middle stands for the 40 year-long and the lower for the 30 year-long shift.

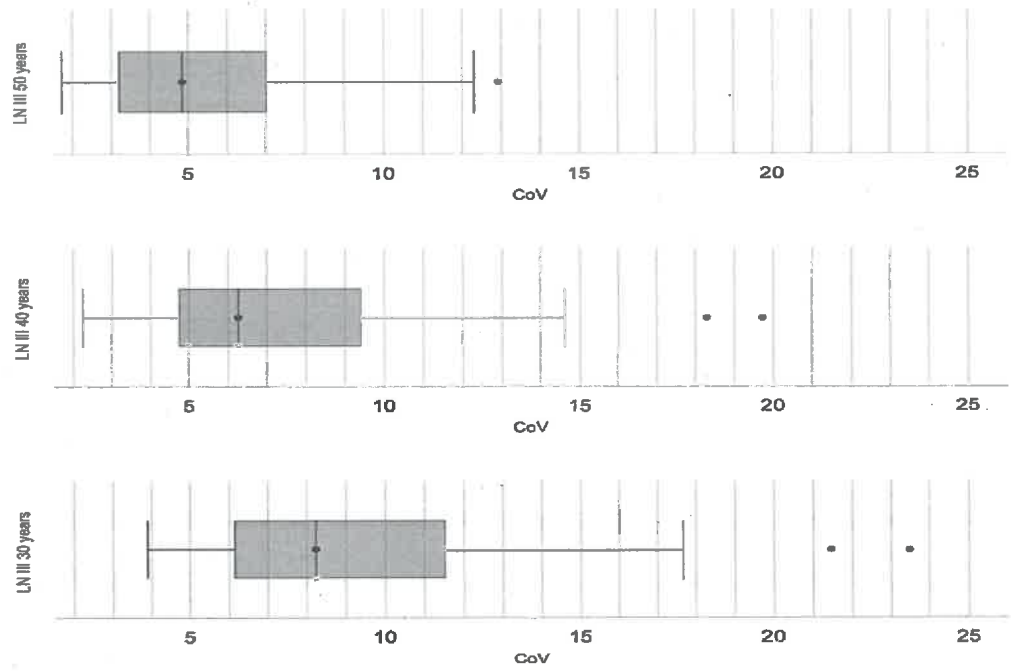

Figure 3.39 Shows the CoV percentages on the x-axis and the function used on the y-axis (LNIII stands for Log Normal III). The dot between the 2 and 3 quartile is the median. The upper box-whisker plot shows the 50 year-long, the middle stands for the 40 year-long and the lower for the 30 year-long shift.

3.3.6 Inter Quartile Range (IQR) Comparison of the 30, 40 and 50 Year-Long Window Shift

The same as described in Subsection 3.3.5 has been done for the IQR, except that the HQ_{100} values have been standardized. Figure 3.40 shows the IQR values (See Subsection 2.2.2 for the calculation details) for all the gauging stations separately. Each time series represents one of the four distribution functions. Afterwards, all the IQR values (standard deviations, sd) for all four functions separately were plotted as box-whisker plots, depending on the time window shift (30, 40 or 50 year-long - Figure 3.41, Figure 3.42, Figure 3.43 and Figure 3.44). The same tendency as for the overall spread (Subsection 3.3.4) as well as the CoV (3.3.5) can be seen for the IQR - the longer the time window shift, the smaller the IQR gets. The biggest spread between the first and the third quartile is reached when calculating with the Pearson III distribution function (df) ranging from 1.69 to 2.20 sd whereas the Gumbel df has the smallest spread between 1.56 to 2.14 sd for the 30 year-long window shift. The same df have the biggest and smallest spread for the 40 year-long shift - the Pearson III df between 1.28 and 1.76 sd and the Gumbel between 1.16 and 1.68 sd. Nevertheless, for the 50 year-long shift the Pearson III df has the smallest spread between 0.69 and 1.20 sd and the Log-Normal III df the biggest between 0.72 and 1.24 sd.

Distribution	Window length	first Quart-ile	Median	third Quart-ile
	[Years]	[SD]	[SD]	[SD]
Weibull	30	1.62	1.96	2.12
	40	1.21	1.51	1.72
	50	0.72	0.98	1.21
Gumbel	30	1.56	1.96	2.14
	40	1.16	1.52	1.68
	50	0.68	1.01	1.24
Pearson III	30	1.69	1.99	2.20
	40	1.28	1.56	1.76
	50	0.69	1.04	1.20
Log-Normal III	30	1.61	1.87	2.18
	40	1.26	1.51	1.70
	50	0.72	0.98	1.24

Table 3.3 Shows the results for the IQR spread in standard deviations for all four functions with respect to the length of the time window applied to the 100 year-long gauging sites' time series.

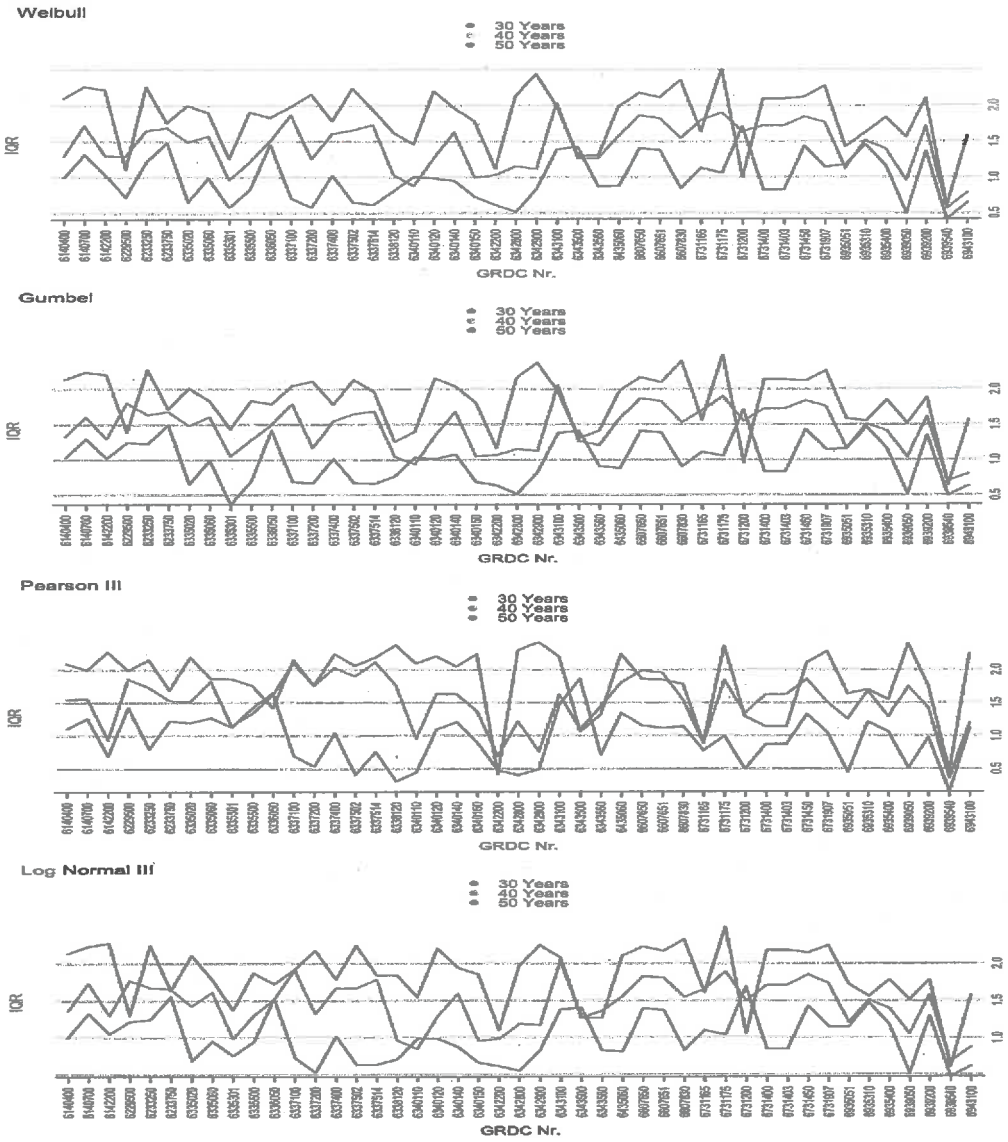

Figure 3.40 Shows the difference of the IQR values for the 30, 40 and 50 year-long time window shift. The name of the function used is displayed as header. The y-axis shows the IQR values in standard deviations (sd). The x-axis shows the GRDC Nr. for the gauging sites.

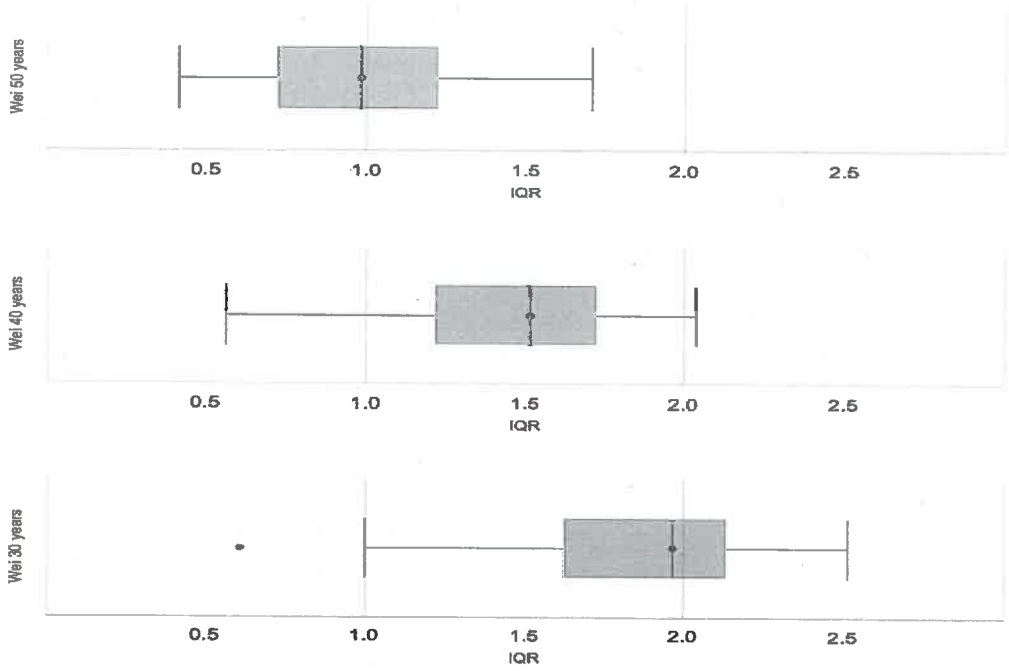

Figure 3.41 Shows the IQR values in standard deviations (sd) on the x-axis and the function used on the y-axis (Wei stands for Weibull distribution function). The dot between the 2 and 3 quartile is the median. The upper box-whisker plot shows the 50 year-long, the middle stands for the 40 year-long and the lower for the 30 year-long window shift.

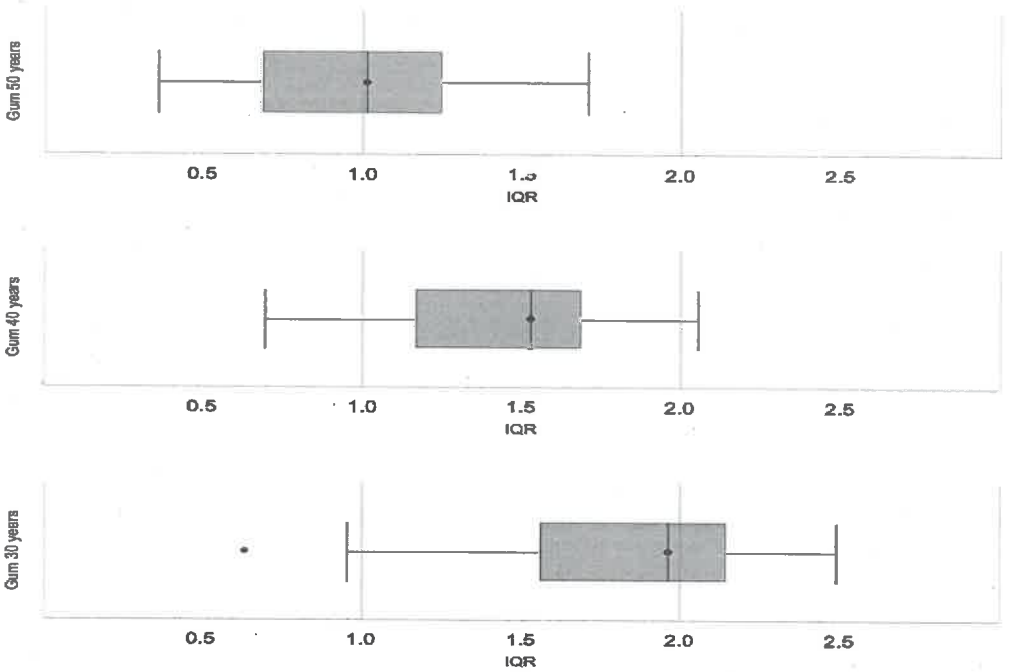

Figure 3.42 Shows the IQR values in standard deviations (sd) on the x-axis and the function used on the y-axis (Gum stands for Gumbel distribution function). The dot between the 2 and 3 quartile is the median. The upper box-whisker plot shows the 50 year-long, the middle stands for the 40 year-long and the lower for the 30 year-long window shift.

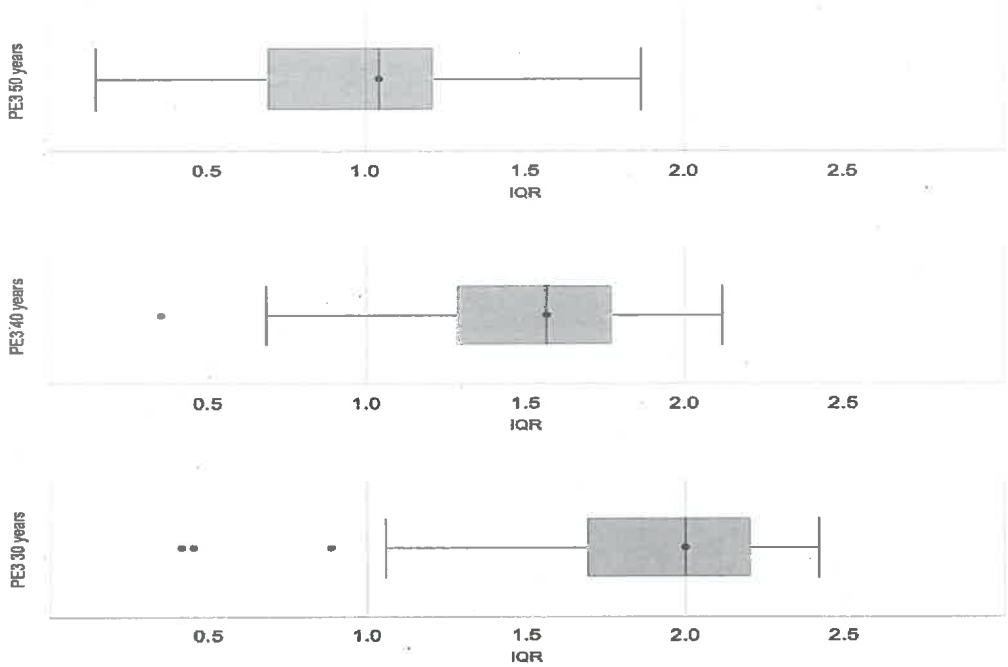

Figure 3.43 Shows the IQR values in standard deviations (sd) on the x-axis and the function used on the y-axis (PeIII stands for Pearson III distribution function). The dot between the 2 and 3 quartile is the median. The upper box-whisker plot shows the 50 year-long, the middle stands for the 40 year-long and the lower for the 30 year-long window shift.

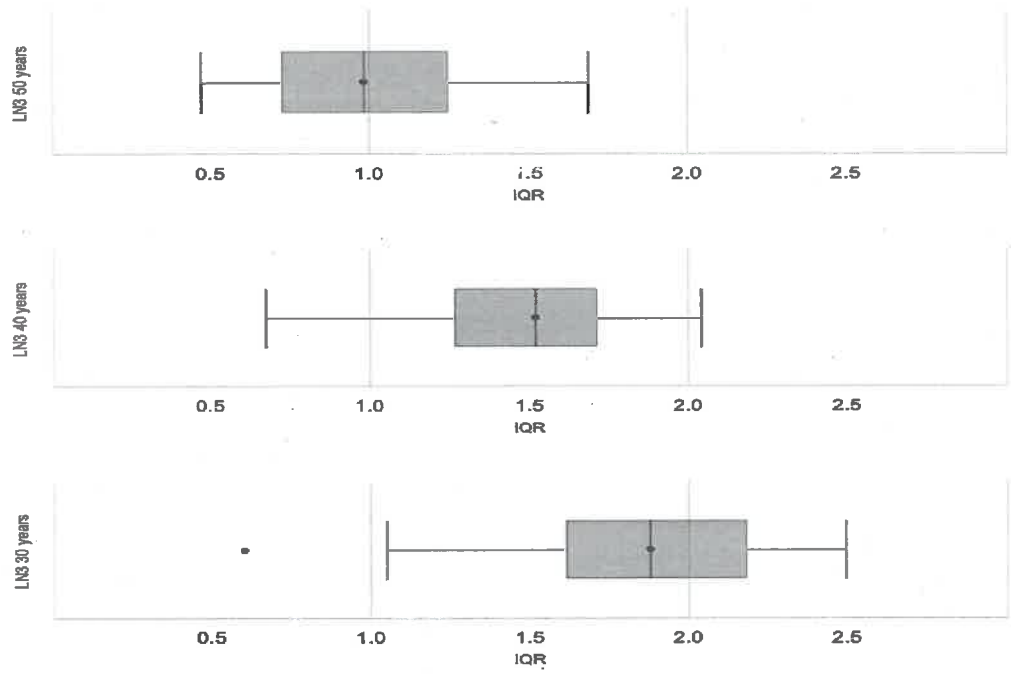

Figure 3.44 Shows the IQR values in standard deviations (sd) on the x-axis and the function used on the y-axis (LNIII stands for Log-Normal III distribution function). The dot between the 2 and 3 quartile is the median. The upper box-whisker plot shows the 50 year-long, the middle stands for the 40 year-long and the lower for the 30 year-long window shift.

3.3.7 Median Absolute Deviation (MAD) Comparison of the 30, 40 and 50 Year-Long Window Shift

The same as described in Subsection 3.3.5 has been done for the MAD, except that the HQ_{100} values have been standardized. Figure 3.45 shows the MAD values in standard deviations (sd) for all the gauging stations separately. Each time series represents one of the four functions (See subsection 2.2.2 for the calculation details). Afterwards, all the MAD values (sd) for all four functions separately are shown as box-whisker plots, depending on the time window shift (30, 40 or 50 year-long - Figure 3.46, Figure 3.47, Figure 3.48 and Figure 3.49). The same tendency as for the overall spread as well as CoV and IQR can be seen for the MAD as well - the longer the time window shift, the smaller the MAD gets. The biggest spread between the first and the third quartile is reached when calculating with the Log-Normal III distribution function (df) ranging from 1.22 to 1.53 sd whereas the Gumbel df has the smallest spread between 1.14 to 1.54 sd for the 30 year-long window shift. As for the 40 year-long shift - the biggest spread is reached when using the Weibull df between 0.87 abd 1.22 sd whereas the Pearson III df has the smallest spread between 0.71 and 1.18 sd. Nevertheless, for the 50 year-long shift the Pearson III df has again the smallest spread between 0.36 and 0.84 sd and the Gumbel df the biggest between 0.57 and 0.83 sd.

Distribution	Window length	first Quart-ile	Median	third Quart-ile
	[Years]	[SD]	[SD]	[SD]
Weibull	30	1.19	1.39	1.52
	40	0.87	1.02	1.22
	50	0.50	0.64	0.85
Gumbel	30	1.14	1.37	1.54
	40	0.85	1.05	1.20
	50	0.57	0.64	0.83
Pearson III	30	1.08	1.44	1.64
	40	0.71	0.99	1.18
	50	0.36	0.60	0.84
Log-Normal III	30	1.22	1.34	1.53
	40	0.89	1.06	1.19
	50	0.49	0.66	0.81

Table 3.4 Shows the results for the MAD spread in standard deviations for all four functions with respect to the length of the time window applied to the 100 year-long gauging sites' time series.

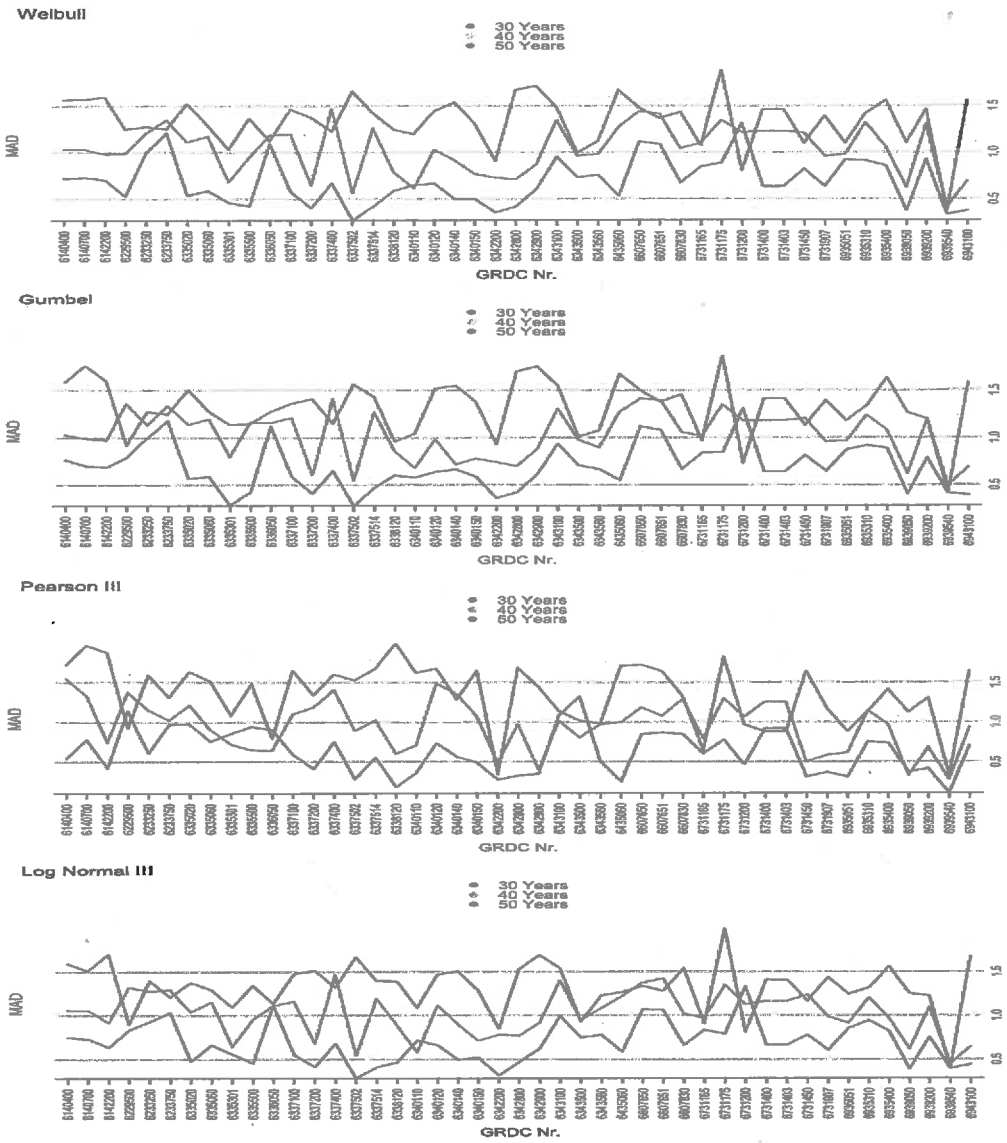

Figure 3.45 Shows the difference of the MAD values in standard deviations (sd) for the 30, 40 and 50 year time window shift. The name of the function used is displayed as header. The y-axis are the MAD values in sd. The x-axis shows the GRDC Nr. for the gauging sites.

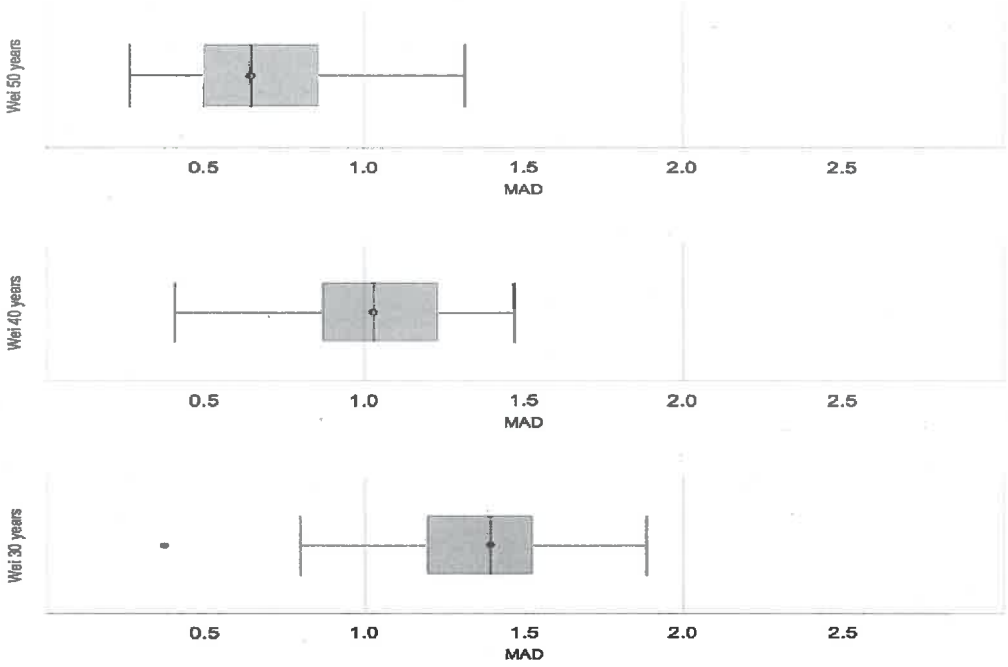

Figure 3.46 Shows the MAD values in standard deviations (sd) on the x-axis and the function used on the y-axis (WEI stands for Weibull distribution function). The dot between the 2 and 3 quartile is the median. The upper box-whisker plot shows the 50 year-long, the middle stands for the 40 year-long and the lower for the 30 year-long window shift.

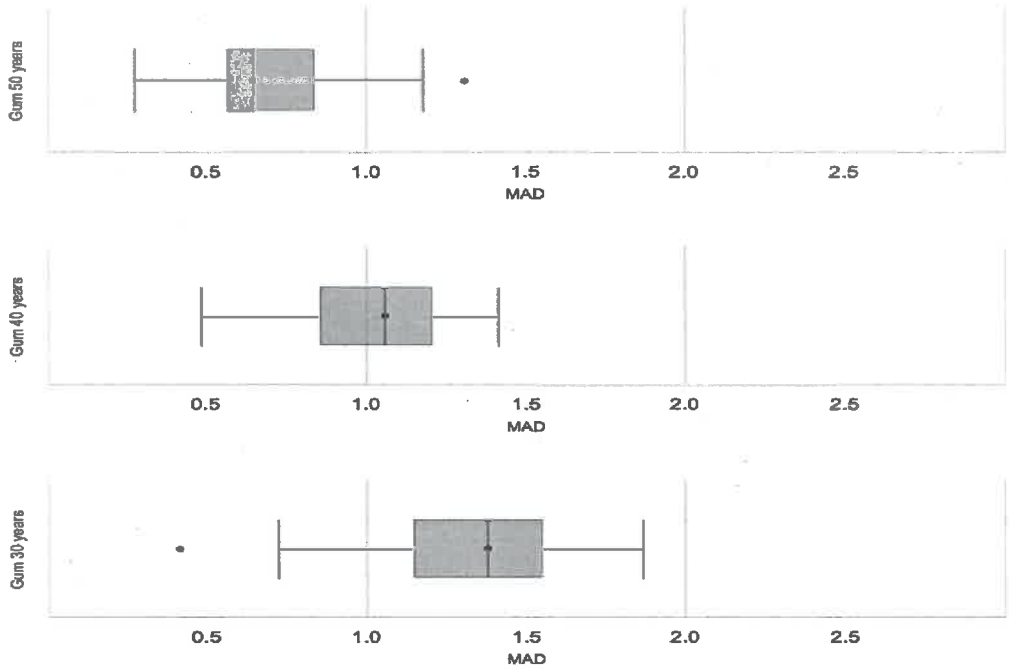

Figure 3.47 Shows the MAD values in standard deviations (sd) on the x-axis and the function used on the y-axis (GUM stands for Gumbel distribution function). The dot between the 2 and 3 quartile is the median. The upper box-whisker plot shows the 50 year-long, the middle stands for the 40 year-long and the lower for the 30 year-long window shift.

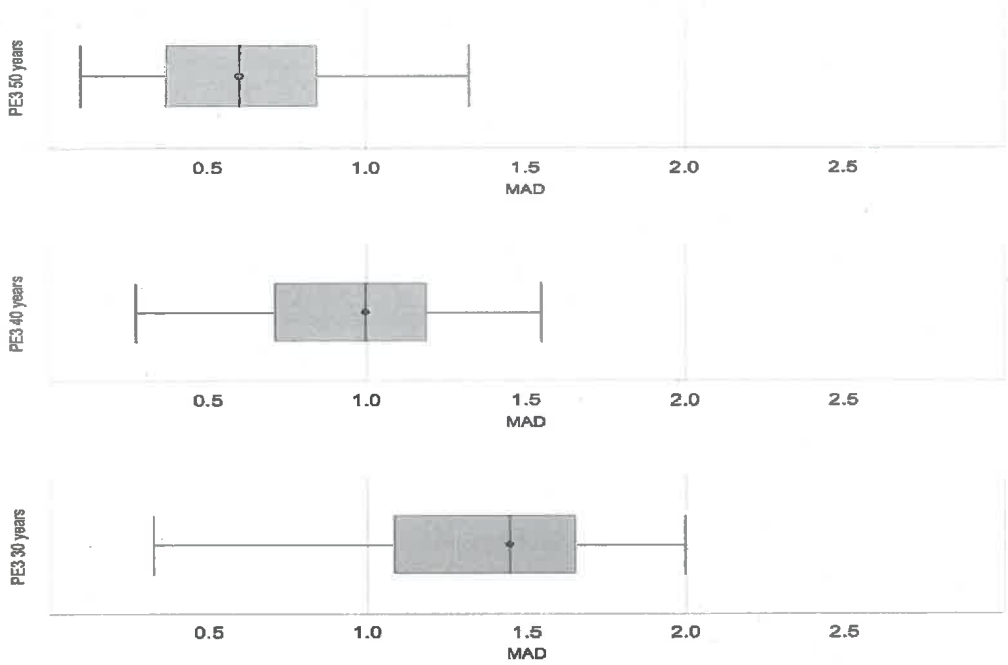

Figure 3.48 Shows the MAD values in standard deviations (sd) on the x-axis and the function used on the y-axis (PeIII stands for Pearson III distribution function). The dot between the 2 and 3 quartile is the median. The upper box-whisker plot shows the 50 year-long, the middle stands for the 40 year-long and the lower for the 30 year-long window shift.

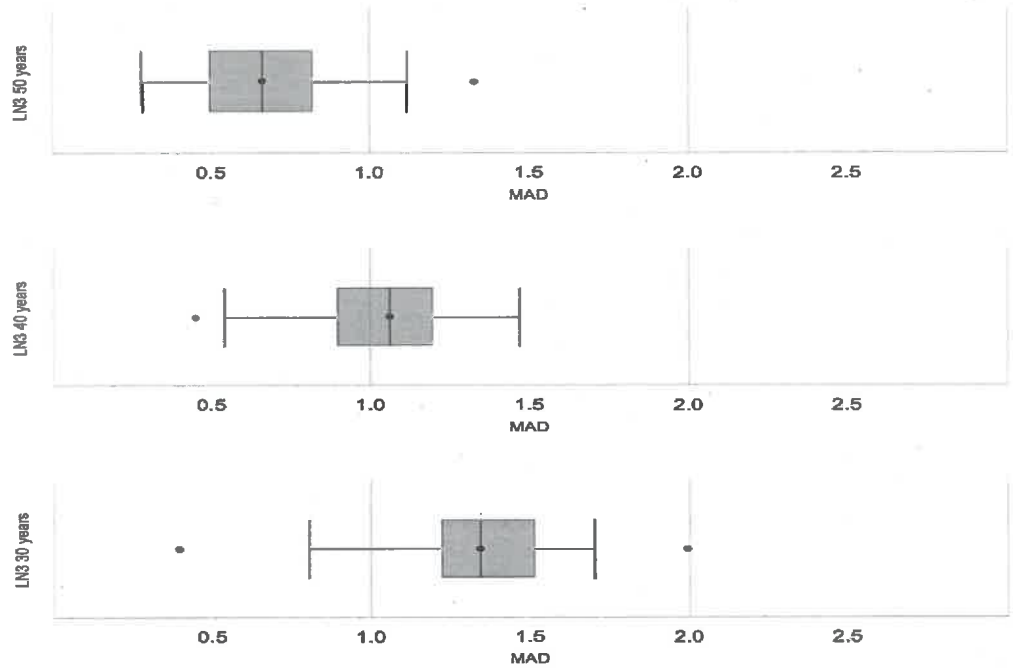

Figure 3.49 Shows the MAD values in standard deviations (sd) on the x-axis and the function used on the y-axis (LNIII stands for Log-Normal III distribution function). The dot between the 2 and 3 quartile is the median. The upper box-whisker plot shows the 50 year-long, the middle stands for the 40 year-long and the lower for the 30 year-long window shift.

3.4 Results for the Generated Stationary Annual Maxima Series

In this section one can see the results of the generated annual maxima (See Section 2.4 for more details regarding the calculation procedure). Figure 3.50 shows the cumulative HQ_{100} values, starting with a time window length of 30 years and ending with a window length of 2000 years for all four functions with their corresponding confidence intervals (CI) - all in all 1970 HQ_{100} values.

The straight black line in Figure 3.50 is the HQ_{100} return level calculated with a time window length of 2000 annual maxima - so always the last value. This line can be seen as some kind of reference HQ_{100} value for a gauging site with a known distribution which fulfills strict stationary conditions. The most precise distribution seems to be the Weibull distribution, however, some HQ_{100} values with their CI do not include the reference value. The relative spread of the CI in relation to the mean of each distribution separately can be seen in Figure 3.51 and 3.52 (See Section 2.4 for the calculation details). There, as one can see in the upper part of Figure 3.51, the Weibull distribution shows the sharpest decrease of the CI spread in relation to the mean. After around 100 years this spread is below 10% and after around 500 years of annual maxima length, it falls below 5%. As for the Gumbel distribution, it falls below 10% of CI spread after roughly 300 years and below 5% after around 1550 years (Lower part of Figure 3.51). The Log-Normal III distributions' CI spread can be seen in the lower part of Figure 3.52, and after around 500 years it decreases below 10% and after around 1550 years, it falls under 5%, despite that it starts with more than 40%, whereas the Gumbel only has a bit more than 30% of CI spread. In the context of CI spread relative to the mean, the Pearson III distribution shows the highest numbers. As one can see in the upper part of Figure 3.52, in the beginning it starts with almost 80% of spread, however, after around 500 years its spread falls below 10% but even after 2000 years of annual maxima length, it does not fall below 5%.

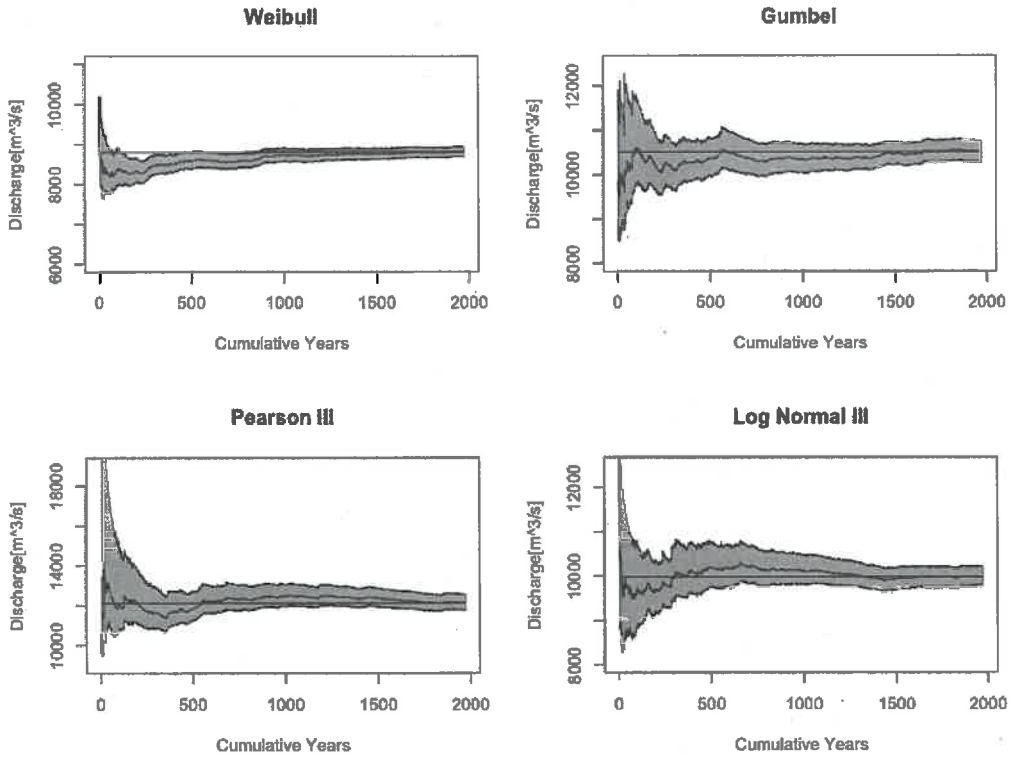

Figure 3.50 Shows the discharge for the calculated HQ_{100} on the y-axis and the length of the years taken into account for the calculation on the x-axis. The gray area is the confidence interval (CI) with a significance level of 0.05 and repetition of 5000. The straight black line is the last value calculated for the whole 2000 years and plotted through the graph.

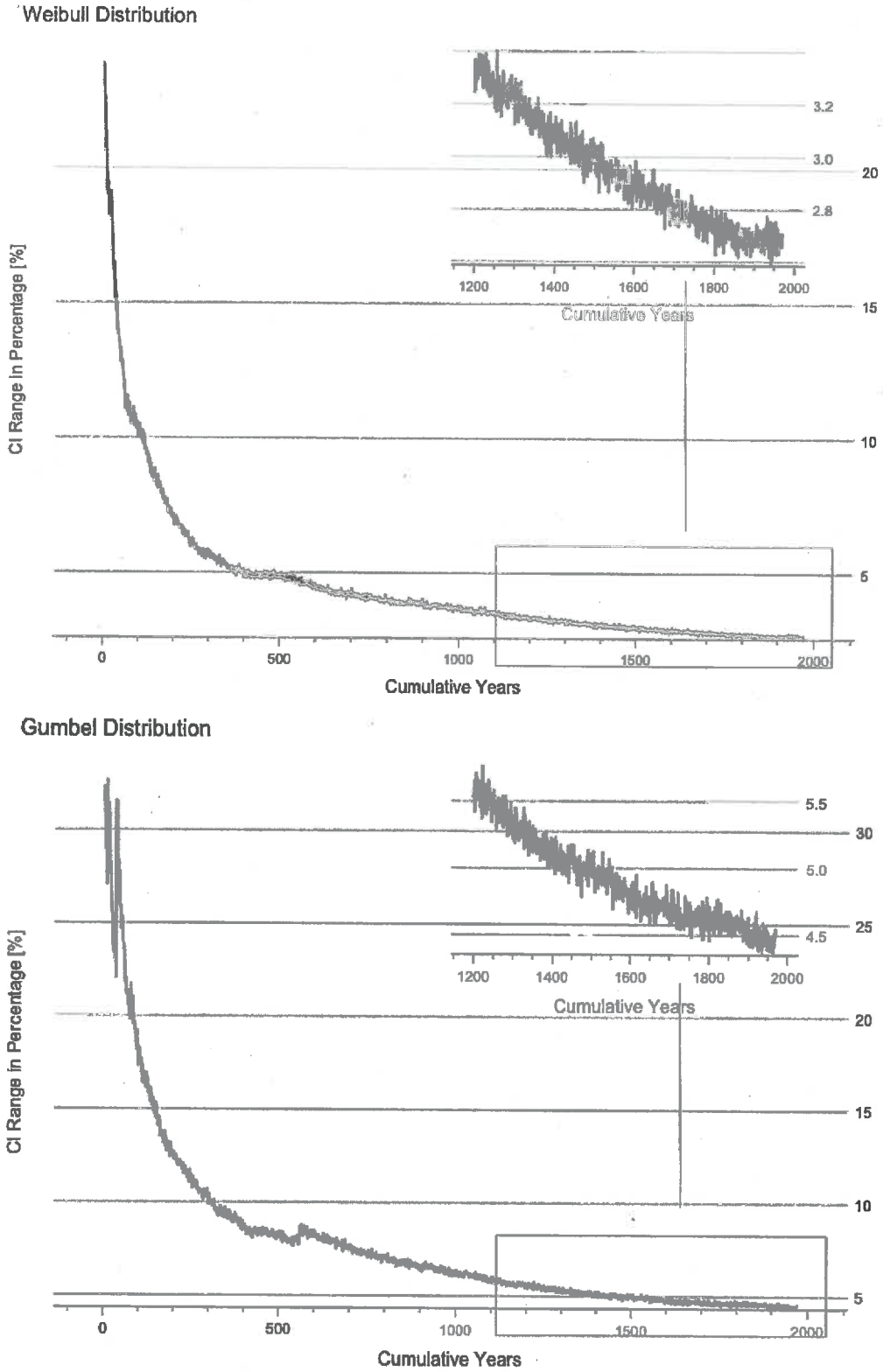

Figure 3.51 Each point shows the CI spread relative to the mean in percentage for the generated annual maximas' HQ_{100} calculated with the Weibull (above) and the Gumbel (below) distribution function. For the calculation details see Section 2.4.

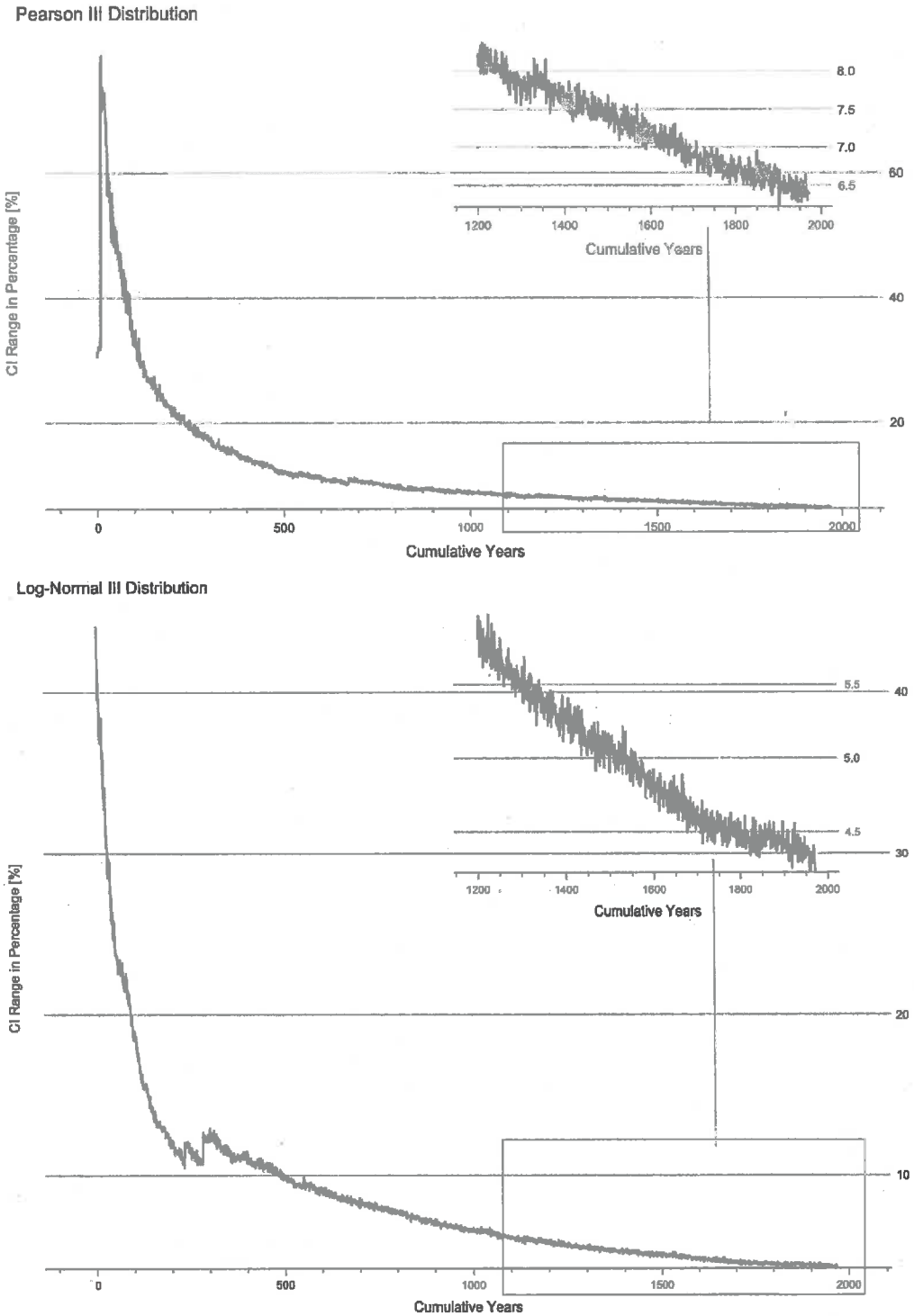

Figure 3.52 Each point shows the CI spread relative to the mean in percentage for the generated annual maximas' HQ_{100} calculated with the Pearson III (above) and the Log-Normal III (below) distribution function. For the calculation details see Section 2.4.

3.4.1 Results for the Cumulative Coefficient of Variation (CoV)

In this Subsection, one can see the results of the CoV results for the generated annual maxima series as described in Section 2.4. Each point on the x-Axis shows a 10 year window of the generated 2000 cumulative years. So basically the first value is the CoV of the 10 HQ_{100} values between the 31 and 40 year windows. The second value stands for the CoV of the 10 HQ_{100} values between the 41 and 50 year window. This means that the CoV for the window of 31 to 40 years is for the Weibull distribution 1.08%, for the Gumbel distribution 1.26%, for the Pearson III distribution 0.95% and for the Log-Normal II Distribution 1.61%. The next window between 41 and 50 years is the one with the highest CoV with 5.37% for the Pearson III distribution. After the time window between 131 and 140 the CoV value drops below 0.6% (Figure 3.53).

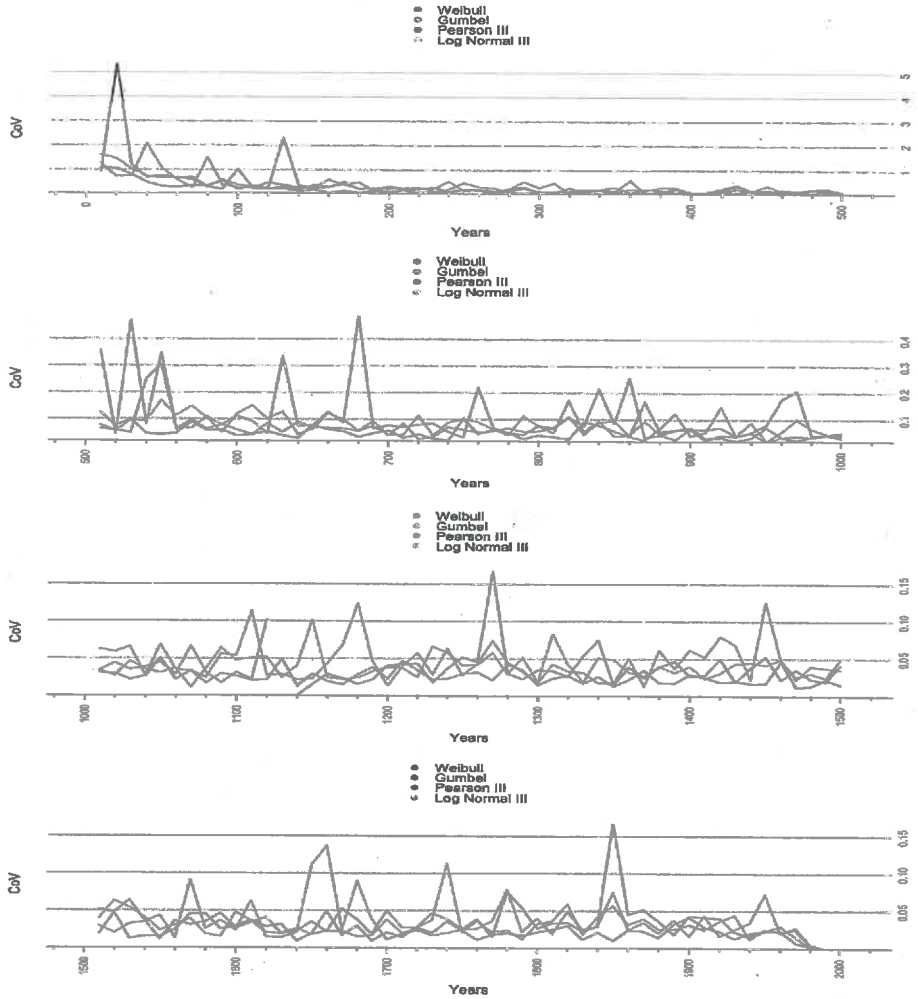

Figure 3.53 Shows the CoV values as percentage on the y-axis. The x-axis shows the modified cumulative year-range as described in Section 2.4. Each 10 years, the CoV has been calculated for the four functions standing in the legend. The CoV value range differs for each row.

3.4.2 Results for the Cumulative Inter Quartile Range (IQR)

In this Subsection, one can see the results for the IQR calculations for the generated annual maxima series. The same as described in the previous Subsection for the CoV has been done for the IQR. The detailed procedure is being described in Section 2.4. The HQ_{100} values have been standardized and then the IQR values (standard deviation (sd)) have been calculated for the same time windows as in the previous Subsection. The IQR for the window of 31 to 40 years is for the Weibull distribution 0.45 sd, for the Gumbel distribution 1.04 sd, for the Pearson III distribution 0.37 sd and for the Log-Normal II Distribution 1.56 sd. The fourth window between 61 and 70 years is the one with the highest IQR values with 2.66 sd for the Gumbel distribution. After the time window between 171 and 180 the IQR value drops below 0.5 sd (Figure 3.54).

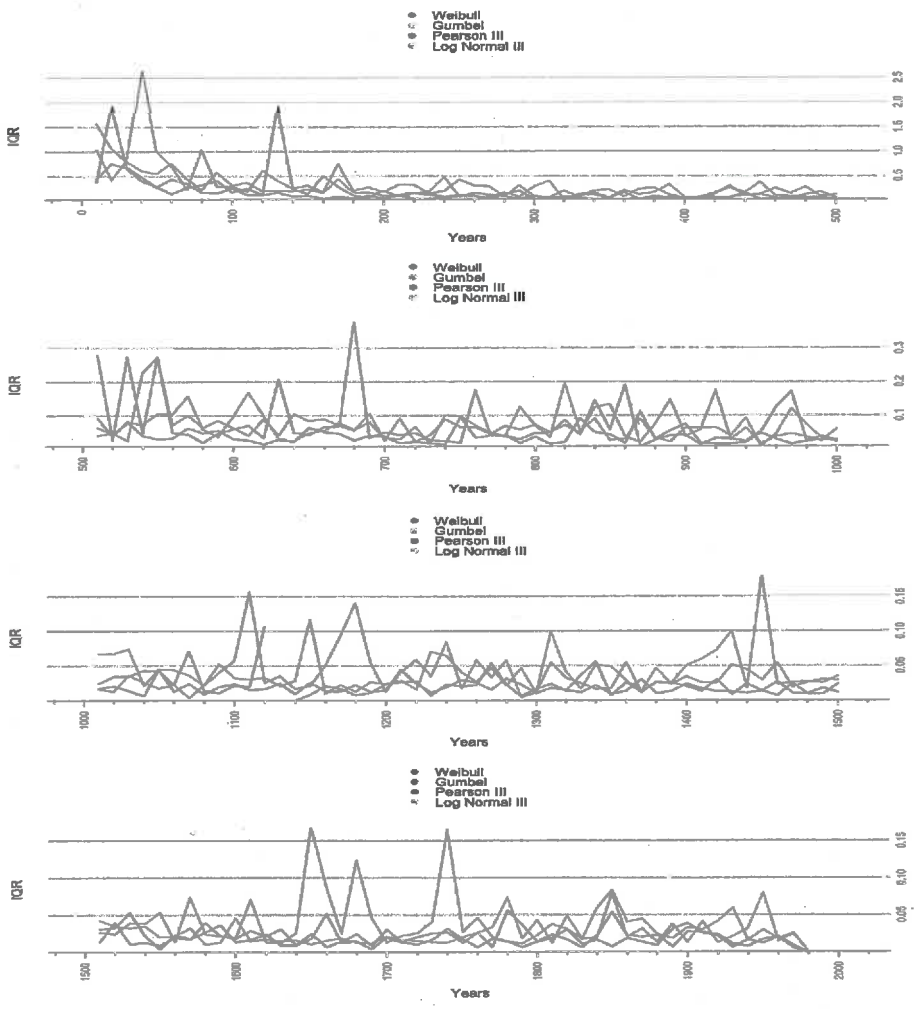

Figure 3.54 Shows the IQR values (sd) on the y-axis. The x-axis shows the modified cumulative year-range as described in Section 2.4. Each 10 years, the IQR has been calculated for the four functions standing in the legend. The IQR value range differs for each row.

3.4.3 Results for the Cumulative Median Absolute Deviation (MAD)

In this Subsection, one can see the results for the MAD calculations for the generated annual maxima series. The same as described in the previous Subsection for the IQR has been done for the MAD. The detailed procedure is being described in Section 2.4. The HQ_{100} values have been standardized and then the MAD values (standard deviation (sd)) have been calculated for the same time windows as in the previous Subsection. This means that the MAD for the window of 31 to 40 years is for the Weibull distribution 0.57 sd, for the Gumbel distribution 0.86 sd, for the Pearson III distribution 0.45 sd and for the Log-Normal II Distribution 0.96 sd. The fourth window between 61 and 70 years is the one with the highest MAD values with 2.10 sd for the Gumbel distribution. After the time window between 131 and 140 the MAD value drops below 0.5 sd (Figure 3.55).

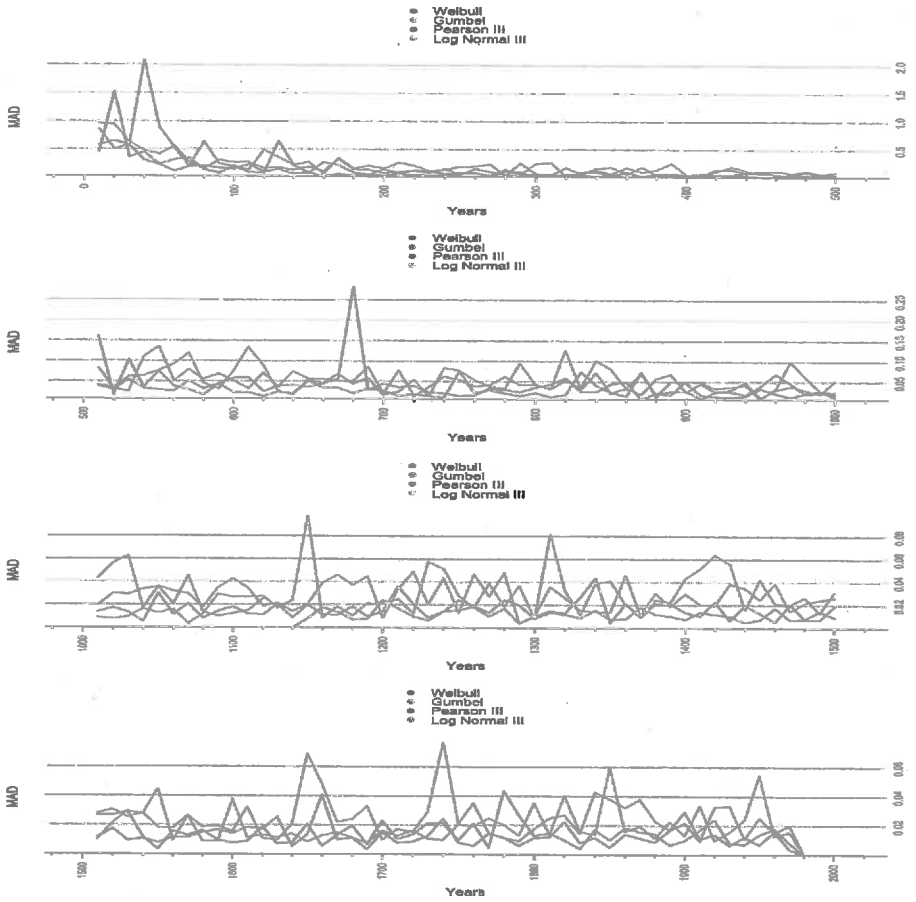

Figure 3.55 Shows the MAD values (sd) on the y-axis. The x-axis shows the modified cumulative year-range as described in Section 2.4. Each 10 years, the MAD has been calculated for the four functions standing in the legend. The MAD value range differs for each row.

Chapter 4

Discussion

As mentioned in the Introduction (Section 1.1), the main research questions were:

1. Are 30 years enough to calculate a "precise" return level?
2. How many years are necessary in order to get a "precise" return level? And,
3. how do 30, 40 and 50 years of time series length impact the return level with regard to the variability of the estimate?

According to the BMLFUW, 2011, 30 years of time series length are enough for extreme value statistic estimations, namely flood return levels. But is that really the case? Are 30 year-long time series enough in order to get a precise return level in a statistical sense under the assumptions of stationarity? By simply looking at the heat-maps in Section 3.2, one can see that the standardized return levels for a HQ_{100} can differ at several gauging sites by more than 2 standard deviations (sd), going up to almost 3 within only a few years - So by simply calculating the HQ_{100} 5 years later, one can get return levels, which can differ substantially from the previous ones and 5 years later one could get a similar result as 10 years before e.g. Figure 3.4 GRDC Nr. 6233366, 6233600, 6335125 or 6335410 or Figure 3.6 GRDC Nr. 6343100, 6357500, 6731150 or 673125. Overall, it is quite obvious that the individual gauging sites' shift HQ_{100} values do vary quite substantially. However, what about the average spread for all the 227 gauging sites? By looking at the first and third quartile for all the gauging sites' HQ_{100} values combined (Figure 3.10), independent of the function being used, is shows that it is between -0.73 and 0.74 standard deviations (sd). So 50% of the HQ_{100} values are within 1.47 sd. This variability is supported by the results of the inter quartile range (IQR) and the median absolute deviation (MAD) of the HQ_{100} values for the 30 year-long window shift over the 60 year-long time series. The IQR results show (3.12), that for all functions the median of the 50% range of the IQR is

expected to be between 1.42 standard deviations (sd) and 1.44 sd, which exceeds the IQR of a normal distribution (1.345), despite being standardized. As for a less robust measure, the Coefficient of Variation (CoV) results in Subsection 3.2.3 show, that the relative variability can go up as high as 20% (Figure 3.10). Of course these extreme examples might already have been identified as not appropriate for the calculation (By either goodness of fit tests, as outliers or by the assumptions necessary (e.g. no anthropogenic influence, etc.)). But still, the overall CoV for the 227 gauging sites shows, that depending on the function, the median for the relative standard deviation to the mean for all 60 year-long time series combined is between 5 and 6.5% of the discharge estimated. The range between the first and third quartile of the CoV for the Weibull and Gumbel is between 3.8% and 8%, the Pearson III has a range between 4.8% and 10.9% CoV and the Log-Normal III distribution one between 4% and 9.8%. So a HQ_{100} return level calculation by a Pearson III distribution and a L-moment parameter estimation method follows a spread with a relative standard deviation of up to almost 11% for the range between the first and third quartile. Nevertheless, as I did use four different functions and no goodness of fit, these variability values might be less prominent, if I would have taken only the HQ_{100} value of the best fit distribution function. However, by looking again at the heat-maps, we see that the Weibull, Gumbel and Log-Normal III distribution function do almost always follow similar patterns and we see that despite maybe a less overall spread of the HQ_{100} values, the pattern of variability and changing of the flood return levels depending on the time would still be the very similar. Moreover, I did not want to calculate the HQ_{100} as accurate as possible, but I wanted to show the variability of them. And all these either robust or non robust measures of variability show us, that when a HQ_{100} is calculated with a 30 year-long time series using the AMS-Method as well as the L-Moment estimation method suggested by the BMLFUW, 2011, the expected return value is a random value, that is somewhat distributed and can vary significantly by up to 3 sd, simply by calculating at a different point of time for the same gauging site. These different HQ_{100} values within only a few years can have several different reasons. Maybe there have been structural changes along the river like dams, dikes or hydro-power plants as well as sealing off the surface, changing the discharge pattern or simply climatic extremes, leading to very extreme floods or draughts, which in turn influence the fitted distribution and leading to higher or lower probabilities for certain return values. Nevertheless the reason for this variability, it is there and the individual as well as overall results shown in this thesis underlines it. This dependency of the length and point of time when the calculation was done, as well as all the implications this does have on a HQ_{100} estimation value, needs to be examined more closely and any kind of guideline should point out such an additional uncertainty.

As for the third question - how do 30, 40 and 50 years of time series length impact the return level - we need to look at Section 3.3.1. In order to understand this question, the $List_{y100}$ has been used for the calculations. Its 45 gauging sites have been taken into consideration, which might be the reason why the values for the 30 year-long shifts' CoV, IQR and MAD are higher than for the 227 gauging sites long $List_{y60}$ 30 year-long shift. Nevertheless, we can see a clear tendency towards a less spread return level with an increased time window length. The robust measures (median absolute deviation (MAD) and the inter quartile range (IQR)) do decrease more prominently than the non-robust measures (Coefficient of Variation (CoV)) between the 30, 40 and 50 year-long window shift, moreover, the decrease between the 40 and 50 year-long window is higher than the one between the 30 and 40 year-long window. This indicates that there is no linear decrease of the variability with longer time windows, but a rather non-linear one. Moreover, this behaviour can also be seen in the generated annual maxima series' HQ_{100} values. The decrease of the variability in the first 500 years is much higher than the decrease over the following 1500 years. It is interesting to see that some gauging sites (e.g. site with the GRDC Nr. 6731200 in Figure 3.45) show contradictory behaviours. So the 50 year-long window lengths' MAD is higher than the 40 year-long window and both of them are even higher than the 30 year-long window for the Weibull, Gumbel and Log-Normal III distribution function. The reason for this might be the distribution of the annual maxima itself and its extraction method. But such a behaviour is very unusual and the overall trend is quite obviously to a more stable return value with a higher window length. Overall the results indicate that especially with only a few year-long (e.g. 30 to 50 years) times series, the variability decrease is very effective and therefore, it is of crucial importance to use as many years as possible for the flood estimation extreme value statistics, especially between 30 and 50 years. But are 50 years already enough in order to decrease this variability? And if not, how many years are necessary? This was the second research question, and by looking at the results in Section 3.4, we can see that the first 100 to 200 years of the generated time series, the HQ_{100} return level is very variable but decreases very quickly. However, the longer the times series gets, the more stable and more precise the calculation and its corresponding confidence intervals (CI) do become. And according to the results in Figure 3.53, 3.54 and 3.55 with a length of more than 120 years, the CoV stays below 1%, which is already very stable. The IQR is permanently under 1 sd with a length of 130 years and drops below 0.7 sd after 170 years. The MAD gets below 0.6 sd after already 130 years, which is already quite precise. So under strict stationary conditions and roughly 140 years of river discharge length, the variability decreases substantially for at least this example. If we add more years, this decrease slows down and almost stops. Nevertheless, as one can see in Figure

3.50 as well, simply by being less variable, the last HQ_{100} return level is sometimes even out of the CI for previous calculations. So being statistically precise does not necessarily lead to good estimation, especially in a statistical accuracy sense. Overall one can see a tendency towards a more stable discharge level after 1500 years in terms of accuracy and precision for this example, however, this is under strict stationary conditions and cannot necessarily be applied for existing rivers. Moreover, the CI decreases with respect to the mean also shows that with an time length increase, the spread of the CI decreases quite sharply in the beginning with all four functions and then, after around 200 to 400 years, depending on the function used, the decreases slows down (See Figure 3.51 and 3.52). The Weibull distribution function has the best fit and highest decrease in the CI spread, however, as the underlying function is also a Weibull distribution function, this might be the reason for it. Nevertheless, one can see by looking at the four Figures, that after 100 years of window length, the CI for the Weibull already drops below 10% of spread relative to the mean. 200 years are necessary for the Gumbel, and around 500 for both, the Pearson III and Log-Normal III distribution function. Those two might do worse, because they both use 3 parameters and are therefore more susceptible to minor changes of the annual maxima. However, the CI spread with regard to the mean of the Pearson III distribution function is unnatural high in the beginning with almost 80%. Nevertheless, throughout almost any of the calculations, the Pearson III distribution did produce the highest variability. This might again be because of the 3 parameters and it is the only one, as the Gumbel has only 2 parameters and the Weibull and Log-Normal III distribution have both a lower bound at 0. The exact reason for this is, however, unknown for the author.

During this thesis, I calculated numerous HQ_{100} time series with the 30 year-long window shift for the 60 year-long gauging sites - all in all 27240 HQ_{100} values. These generated HQ_{100} time series do have certain behaviours regarding their tendency over time. In order to find similarities of increased or decreased HQ_{100} values, I compared them and put gauging sites with similar tendencies in different regions (Subsection 2.2.1). These regions do show that throughout the gauging sites I used (227 in total throughout Europe), most rivers tend to have an increased HQ_{100} value, if calculated with the last 30 year-long time window than HQ_{100} values with the first 30 year-long window. The reason for this is unknown, but it might be due to anthropogenic influences as structural changes along the river or land sealing. It is interesting to see, that most gauging sites do have an increased HQ_{100} value if calculated today than 30 years ago with the same time series length. Nevertheless, the regions need to be split up more in order to generate higher R^2 values (the highest value is within region two, with 0.629) and eliminate all unfit gauging sites. The information value is therefore

limited and to make any significant conclusions, more research needs to be done on this topic.

Overall, the main takeaway message should be that return levels are distributed and the spread of this distribution is also depending on the time lengths of the time series being used. This behaviour exists and even 2000 years of time series length cannot get rid of it indefinitely. Therefore, this effect needs to be addressed more often and peoples' awareness towards it should be raised. Moreover, the additional uncertainty arising from it for any statistical outcome depending on finite time series needs to be accounted for and taken into consideration.

References

[1] Lorenzo Alfieri, Luc Feyen and Giuliano Baldassarre. "Increasing flood risk under climate change". In: *Climatic Change* 136.3 (2016), pp. 507–521.

[2] Lorenzo Alfieri, Luc Feyen, Francesco Dottori et al. "Ensemble flood risk assessment in Europe under high end climate scenarios". In: *Global Environmental Change* (2015). ISSN: 09593780. DOI: 10.1016/j.gloenvcha.2015.09.004.

[3] Rodrigo J Aristizabal. "Estimating the Parameters of the Three-Parameter Lognormal Distribution". In: (2012).

[4] J. I. Barredo. "Major flood disasters in Europe: 1950-2005". In: *Natural Hazards* (2007). ISSN: 0921030X. DOI: 10.1007/s11069-006-9065-2.

[5] Gunter Bloschl and Alberto Montanari. *Climate change impacts-throwing the dice?* 2010. DOI: 10.1002/hyp.7574.

[6] BMLFUW. *Leitfaden - Verfahren zur Abschätzung von Hochwasserkennwerten.* Tech. rep. BMLFUW, 2011, p. 113.

[7] Wenju Cai, Simon Borlace and Matthieu Lengaigne. "Increasing frequency of extreme El Niño events due to greenhouse warming". In: *Nature Climate Change* 4 (2014).

[8] Chakravarti, Laha and Roy. *Handbook of Methods of Applied Statistics.* Volume 1. John Wiley and Sons, 1967, pp. 392–294.

[9] John Chambers. *R Programming Language.* URL: https://www.r-project.org/about.html.

[10] S. Defays. "The Comparison of GEV Log-Pearson Type 3 and Gumbel Distribution". In: *The Computer Journal* 364-366 (1977).

[11] DWA. *Ermittlung von Hochwasserwahrscheinlichkeiten.* 2012.

[12] EEA. *River Floods.* 2012. URL: http://www.eea.europa.eu/data-and-maps/indicators/river-floods-1.

[13] European Comission. "Water Framework Directive 2000/60/EC". In: *Official Journal of the European Parliament* L327.September 1996 (2000), pp. 1–82. ISSN: 0144557X. DOI: 10.1039/ap9842100196.

[14] European Commission. *Links between the Floods Directive and Water Framework Directive - Resource Document.* Tech. rep. European Union, 2014, p. 37.

[15] Brian Everitt. *The Cambridge Dictionary of Statistics.* Cambridge University Press, 1998. ISBN: 0521593468.

[16] Luc Feyen, Jos. I. Barredo and R. Dankers. *Implications of global wariming and urban land use change on flooding in europe.* Tech. rep. Institute for Environment and Sustainability, 2009, pp. 217–225. URL: http://publications.jrc.ec.europa.eu/repository/handle/JRC47337.

References

[17] FOEN. *Natural hazards: In brief*. 2016. (Visited on 01/01/2016).

[18] P D Sven Fuchs. *Risk management and vulnerability assessment – Introduction*. Tech. rep. 2014, pp. 1–32.

[19] Elisabetta Genovese. *A Methodological Approach to Land Use Based Flood Damage Assessment in Urban Areas- PRague Case Study*. Tech. rep. EU-Joint Research Centre. Institute for Environment et al., 2006, p. 49. URL: http://natural-hazards.jrc.it.

[20] GRDC. *Global Runoff Data Base*. 2014.

[21] Stéphane Hallegatte et al. "Future flood losses in major coastal cities". In: *Nature Climate Change* 3.9 (2013), pp. 802–806. ISSN: 1758-678X. DOI: 10.1038/nclimate1979. arXiv: arXiv:1011.1669v3. URL: http://www.nature.com/nclimate/journal/v3/n9/full/nclimate1979.html$%5Cbackslash$nhttp://www.nature.com/nclimate/journal/v3/n9/pdf/nclimate1979.pdf.

[22] J. R. M. Hosking. "L-Moments: Analysis and Estimation of Distributions Using Linear Combinations of Order Statistics". In: *Journal of the Royal Statistical Society. Series B (Methodological)* 52.1 (1990), pp. 105–124. ISSN: 00359246. URL: http://www.jstor.org/stable/2345653.

[23] IPCC. "Climate Change 2014 Synthesis Report Summary Chapter for Policymakers". In: *Ipcc* (2014), p. 31. ISSN: 1476-4687. DOI: 10.1017/CBO9781107415324. arXiv: arXiv:1011.1669v3.

[24] Shaleen Jain and Upmann Lall. "Floods ina changing climate- does the past represent the future?" In: *WATER RESOURCES RESEARCH* 37.12 (2001), pp. 3193–3205.

[25] Katarína Jeneiová et al. "Potential of Global Runoff Data for evaluation of seasonal flood patterns in Europe". In: 17 (2015), p. 2015.

[26] A. F. Jenkinson. "The frequency distribution of the annual maximum (or minimum) values of meteorological elements". In: *Q.J.R. Meteorol. Soc* 81 (1955), pp. 158–171. DOI: 10.1002.

[27] Abhas K. Jha, Robin Bloch and Jessica Lamond. *Cities and flooding*. Tech. rep. World Bank & GFDRR, 2012, p. 638. DOI: 10.1596/978-0-8213-8866-2. URL: www.worldbank.org.

[28] Erwin Kryszig. *Advanced Engineering mathematics*. 4th. John Wiley & Sons Inc, 1979, p. 1052. ISBN: 0471021407.

[29] Jian Liu et al. "Divergent global precipitation changes induced by natural versus anthropogenic forcing". In: *Nature* 493 (2013), pp. 656–659.

[30] B Merz et al. "Fluvial flood risk management in a changing world". In: *Natural Hazards and Earth System Sciences* 10 (2010), pp. 509–527.

[31] P. C. D. Milly et al. "Increasing risk of great ¯oodsin a changing climate". In: *Nature* 415 (2002), pp. 514–517.

[32] Munich Re. *Economic consequences of natural catastrophes: Emerging and developing economies particularly affected – Insurance cover is essential*. Tech. rep. 80802 Munich: Munich Re Economic Research, 2013, p. 9.

[33] P. E. O'Connell et al. "Is there a link between agricultural land-use management and flooding?" In: *Hydrology and Earth System Sciences* 11.1 (2007), pp. 96–107. ISSN: 1607-7938. DOI: 10.5194/hess-11-96-2007.

[34] T N Palmer and J Räisänen. "Quantifying the risk of extreme seasonal precipitation events in a changing climate." In: *Nature* 415.6871 (2002), pp. 512–514. ISSN: 00280836. DOI: 10.1038/415512a.

[35] European Parliament and Social Comission. "Flood Directive 2007/60/EC". In: 2455 (2007), pp. 27–34.

[36] Edmund C. Penning-Rowsell and Sally J. Priest. "Sharing the burden of increasing flood risk: who pays for flood insurance and flood risk management in the United Kingdom". In: *Mitigation and Adaptation Strategies for Global Change* 20.6 (2014), pp. 991–1009. ISSN: 15731596. DOI: 10.1007/s11027-014-9622-z.

[37] Iwona Pinskwar et al. "Changing floods in Europe". In: *Changes in Flood Risk in Europe* (2012). ISSN: 01447815. DOI: 10.1201/b12348.

[38] RIWA-T. *TECHNISCHE RICHTLINIEN FÜR DIE BUNDES- WASSERBAUVERWALTUNG RIWA-T GEMÄSS § 3 ABS 2 WBFG FASSUNG 2016*. 2015.

[39] Peter Schwerdtfeger. "Rabbits and Climate.pub". 1993. URL: http://www.airborneresearch.com.au/peter%7B%5C_%7Dschwerdtfeger.htm.

[40] Graham Upton and Ian Cook. *Understanding Statistics*. Oxford University Press, 1996. ISBN: 0-19-914391-9.

[41] W.N. Venables and B.D. Ripley. *No TitleModern Applied Statistics with S-Plus*. Springer, 1999, p. 128. ISBN: 0-387-98825-4.

[42] Gabriele Villarini et al. "Flood frequency analysis for nonstationary annual peak records in an urban drainage basin". In: *Advances in Water Resources* (2009). ISSN: 03091708. DOI: 10.1016/j.advwatres.2009.05.003.

[43] Frank Wentz et al. "How Much More Rain Will Global Warming Bring?" In: *Science* 317.5835 (2007), pp. 233–235.

[44] S. Westra et al. "Addressing Climatic Non Stationarity in the Assessment of Flood Risk". In: *Australian Journal of Water Resources* 14 (2015), pp. 1–16.

[45] Boeing Phantom Works, Computing Technology and Applied Statistics. "Weibull Reliability Analysis = ‚áí". In: (2002), pp. 1–76.

Appendix A

Calculation List & Packages

A.1 List for the 227 and 45 Gauging Sites with 60 and 100 years of time series length

This list was extracted from the GRDC's database and consists of the gauging sites, which were used in the calculations.

Table A.1 Summary of the streamflow dataset containing the years between 1948 and 2009.

Country	River	Station	Lat	Long	Area [km^2]	GRDC-No.
FR	GAVE D'OLORON	OLORON-SAINTE-MARIE (OLORON-SNCF)	43.2	−0.61	1085	6119030
FR	CHER	TEILLET-ARGENTY	46.24	2.67	1600	6123370
FR	ANCE DU NORD	SAINT-JULIEN-D'ANCE (LAPRAT)	45.31	3.94	354	6123760
FR	DUNIERE	SAINTE-SIGOLENE (VAUBARLET)	45.21	4.21	228	6123770
FR	AUDE	PUYVALADOR	42.82	2.12	134	6128101
FR	VERDON	DEMANDOLX (CASTILLON)	43.88	6.54	655	6139201
FR	DURANCE	ESPINASSES (SERRE-PONCON)	44.47	6.28	3580	6139280
FR	AIN	CERNON (VOUGLANS)	46.4	5.67	1120	6139501
FR	TORRENT LE FIER	VALLIERES	45.9	5.92	1350	6139850
CZ	ELBE RIVER	DECIN	50.79	14.23	51123	6140400
CZ	LOUCNA	DASICE	50.04	15.91	624	6140600
CZ	DIVOKA ORLICE	NEKOR	50.07	16.55	182	6140700
CZ	MORAVA	STRAZNICE	48.93	17.32	9146	6142120
CZ	ODER RIVER	BOHUMIN	49.92	18.33	4665	6157100
SK	MORAVA	MORAVSKY JAN	48.6	16.94	24129	6142150
SK	DANUBE RIVER	BRATISLAVA	48.14	17.11	131331	6142200
SK	NITRA	NITRIANSKA STREDA	48.52	18.17	2094	6142520
SK	VAH	SALA	48.16	17.88	11218	6142620
SK	HRON	BANSKA BYSTRICA	48.73	19.13	1766	6142650
SK	HRON	BREHY	48.41	18.65	3821	6142660
SK	VAH	LIPTOVSKY MIKULAS	49.09	19.61	1107	6142680
SK	SAJO	LENARTOVCE	48.31	20.31	1830	6144100
SK	TORYSA	KOSICKE OLSANY	48.73	21.34	1298	6144350
SK	TOPLA	HANUSOVCE	49.03	21.5	1050	6144400
SK	POPRAD	CHMELNICA	49.29	20.73	1262	6158100
SE	ENNINGDALSAELVEN	VASSBOTTEN	58.88	11.54	624.1	6229100
SE	GOETA AELV	VARGOENS KRV	58.36	12.37	46885.5	6229500
SE	TORNETRAESK	ABISKO	68.36	18.82	3345.5	6232101
SE	VISKAN	ASBRO 3	57.24	12.31	2160.2	6233100
SE	FYLLEAN	SIMLANGEN	56.72	13.12	259.7	6233150
SE	LAGAN	AENGABAECKS KRV	56.49	13.51	5479.5	6233170
SE	GROETSJOEN	GROETSJOEN	61.81	12.44	565	6233200
SE	VAESTERDALAELVEN	ERSBO	61.31	13.01	1103.8	6233205
SE	TAENNAN	TAENNDALEN	62.54	12.35	226.6	6233220
SE	TAENNAN	LILLGLAEN	62.64	12.13	64.6	6233222
SE	LJUSNAN	LJUSNEDAL OEVRE	62.55	12.6	340.3	6233227
SE	VESANKANALEN	HALABAECK	56.12	14.62	4.7	6233240
SE	HELGE A	TORSEBRO KRV (POWERSTATION)	56.1	14.13	3664.5	6233250
SE	MOSSAN	VELEN 2	58.71	14.31	45	6233300
SE	MOTALA STROEM	HOLMEN	58.59	16.17	15384	6233301
SE	ALSTERAN	GETEBRO	57.01	16.16	1332.7	6233350
SE	SOLGENAN	SKAERSBODA	57.58	14.86	157.2	6233366

A.1 List for the 227 and 45 Gauging Sites with 60 and 100 years of time series length

Country	River	Station	Lat	Long	Area [km^2]	GRDC-No.
SE	FYRSJOEN	FYRAS	63.52	15.39	2428.4	6233400
SE	NYKOEPINGSAN	HALLBOSJOEN	58.86	16.7	1992.3	6233440
SE	ANKARVATTNET	ANKARVATTNET	64.88	14.22	427.8	6233450
SE	AECKLINGEN	AECKLINGEN	63.74	13.01	155.8	6233460
SE	HARKAN	RENGEN	64.07	14.1	1110.1	6233470
SE	UMEAELVEN	STORNORRFORS KRV	63.85	20.05	26567.8	6233502
SE	VINDELAELVEN	GRANAKER	64.24	19.67	11850.5	6233510
SE	VATTHOLMAAN	VATTHOLMA 2	60.02	17.73	293.8	6233600
SE	ANGERMANAELVEN	SOLLEFTEA KRV	63.17	17.27	30638	6233650
SE	VINDELAELVEN	SORSELE 2	65.54	17.51	6056.3	6233680
SE	MOAELVEN	VAESTERSEL	63.43	18.3	1465.2	6233700
SE	PITEAELVEN	SIKFORS KRV	65.53	21.21	10816.1	6233710
SE	LULEAELVEN	BODENS KRV (+ VATTENVERK, TRANGFORS)	65.81	21.67	24923.5	6233750
SE	RANEAELVEN	NIEMISEL	66.02	21.97	3780.8	6233780
SE	ROERAN	YTTERHOLMEN	66.17	21.81	1012	6233800
SE	KALIXAELVEN	RAEKTFORS	66.17	22.82	23102.9	6233850
SE	MUONIOAELVEN, MUONIONJOKI	KALLIO 2	67.22	23.54	14477.1	6233901
SE	TORNEAELVEN, TORNIONJOKI	KUKKOLANKOSKI OEVRE	65.98	24.06	33929.6	6233910
DE	RHINE RIVER	REES	51.76	6.4	159300	6335020
DE	RHINE RIVER	DUESSELDORF	51.23	6.77	147680	6335050
DE	RHINE RIVER	KOELN	50.94	6.96	144232	6335060
DE	RHINE RIVER	ANDERNACH	50.44	7.39	139549	6335070
DE	RHINE RIVER	KAUB	50.09	7.76	103488	6335100
DE	NAHE	GROLSHEIM	49.91	7.91	4013	6335115
DE	KINZIG	SCHWAIBACH	48.39	8.03	954	6335125
DE	RHINE RIVER	MAINZ	50	8.28	98206	6335150
DE	RHINE RIVER	WORMS	49.64	8.38	68827	6335180
DE	RHINE RIVER	MAXAU	49.04	8.31	50196	6335200
DE	KOCHER	NEUENSTADT / KOCHER	49.23	9.33	1410	6335300
DE	MAIN	SCHWEINFURT - NEUER HAFEN	50.03	10.22	12715	6335301
DE	LAHN	LEUN (NEU)	50.55	8.36	3571	6335350
DE	RHINE RIVER	RHEINFELDEN	47.56	7.8	34550	6335400
DE	WUTACH	OBERLAUCHINGEN	47.62	8.33	627.13	6335410
DE	ARGEN	GIESSEN	47.63	9.6	639.34	6335450
DE	SCHUSSEN	GERBERTSHAUS	47.67	9.53	782.01	6335460
DE	MAIN	WUERZBURG	49.8	9.93	14031	6335500
DE	NECKAR	PLOCHINGEN	48.71	9.42	3995	6335602
DE	MOSELLE RIVER	COCHEM	50.14	7.17	27088	6336050
DE	WESER	VLOTHO	52.18	8.86	17618	6337100
DE	WESER	INTSCHEDE	52.96	9.12	37720	6337200
DE	ALLER	RETHEM	52.79	9.38	14730	6337250
DE	WESER	HANN.-MUENDEN	51.43	9.64	12442	6337400

Country	River	Station	Lat	Long	Area [km^2]	GRDC-No.
DE	LEINE	GREENE	51.86	9.94	2916	6337500
DE	ALLER	MARKLENDORF	52.68	9.7	7209	6337501
DE	ALLER	CELLE	52.62	10.06	4374	6337502
DE	DIEMEL	HELMINGHAUSEN	51.38	8.73	103	6337503
DE	EDER	SCHMITTLOTHEIM	51.16	8.9	1202	6337504
DE	EDER	AFFOLDERN	51.17	9.09	1452	6337505
DE	FULDA	GUNTERSHAUSEN	51.23	9.47	6366	6337507
DE	FULDA	ROTENBURG	51	9.72	2523	6337508
DE	LEINE	HERRENHAUSEN	52.39	9.68	5304	6337509
DE	LEINE	SCHWARMSTEDT	52.68	9.6	6443	6337510
DE	WERRA	ALLENDORF (BAD SOODEN)	51.27	9.97	5166	6337511
DE	WERRA	LETZTER HELLER	51.41	9.71	5487	6337513
DE	WESER	BODENWERDER	51.97	9.52	15924	6337514
DE	WESER	KARLSHAFEN	51.65	9.44	14794	6337516
DE	WESER	PORTA	52.25	8.92	19162	6337518
DE	WESER	WAHMBECK	51.62	9.52	12996	6337519
DE	EMS	VERSEN - GESAMT	52.74	7.24	8369	6338100
DE	EMS	GREVEN	52.09	7.6	2842	6338120
DE	EMS	RHEINE UNTERSCHLEUSE UP	52.29	7.43	3740	6338130
DE	ELBE RIVER	NEU-DARCHAU	53.23	10.89	131950	6340110
DE	ELBE RIVER	DRESDEN	51.06	13.74	53096	6340120
DE	ELBE RIVER	BARBY	51.99	11.88	94060	6340140
DE	ELBE RIVER	WITTENBERGE	52.99	11.76	123532	6340150
DE	ELBE RIVER	AKEN	51.86	12.06	70093	6340170
DE	ELBE RIVER	MAGDEBURG-STROMBRUECKE	52.13	11.64	94942	6340180
DE	ELBE RIVER	TORGAU 1	51.56	13.01	55211	6340190
DE	UNSTRUT	LAUCHA	51.23	11.68	6218	6340200
DE	SAALE	CALBE-GRIZEHNE	51.92	11.81	23719	6340300
DE	HAVEL	KETZIN	52.48	12.85	16173	6340510
DE	ILLER	KEMPTEN	47.73	10.32	954.6	6342200
DE	DANUBE RIVER	INGOLSTADT	48.75	11.42	20001	6342500
DE	ALTMUEHL	EICHSTAETT	48.89	11.2	1400	6342520
DE	DANUBE RIVER	REGENSBURG/SCHWABELWEIS	49.02	12.14	35399	6342600
DE	DANUBE RIVER	HOFKIRCHEN	48.68	13.12	47496	6342800
DE	DANUBE RIVER	ACHLEITEN	48.58	13.5	76653	6342900
DE	DANUBE RIVER	OBERNDORF	48.95	12.01	26448	6342910
DE	DANUBE RIVER	PFELLING	48.88	12.75	37687	6342920
DE	ISAR	LANDAU	48.67	12.69	8467	6342925
DE	ISAR	MITTENWALD-KARWENDELSTEG	47.44	11.27	404	6342928
DE	LOISACH	KOCHEL	47.67	11.36	684.9	6342930
DE	LOISACH	GARMISCH BELOW PARTNACH (UDP)	47.5	11.06	393.5	6342931

A.1 List for the 227 and 45 Gauging Sites with 60 and 100 years of time series length

Country	River	Station	Lat	Long	Area [km^2]	GRDC-No.
DE	DANUBE RIVER	HUNDERSINGEN	48.07	9.4	2647.01	6342970
DE	INN	WASSERBURG	48.06	12.23	11983	6343100
DE	SALZACH	BURGHAUSEN	48.16	12.83	6649	6343500
DE	TRAUN	STEIN	47.99	12.54	367.4	6343530
DE	RAMSAUER ACHE	ILSANK	47.62	12.95	122.5	6343555
DE	SAALACH	UNTERJETTENBERG	47.68	12.82	927.3	6343560
DE	TIROLER ACHEN / GROSSACHE	STAUDACH	47.78	12.48	951.9	6343570
DE	INN	PASSAU-INGLING	48.56	13.44	26084	6343900
DE	ODER RIVER	HOHENSAATEN-FINOW AP	52.87	14.14	109564	6357010
DE	ODER RIVER	EISENHUETTENSTADT	52.15	14.69	52033	6357500
DE	NEISSE RIVER	GOERLITZ	51.16	14.99	1621	6357502
IS	THJORSA	THJORSARTUN	63.93	−20.64	7380	6401120
IS	SVARTA, SKAGAFIROI	REYKJAFOSS	65.49	−19.39	393	6401601
NL	RHINE RIVER	LOBITH	51.84	6.11	160800	6435060
SI	SAVA	RADOVLJICA I	46.34	14.17	908	6545190
SI	KRKA	PODBOCJE	45.86	15.46	2238	6545200
SI	LJUBLJANICA	MOSTE	46.05	14.55	1763	6545400
SI	MUR	GORNJA RADGONA 1	46.68	16	10197	6546610
SI	SOCA / INSONZO	SOLKAN I	45.98	13.66	1573	6549100
SI	SOCA / INSONZO	KOBARID	46.25	13.59	437.02	6549101
SI	SOCA / INSONZO	LOG CEZSOSKI	46.31	13.49	325	6549180
GB	DEE	WOODEND	57.05	−2.6	1370	6604800
GB	LEVEN	NEWBY BRIDGE FMS	54.27	−2.97	247	6605390
GB	BEDFORD OUSE	BEDFORD	52.13	−0.46	1460	6606400
GB	THAMES	KINGSTON	51.41	−0.31	9948	6607650
GB	THAMES	KINGSTON (NATURALISED DISCHARGE)	51.41	−0.31	9948	6607651
GB	THAMES	DAYS WEIR	51.64	−1.18	3445	6607701
GB	LEE RIVER	FEILDES WEIR	51.76	0.01	1036	6607830
GB	DEE	MANLEY HALL	52.97	−2.97	1019.3	6608100
GB	WYE	REDBROOK	51.8	−2.68	4010	6608501
GB	AVON	EVESHAM	52.09	−1.94	2210	6609400
GB	SEVERN	BEWDLEY	52.38	−2.32	4325	6609500
NO	TANA (NO, FI)	POLMAK NYE	70.07	28.02	14160	6730501
NO	ENGESETELV	ENGESETVATN	62.53	6.62	41.7	6731010
NO	STJORDALSELVA	HOGGAS BRU	63.49	11.32	491	6731050
NO	NORDELVA	KRINSVATN	63.79	10.23	205	6731070
NO	ETNEELV	STORDALSVATN	59.68	6.02	127	6731130
NO	KINSO	HOLEN	60.38	6.74	229	6731140
NO	OSELV	ROYKENES	60.25	5.43	50	6731150
NO	GAULAR	VIKSVATN	61.33	5.87	505	6731165
NO	EIDSELV	HORNINDALSVATN	61.92	6.09	378	6731175
NO	VOSSO	BULKEN	60.63	6.28	1102	6731200

Country	River	Station	Lat	Long	Area [km^2]	GRDC-No.
NO	LYGNA	TINGVATN	58.4	7.23	266	6731250
NO	OTRA	HEISEL	58.25	7.95	3689	6731260
NO	AUSTENA	AUSTENA	58.85	8.1	286	6731280
NO	JONDALSELV	JONDAL	59.7	9.55	150	6731320
NO	GLAMA	LANGNES	59.61	11.12	40540	6731400
NO	GLAMA	SOLBERGFOSS	59.64	11.15	40540	6731403
NO	LOSNA	LOSNA	61.33	10.28	11210	6731450
NO	ARGARDSELV	OEYUNGEN	64.25	11.08	237	6731550
NO	KLARA	NYBERGSUND	61.26	12.23	4410	6731570
NO	FUSTA	FUSTVATN	65.9	13.3	520	6731610
NO	KJERRINGA	VASSVATN	66.4	13.18	16.1	6731650
NO	SALTELV	JUNKERDALSELV	66.82	15.43	422	6731680
NO	MAALSELV	MALANGSFOSS	69.03	18.66	3239	6731907
RO	DANUBE RIVER	HARSOVA	44.68	27.09	709100	6742800
FI	KOKEMAENJOKI	HARJAVALTA	61.34	22.11	26117	6854101
FI	LAPUANJOKI	KEPPO	63.36	22.7	3949	6854200
FI	LESTIJOKI	LAKE LESTIJARVI OUTLET	63.58	24.72	363	6854300
FI	KIIMINGINJOKI	HAUKIPUDAS	65.19	25.41	3814	6854400
FI	OULUJOKI	LAKE LENTUA OUTLET	64.19	29.58	2045	6854590
FI	IIJOKI	RAASAKKA (NEAR THE MOUTH)	65.33	25.41	14191	6854600
FI	KYRONJOKI	SKATILA (LANSORSUND)	63.09	21.88	4833	6854900
FI	VANTAANJOKI	OULUNKYLA (NEAR THE MOUTH)	60.23	24.98	1680	6855100
FI	VUOKSI	KALLAVESI - KONNUS + KARVIO	62.55	27.77	16270	6855402
FI	VUOKSI	LATOSUONOJA	61.37	28.69	5.34	6855403
FI	KARJAANJOKI	LOHJANJARVI-PELTOKOSKI	60.15	23.83	1935	6855500
CH	AARE	BERN-SCHOENAU	46.93	7.45	2945	6935020
CH	RHINE RIVER	BASEL, RHEINHALLE	47.56	7.62	35897	6935051
CH	RHINE RIVER	RHEINFELDEN, MESSSTATION	47.56	7.8	34526	6935053
CH	RHINE RIVER	REKINGEN	47.57	8.33	14718	6935054
CH	BIRSE	MONTIER (LA CHARRUE)	47.28	7.38	183	6935060
CH	ERGOLZ	LIESTAL	47.49	7.73	261	6935070
CH	GUERBE	BELP	46.89	7.5	117	6935080
CH	RHINE RIVER	DOMAT/EMS	46.84	9.46	3229	6935145
CH	AARE	UNTERSIGGENTHAL, STILLI	47.52	8.23	17601	6935300
CH	AARE	BRUGG	47.48	8.19	11726	6935301
CH	AARE	MURGENTHAL	47.27	7.83	10119	6935302
CH	REUSS	MELLINGEN	47.42	8.27	3382	6935310
CH	EMME	EMMENMATT	46.95	7.75	443	6935320
CH	SIMME	OBERWIL	46.66	7.44	344	6935330
CH	SIMME	OBERRIED / LENK	46.43	7.47	35.7	6935331
CH	SENSE	THOERISHAUS	46.89	7.35	352	6935350

A.1 List for the 227 and 45 Gauging Sites with 60 and 100 years of time series length

Country	River	Station	Lat	Long	Area [km^2]	GRDC-No.
CH	BROYE	PAYERNE	46.84	6.94	392	6935390
CH	THUR	ANDELFINGEN	47.6	8.68	1696	6935400
CH	SITTER	APPENZELL	47.33	9.41	74.2	6935412
CH	HINTERRHEIN	HINTERRHEIN	46.53	9.2	53.7	6935510
CH	LANDQUART	FELSENBACH	46.97	9.61	616	6935540
CH	TOESS	NEFTENBACH	47.52	8.65	342	6935560
CH	MUOTA	INGENBOHL	47	8.6	316	6935590
CH	RHONE	CHANCY, AUX RIPES	46.15	5.97	10323	6939050
CH	RHONE	PORTE DU SCEX	46.35	6.89	5244	6939200
CH	GRANDE EAU	AIGLE	46.32	6.97	132	6939205
CH	RHONE	BRANSON	46.13	7.09	3752	6939500
CH	MASSA	BLATTEN BEI NATTERS	46.39	8.01	195	6939510
CH	LUETSCHINE	GSTEIG	46.66	7.87	379	6939540
CH	WEISSE LUETSCHINE	ZWEILUETSCHINEN	46.63	7.9	164	6939541
CH	INN	MARTINSBRUCK	46.89	10.47	1945	6943100
CH	TICINO	BELLINZONA	46.19	9.01	1515	6948100
CH	POSCHIAVINO	LE PRESE	46.3	10.08	169	6948110
RU	NEVA	NOVOSARATOVKA	59.84	30.53	281000	6972430

Table A.2 Summary of the streamflow dataset containing the years between 1908 and 2009.

Country	River	Station	Lat	Long	Area [km^2]	GRDC-No.
CZ	ELBE RIVER	DECIN	50.79	14.23	51123	6140400
CZ	DIVOKA ORLICE	NEKOR	50.07	16.55	182	6140700
SK	DANUBE RIVER	BRATISLAVA	48.14	17.11	131331	6142200
SE	GOETA AELV	VARGOENS KRV	58.36	12.37	46885.5	6229500
SE	HELGE A	TORSEBRO KRV (POWERSTATION)	56.1	14.13	3664.5	6233250
SE	LULEAELVEN	BODENS KRV (+ VATTENVERK, TRANGFORS)	65.81	21.67	24923.5	6233750
DE	RHINE RIVER	REES	51.76	6.4	159300	6335020
DE	RHINE RIVER	KOELN	50.94	6.96	144232	6335060
DE	MAIN	SCHWEINFURT - NEUER HAFEN	50.03	10.22	12715	6335301
DE	MAIN	WUERZBURG	49.8	9.93	14031	6335500
DE	MOSELLE RIVER	COCHEM	50.14	7.17	27088	6336050
DE	WESER	VLOTHO	52.18	8.86	17618	6337100
DE	WESER	INTSCHEDE	52.96	9.12	37720	6337200
DE	WESER	HANN.-MUENDEN	51.43	9.64	12442	6337400
DE	ALLER	CELLE	52.62	10.06	4374	6337502
DE	WESER	BODENWERDER	51.97	9.52	15924	6337514
DE	EMS	GREVEN	52.09	7.6	2842	6338120
DE	ELBE RIVER	NEU-DARCHAU	53.23	10.89	131950	6340110
DE	ELBE RIVER	DRESDEN	51.06	13.74	53096	6340120
DE	ELBE RIVER	BARBY	51.99	11.88	94060	6340140
DE	ELBE RIVER	WITTENBERGE	52.99	11.76	123532	6340150
DE	ILLER	KEMPTEN	47.73	10.32	954.6	6342200
DE	DANUBE RIVER	HOFKIRCHEN	48.68	13.12	47496	6342800
DE	DANUBE RIVER	ACHLEITEN	48.58	13.5	76653	6342900
DE	INN	WASSERBURG	48.06	12.23	11983	6343100
DE	SALZACH	BURGHAUSEN	48.16	12.83	6649	6343500
DE	SAALACH	UNTERJETTENBERG	47.68	12.82	927.3	6343560
NL	RHINE RIVER	LOBITH	51.84	6.11	160800	6435060
GB	THAMES	KINGSTON	51.41	−0.31	9948	6607650
GB	THAMES	KINGSTON (NATURALISED DISCHARGE)	51.41	−0.31	9948	6607651
GB	LEE RIVER	FEILDES WEIR	51.76	0.01	1036	6607830
NO	GAULAR	VIKSVATN	61.33	5.87	505	6731165
NO	EIDSELV	HORNINDALSVATN	61.92	6.09	378	6731175
NO	VOSSO	BULKEN	60.63	6.28	1102	6731200
NO	GLAMA	LANGNES	59.61	11.12	40540	6731400
NO	GLAMA	SOLBERGFOSS	59.64	11.15	40540	6731403
NO	LOSNA	LOSNA	61.33	10.28	11210	6731450
NO	MAALSELV	MALANGSFOSS	69.03	18.66	3239	6731907
CH	RHINE RIVER	BASEL, RHEINHALLE	47.56	7.62	35897	6935051
CH	REUSS	MELLINGEN	47.42	8.27	3382	6935310
CH	THUR (CH)	ANDELFINGEN	47.6	8.68	1696	6935400
CH	RHONE	CHANCY, AUX RIPES	46.15	5.97	10323	6939050
CH	RHONE	PORTE DU SCEX	46.35	6.89	5244	6939200
CH	LUETSCHINE	GSTEIG	46.66	7.87	379	6939540
CH	INN	MARTINSBRUCK	46.89	10.47	1945	6943100

A.2 R-Packages

The following R-Packages have been used at any point during the Thesis:

1. boot
2. corrplot
3. evd
4. extRemes
5. grid
6. gtable
7. hexbin
8. Hmisc
9. ismev
10. lattice
11. latticeExtra
12. lmom
13. MASS
14. NMF
15. plyr
16. scales